

For Reference

NOT TO BE TAKEN FROM THIS ROOM

Ex libris
UNIVERSITATIS
ALBERTAENSIS





THE UNIVERSITY OF ALBERTA

PRECAMBRIAN GEOLOGY ALONG THE FRASER RIVER BETWEEN
MOUNT ROBSON AND TÊTE JAUNE CACHE, BRITISH COLUMBIA

by



ROBERT HUGH PINSENT

A THESIS

SUBMITTED TO THE FACULTY OF GRADUATE STUDIES
AND RESEARCH IN PARTIAL FULFILMENT OF THE
REQUIREMENTS FOR THE DEGREE OF MASTER OF SCIENCE

DEPARTMENT OF GEOLOGY

EDMONTON, ALBERTA

Fall, 1971



Digitized by the Internet Archive
in 2020 with funding from
University of Alberta Libraries

<https://archive.org/details/Pinsent1971>

THE UNIVERSITY OF ALBERTA
FACULTY OF GRADUATE STUDIES AND RESEARCH

The undersigned certify that they have read, and recommend to the Faculty of Graduate Studies and Research for acceptance, a thesis entitled "Precambrian Geology along the Fraser River between Mount Robson and Tête Jaune Cache, British Columbia" submitted by Robert Hugh Pinsent B.Sc., in partial fulfilment of the requirements for the degree of Master of Science

Date .28th. October..1971.



i

ABSTRACT

A 13 mile section through the Selwyn Range of the Canadian Rocky Mountains was mapped at a scale of 6 inches to 1 mile. The section extends along the Fraser River valley between Kinney Lake at the foot of Mount Robson, and Tête Jaune Cache in the Rocky Mountain Trench.

The rocks exposed belong to the uppermost Precambrian Miette Group and the basal Cambrian Gog Group. The strata are assigned to 8 informal stratigraphic units which correlate with the stratigraphy both in the Cariboo Mountains to the west, and in the eastern Main Ranges to the east. Cambrian quartzites are underlain by a mixed sequence of commonly graded argillaceous sandstones and shales. The quartz, feldspar and clay mineral content of the sediments varies considerably on all scales.

Structurally, the rocks are relatively undeformed in the northeast and highly deformed in the southwest. Ductility increased southwestwards during deformation. An older schistosity developed in argillaceous rocks was largely obliterated during the main deformation period. Fold axes associated with this period plunge to the west northwest except in the east where they plunge east southeast. Younger crenulations are evident in the southwest.

Metamorphism increases southwestwards. At the biotite isograd, the appearance of biotite is controlled by rock chemistry. The onset of biotite-grade metamorphism was a syn- to post-kinematic event.

Coexisting micas from eight rock samples taken above the biotite isograd were analysed by means of the Electron Microprobe, and element partitioning patterns indicate an equilibrium assemblage. The ubiquitous occurrence of a carbonate phase, usually ankerite, has a pronounced effect on the $Mg/Mg+Fe$ ratio of the rock system, and is thought to 'buffer' the chlorite phase at a maximum value. Muscovites have a low phengite content relative to comparable published analyses, possibly a result of the carbonate 'buffer'.

The whole-rock chemistry suggests that there was only one clay mineral in the original sediment, namely illite. A period of alkali exchange appears to have albitized detrital feldspar clasts at the onset of chlorite-grade conditions. The cell parameters and structural state of chessboard albite formed by this process, together with detrital microcline, were determined using an X-ray diffractometer.

ACKNOWLEDGEMENTS

The writer would like to express his gratitude to Dr. H.A.K. Charlesworth for introducing him to the thesis topic, and for supervising the various aspects of it. In particular the writer would like to acknowledge the guidance and aid given him in the field of computing structural data, and in the construction of the finished manuscript. His help and encouragement throughout are gratefully acknowledged.

The writer is also indebted to Dr. D.G.W. Smith for his assistance in the use of the Electron Microprobe, and his APL Language computer programmes. Permission to utilize data contained in his doctoral dissertation is also gratefully received.

Dr. H. Baadsgaard supervised the wet chemical analyses which were carried out by the writer with the help of Mr. A. Stelmach. The assistance of both was appreciated.

The writer would also like to thank Dr. R.D. Morton for his advice on operating the X-ray diffractometer.

Discussions with the above, and many other faculty members and graduate students contributed much to the understanding of the problem. In particular the writer is happy to acknowledge the assistance given by Dr. R. St. J. Lambert on the metamorphic petrology of the rocks, and Dr. J. Krupicka for his discussion of the feldspar component in the rocks.

The writer is indebted to Mr. D. Tomlinson for operation of the Electron Microprobe during the analyses, and to Mr. F. Dimitrov for the photography and part of the drafting. Mr. J. Ramsden kindly helped

with the Fortran IV computing, and Miss. P. Lumsden with the typing. The assistance of each is appreciated.

Financial assistance has been provided by Graduate Teaching Assistantships, and National Research Council Research Grants.

Finally the writer would like to express his thanks to Miss A. Wright and the Cochrane family for their hospitality and assistance during his visit to the Mount Robson Ranch.

TABLE OF CONTENTS

	Page
Chapter I. INTRODUCTION	
Geological Setting	1
Location of Map Area	3
History of Research in the Vicinity of Mount Robson	4
Study Objectives	6
Geographic Setting	6
Chapter II. STRATIGRAPHY	
Introduction	9
Lithology	10
Sedimentary Structures	12
Stratigraphic Succession	12
Correlation	16
Discussion	18
Chapter III. STRUCTURE	
Introduction	21
Western Zone	21
Central Zone	23
Eastern Zone	27
Chapter IV. FOLIATION AND LINEATION	
Foliation	28
Schistosity - S_1	28
Schistosity - S_2	30
Schistosity - S_3	31
Lineations	
Lineation 1	32
Lineation 2	33
Lineation 3	33
Lineation 4	33
Chapter V. FOLDS	
F_1 Folds	34
F_2 Folds	43
Structural Assessment	46

	Page
Chapter VI. METAMORPHISM AND PETROGRAPHY	
Metamorphic Setting	48
Petrography	50
Chapter VII. GEOCHEMISTRY AND MINERALOGY	
Samples	54
Whole-rock Chemistry	56
Discussion	65
Muscovite Chemistry	70
Muscovite Structural Formulae	74
Discussion	79
Biotite Chemistry	91
Biotite Structural Formulae	95
Discussion	96
Chlorite Chemistry	99
Chlorite Structural Formulae	102
Discussion	103
Carbonate Chemistry	108
Carbonate Structural Formulae	108
Discussion	110
Mg/Mg+Fe	115
Albite Occurrence	121
Albite X-ray Diffraction Data	122
Microcline X-ray Diffraction Data	126
Chapter VIII. PHYSICAL AND CHEMICAL CONSIDERATIONS	
Physical Conditions	140
Fugacity of Oxygen	131
Fugacity of Sulphur	131
Fugacity of Carbon Dioxide	133
Pressure	135
Temperature	135
Mineralogical Evolution of Miette Group Sediment	136
Biotite Isograd	139
Age Determinations	144
References	R-1
Appendix A. Maps	A-1
Appendix B. Analytical Methods	A-3
Appendix C. Computer Programmes	A-8
Appendix D. Petrographic Descriptions	A-9

LIST OF TABLES

	Page
1. Precambrian and Lower Cambrian Stratigraphic Successions	17
2. Schistosity Pole Maxima	37
3. Mean Trend and Plunge of Fold Axes	41
4. Whole-rock Chemical Analyses	57
5. Whole-rock Chemical Analyses	58
6. Composition of Pelitic Rocks	63
7. Mineral Assemblages	68
8. Muscovite Chemical Analyses	69
9. Muscovite Structural Formulae	72
10. Muscovite Structural Formulae	73
11. Biotite Chemical Analyses	90
12. Biotite Structural Formulae	93
13. Biotite Structural Formulae	94
14. Chlorite Chemical Analyses	98
15. Chlorite Structural Formulae	100
16. Chlorite Structural Formulae	101
17. Carbonate Chemical Analyses	107
18. Carbonate Structural Formulae	109
19. Albite Cell Parameters	126
20. Microcline Cell Parameters	129
21. Radiometric Age Dates	146

LIST OF FIGURES

	Page
1. Relationship between S_1 and S_2 Schistosities	29
2. Fold Synopsis. Total Bedding	38
3. Schistosity Pole Maxima in Grouped Domains	39
4. Fold Synopsis. Total Schistosity	42
5. Formation of S_3 Schistosity in Western Zone	45
6. Schematic View of the section between Mount Robson and Tête Jaune Cache	47
7. Whole-rock Chemical Distribution of Major Elements	59
8. Whole-rock Si,Al,FeMgMnTi Plot	60
9. Whole-rock Matrix Composition	62
10. AKF Diagram	67
11. Na^+ and K^+ Cation Content of Muscovite	75
12. Na^+ Cation Distribution between coexisting Biotite and Muscovite Pairs	75
13. Distribution of Large Cations in coexisting Muscovite and Biotite Pairs	77
14. Octahedral Al^{VI} Content in coexisting Mica Pairs	78
15. Tetrahedral Al^{IV} Content in Coexisting Mica Pairs	78
16. Octahedral Site Content in Cation Percent	80
17. Distribution of $FeO + Fe_2O_3$ and Al_2O_3 in Phengitic Muscovites as a Function of Metamorphic Grade	82
18. Stability Curves for Phengitic Micas	84
19. Modified AKF Diagram. Stylized Phase Fields and Joins	86
20. Modified AKF Diagram	87
21. Modified AKF Diagram	88
22. Modified AKF Diagram	89
23. AFM Diagram	92

	Page
24. Biotite and Muscovite Al/Mg+Fe Plot	106
25. Biotite and Chlorite Al/Mg+Fe Plot	106
26. Subsolidus Relations in the System FeCO_3 - CaCO_3 - MgCO_3	111
27. Chlorite and Ankerite Mg/Mg+Fe Plot	116
28. Muscovite and Chlorite Mg/Mg+Fe Plot	116
29. Muscovite and Biotite Mg/Mg+Fe Plot	117
30. Muscovite and Ankerite Mg/Mg+Fe Plot	117
31. Biotite and Ankerite Mg/Mg+Fe Plot	118
32. Biotite and Chlorite Mg/Mg+Fe Plot	118
33. Structural State of Alkali Feldspars using the Unit Cell Parameters b and c.	124
34. Weight Percent Orthoclase in Alkali Feldspars using 201 Spacings	124
35. Structural State of Alkali Feldspars using the Reciprocal Lattice Parameters γ^* and α^*	125
36. Structural State of Alkali Feldspars using the Unit Cell Parameters γ and α	125
37. Range of S_2 , O_2 , and CO_2 Fugacities at 600°K, as defined by the Mixed Assemblages	132
38.. Minimum Temperature of Formation of Pyrrhotite using Arnold's (1962) Geothermometer	134

Chapter 1

INTRODUCTION

Geological Setting

The eastern part of the Southern Canadian Cordillera is divisible into the Columbia and Rocky Mountains. Although the two areas are geologically distinct, the boundary between them is gradational and the Rocky Mountain Trench, which forms their geographic divide, is not considered to be a major tectonic discontinuity (Map 1).

At the latitude of Mount Robson, the Columbia Mountains consist of the Cariboo Mountains, a range which passes to the south and east into the Monashee Mountains. The Rocky Mountains at the same latitude may be subdivided from southwest to northeast into the Main Ranges, Front Ranges, and Foothills. Characteristically, the Foothills consist of tightly folded and imbricately thrust-faulted Mesozoic clastics, and the Front Ranges of thick plates of Upper Palaeozoic carbonates thrust onto Mesozoic clasts. The Main Ranges expose highly folded Precambrian and thrust-faulted Lower Palaeozoic clastics and carbonates.

Sediments exposed in the Main Ranges are pre-Devonian in age and part of a thick miogeosynclinal shelf sequence consisting of carbonates and clastics. The mode of deformation changes from thrust faulting in the Palaeozoic to folding in the Precambrian. Unlike the

Palaeozoic strata the Precambrian clastics have been metamorphosed and complexly deformed on all scales. At the latitude of Mount Robson the fold-axes deviate from the normal and trend west northwest. High-angle thrust and normal faults occur in the western Main Ranges. The Malton gneiss straddles the Trench south of the latitude of Mount Robson and crops out in both the Monashee and Rocky Mountains. The origin of this and other gneiss domes in the Columbia Mountains is uncertain, but some may prove to be reactivated basement (Campbell, 1970).

In the Columbia Mountains the structural style is intimately related to the gneiss domes which occur throughout. In the Cariboo Mountains where the layered rocks are stratigraphically equivalent to those in the western Main Ranges of the Rocky Mountains, metamorphism and deformation are apparently related to the emplacement of the Shuswap and Wolverine metamorphic complexes. These form a high-grade metamorphic "infrastructure" exposed beneath a deformed "superstructure" of Windermere sediments. Metamorphism associated with the Shuswap metamorphic complex forms an aureole which extends across the Trench into the Rocky Mountains.

Metasedimentary rocks lying in a thermal saddle between the Shuswap and Wolverine metamorphic complexes have experienced ductile flow at high temperatures. The rocks are isoclinally and recumbently folded such that both bedding and schistosity now define a simple antiformal structure. Strata overlying this antiform are isoclinally as uprightly folded and occur in anticlinoria and synclinoria. The rheidity of a rock is largely a function of composition and temperature; thus as one rises structurally and stratigraphically the ductility decreases and the amount of brittle behaviour increases. Away from the "infra-

structure" flow folds are replaced by buckle folds and at higher levels still stress was relieved by faulting.

Although late faults have been mapped in the vicinity of the Rocky Mountain Trench, the 20-mile offset of the garnet isograd across the Trench is not itself evidence for large lateral displacement, as the angle of dip of the isograd is unknown. Normal faults are thought to occur at intervals along the Trench and it may also be the locus of high-angle thrust faults. Regardless of this, the structural style and orientation in the Cariboo Mountains continues across into the Main Ranges of the Rocky Mountains. Precambrian sandstones, because of their argillaceous nature, carry the imprint of the Shuswap metamorphism into the Main Ranges. Thrust faulting in the overlying strata is a brittle response to the same orogenic processes which caused deformation in the Cariboo Mountains. "Rocky Mountain Orogenesis" is thus integrally related to the evolution of the Canadian Cordillera farther west.

The Precambrian Miette Group, which crops out in the western Main Ranges, represents the lowest structural and stratigraphic level exposed in the Rocky Mountains. These sediments, which roughly correlate with the Kaza Group and the Isaac Formation of the Cariboo Mountains, are the structural and stratigraphic link between the Columbia and Rocky Mountains. Comparatively little is known about the detailed structure and stratigraphy of the Miette Group in the western part of the Main Ranges.

Location of Map Area

At the latitude of Mount Robson the Fraser and Robson Rivers have cut a pass across the structural grain of the western Main Ranges.

This section from Kinney Lake on the Robson River to Tête Jaune Cache, where the Fraser River enters the Rocky Mountain Trench, is approximately 13 miles long and presents a readily accessible although incomplete section through the Miette Group.

The area mapped for this study extends through the Fraser Valley from Tête Jaune Cache in the southwest to a point on the Robson River just short of Kinney Lake in the northeast.

The area was mapped in the autumn of 1969, at a scale of 6 inches to the mile, on air photographs obtained from the British Columbia Department of Lands and Forests.

History of Research in the Vicinity of Mount Robson

In the autumn of 1898 J. McEvoy followed the trail from Jasper through the map area out into the Trench. He noted the occurrence of 'grits' which he assigned to the Lower Cambrian Bow River conglomerate (McEvoy, 1901).

The Trench section from Prince George to Tête Jaune Cache was examined by G.S. Malloch in 1909, and Mount Robson was visited by C.D. Walcott in 1912 and L. Burling in 1915. These early workers established the stratigraphic position of McEvoy's grit sequence as Late Precambrian, and Walcott assigned them to the "Miette Formation", later raised to group status (Mountjoy, 1962).

Although M. Sorensen examined the area in the early 1930's, his work remained unpublished until 1955. Sorensen considered that the argillites exposed on the eastern part of the map-area form the core of an anticline whose westerly limb forms the Selwyn Range. The 'grits'

in this limb were reported to become progressively more deformed towards the Trench.

More recently the area has fallen within the range of several regional geological studies. The western part of the area has been mapped at a scale of 4 miles to the inch (Campbell, 1967 and 1970). The Main Ranges of the Rocky Mountains between the latitudes of Mount Robson and Banff have been mapped on the same scale (Price and Mountjoy, 1970).

Additional information relating to the regional setting of the map area is presented by Mountjoy and also Campbell and Charlesworth as papers in the Edmonton Geological Society Guidebook (1970).

More specific reference to the map area is made by Weiner (1966) who radiometrically dated a biotite separate, a muscovite separate and a whole-rock phyllite from the area by the K^{40}/Ar^{40} method.

Although the map area lies outside the McBride map sheet, work by A. Brown (1967) on the northwesterly extension of the Selwyn Range in the vicinity of McBride is relevant to the present study.

Study Objectives

One of the primary objectives of the study was to examine the stratigraphy and structure of the Precambrian Miette Group and compare them with equivalent strata found both near the town of Jasper, approximately 50 miles to the east, and also in the Cariboo Mountains west of the Trench.

In the Cariboo Mountains the Precambrian and Early Palaeozoic Cariboo and Kaza Group are known only from regional studies undertaken by Dr. R.A. Campbell of the Geological Survey of Canada. The Miette Group at Jasper is known in more detail through the work of Dr. H.A.K. Charlesworth and graduate students at the University of Alberta.

In addition to the above, which relies heavily on field relationships, the study included an examination of the mineralogy and metamorphic petrology of the Miette Group near the Rocky Mountain Trench.

The geochemistry and chemical evolution of the sediments, now regionally metamorphosed up to the biotite grade, were examined and an attempt made to explain the nature of the biotite isograd in terms of bulk whole-rock chemistry and the chemistry of coexisting phases.

Coexisting carbonates and micas were analysed with the A.R.L. Electron Microprobe in an attempt to establish patterns of element distribution between coexisting phases. The samples were examined for evidence of chemical equilibrium and the effects of bulk chemistry and the physical environment on the silicate mineralogy.

Geographic Setting

Eight miles southwest of Mount Robson the Fraser River is joined by a tributary, the Robson River. Upstream from this point the Fraser

River flows northwestward, parallel to the regional structural trend, between the Rainbow and Selwyn Ranges. Downstream it cuts southeastward through the Selwyn Range towards the Rocky Mountain Trench. The valley floor, between Kinney Lake situated on the Robson River five miles northeast of its confluence with the Fraser River and Tête Jaune Cache, where the Fraser River enters the Trench, exposes a readily accessible structural section through the western part of the Main Ranges of the Rocky Mountains (Map 1). In the six miles upstream from its confluence with the Robson River, the Fraser River falls 500 feet, from 3,200 to 2,700 feet, and is incised into a broad glaciated valley. Above this section the gradient decreases and the valley, partially occupied by Moose Lake, drops only 400 feet in 25 miles. Downstream from its confluence with the Robson River, the Fraser River occupies a glacial valley encompassing the lower reaches of the Robson River and the Fraser River downstream as far as Rearguard Station. The gradient is less steep and falls only 300 feet in the 12 miles downstream to the Trench. Between Rearguard Station and the Trench the valley is confined and sinuous; there is, however, little apparent increase in gradient as the Fraser River makes its way into the flat lying floor of the Trench near Tête Jaune Cache.

The Mount Robson Ranch, below Emperor Station, lies on an abandoned river channel through which the Fraser River used to flow into the Robson River at the mouth of Swiftcurrent Creek. The Fraser River subsequently broke through the spit of land separating it from the Robson River, and has cut a canyon close to the Robson Ranch fault.

Within the map area the valley walls of the Fraser and Robson Rivers are commonly steep. They give a local relief of up to 5,000 feet,

such as below Mount Chamberlin and Cinnamon Peak. These two peaks are separated by a major tributary, Swiftcurrent Creek, which cuts a substantial notch out of the valley wall and joins the Fraser River downstream from its confluence with the Robson River.

Outcrop in the valley floor is best between Rearguard Station and the Trench. The bottom of the valley along this stretch has been eroded by the Fraser River since glacial times. Two railway tracks, a road, and the river contribute to the availability of outcrop in this region. Between Rearguard Station and the ridge which used to separate the Fraser and Robson Rivers, there is no outcrop in the floor of the valley. Except for the slopes of Mount Chamberlin exposure on the valley walls is generally poor.

The valley of the Fraser River is one of the few good lines of communication between the western plains and the Cordilleran region west of the Trench. The Yellowhead Highway lies in the floor of the valley and follows the north bank of the Fraser River down to Tête Jaune Cache. The Highway crosses the Fraser River at Tête Jaune Cache, at its junction with Highway #5 to Kamloops. The road mileage from this junction to Edmonton is 300 miles, and to Vancouver 497 miles.

Both railway lines, which are owned by Canadian National Railways, follow the south bank of the river, where they have been cut at different levels into the steep and wooded valley wall (Plate I, #2). The lower of the two lines goes from Jasper, Alberta, to Prince Rupert on the west coast of British Columbia. The upper track, also from Jasper, turns south on entering the Trench and goes to Vancouver.

An oil pipeline also lies in the valley floor, giving, along with the river, five potential sections across the geological strike.

Chapter II

STRATIGRAPHY

Introduction

The rocks found in the map area are of sedimentary origin. However, they become progressively more deformed and metamorphosed as one approaches the Trench.

The sediments, especially in the lower two thirds of the stratigraphic succession, are monotonous and repetitious, consisting largely of interbedded coarse argillaceous sandstones and argillites. This lower mixed clastic sequence may itself be subdivided into a number of informal units of approximately 1,500 feet thick, which facilitate mapping in an otherwise uniform succession. This subdivision is based on the relative proportions of coarse arenaceous to fine argillaceous material and the units thus alternate from "arenaceous" to "argillaceous". The upper third may also be subdivided; this subdivision is more clear cut as each unit is uniform and lithologically distinct.

The lack of continuous outcrop and the complexity of deformation make correlation from one outcrop to another extremely difficult. The thicknesses assigned to the various units are estimates based on the available outcrop and structural data and are not based on measured stratigraphic sections. The succession is thought to be conformable throughout, although critical outcrops are largely missing.

Lithology

The proportions of detrital quartz, feldspar and clay minerals (now metamorphosed) vary widely. The rock types encountered thus range from shale to sandstone; the feldspar content of the latter tends to increase with detrital quartz content and grain size. Poor sorting and the common occurrence of small-scale graded bedding makes it difficult to give a precise name to many beds. Many comparatively thin beds range from quartzo-feldspathic pebble-conglomerate to shale.

The lithologies commonly encountered may be loosely classified as shale, siltstone, argillaceous sandstone (with or without feldspar), feldspathic sandstone and quartzo-feldspathic pebble-conglomerate. This sedimentary classification is complicated by the variable metamorphism experienced by the rocks (see Chapter 6).

Shale

None of the original detrital clay minerals remain: the shales have generally been recrystallised into slates or phyllitic schists. Shale is found both as thicker interbeds separating distinctly more arenaceous layers and as comparatively thin layers in the upper parts of graded beds. It commonly is greenish-grey or black and finely laminated. Some shale horizons contain carbonate (up to 50%) which is either finely disseminated or occurs as porphyroblasts.

Siltstone

Siltstone is commonly associated with shale as an intermediate step in graded horizons. It is also found as discrete beds interbedded with shale in the thicker shale sequences and may be interbedded with

arenaceous material without the presence of shale.

Siltstone tends to be flaggy, poorly bedded and uniform.

Argillaceous Sandstone

Siltstones pass imperceptibly into argillaceous sandstones with increase in grain size and quartz content. The proportions of original clay matrix and detrital quartz with feldspar is variable. In graded units argillaceous sandstones may pass from coarse to fine in a matter of feet, or alternatively, in less graded parts of the succession they may be constant in grain size over great stratigraphic thicknesses. The feldspar content increases with grain size and quartz content. The quartz and feldspar grains are set in a matrix of clay-sized material capable of isolating the original clastic grains and preserving the original texture of the rock. The quartz, commonly blue, is subangular to subrounded. The chloritic matrix gives a greenish tint to the rock in hand specimen. Large cubes of pyrite 1-2 cm in width are common in this rock type; on weathering to limonite they give a rusty blotched appearance to exposed surfaces.

Feldspathic Sandstones

Feldspathic sandstones show much less variation in grain size within a bedded sequence. They are thickly bedded, commonly cross-bedded, and massive in appearance. The feldspar is white, and the overall texture of the rock is granular.

Quartzite

True quartzites are rare; impure quartzites are found with argillaceous sandstones where they tend to be gradational into pebble-

conglomerate. More commonly, quartzites are found interbedded with feldspathic quartzites and differ little from that lithology except in the reduced feldspar component. The sediment tends to be coarse and granular; there appears to be little fusion of detrital grains.

Quartzofeldspathic Pebble-Conglomerates

Lenses of pebble-conglomerate are found throughout the coarse argillaceous sandstone beds. They characteristically make up the base of the coarser graded horizons and usually pass imperceptibly into argillaceous sandstones. Interbed scour channels are usually found to contain coarse sandstone or pebble conglomerate. The pebbles are sub-angular to rounded and may contain a high feldspar percentage; the argillaceous matrix content is low, but variable.

Sedimentary Structures

Graded bedding is common. Graded sediments are argillaceous throughout, although the amount and grain size of granular quartz and feldspar decreases from bottom to top. Individual graded units tend to pass from conglomerate to coarse argillaceous sandstone, finer argillaceous sandstone and through siltstone to shale, although not all these lithologies need be present and the thickness of each is variable. Graded beds range in thickness from a few feet to a few tens of feet.

Scour-and-fill structures commonly occur between individual graded beds, particularly where pebble-conglomerate and coarse argillaceous sandstone overlie shales (Plate II, #6).

Evidence for fluxoturbidite-type deposition is found in the form of convolute bedding or flame structures (Plate II, #3).

Cross-bedding on a scale of one or two feet is restricted to quartzites and feldspathic sandstones at the top of the succession.

Stratigraphic Succession

The succession has been divided into lithologic units A-H, brief descriptions of which follow.

Unit A

Unit A is predominantly arenaceous, consisting of coarse argillaceous sandstone and quartzo-feldspathic pebble-conglomerate, and is poorly exposed. Massive ribs of arenaceous sandstone marking the top of the unit are readily accessible 1/2 mile northwest of Emperor Station. These have been correlated with pebble-conglomerates cropping out in the extreme southwest (Plate II, #8). This correlation implies a coarsening of the unit towards the southwest.

Unit B 1,300'

Unit B is predominantly argillaceous and contains only a few arenaceous interbeds near the base. It conformably overlies Unit A and consists of finely bedded greenish-grey interbedded shales and siltstones. Chlorite and phengitic muscovite are largely responsible for the greenish colouration. Increase in metamorphic grade and deformation has transformed the slates which crop out just northwest of Emperor Station into a coarse-grained, phyllitic schist further west. The unit is best exposed along the lower railway track northeast of Rearguard Station. At this locality, however, the unit is more highly metamorphosed and is intensely deformed on a mesoscopic scale.

Unit C 1,750'

Unit C marks a return to predominantly arenaceous deposition, consisting of argillaceous sandstone (Plate II, #1) with interbedded subordinate shale and siltstone. The sandstones are graded near the base of the unit and pass upward into more massive, thickly bedded, argillaceous sandstone. Irregular and angular clasts of shale are found in some of the more massive strata which locally resemble mud-flake conglomerates.

Unit C crops out sporadically over much of the section between Emperor Station and Rearguard Station where it is best displayed.

Unit D 1,000'

Unit D differs from Unit C in that it appears to be thinner bedded and more argillaceous. Individual arenaceous units contain a higher proportion of argillaceous matrix and there is a greater development of shale and siltstone. Graded bedding and thick arenaceous units are largely absent.

Unit D is best exposed above the highway in the face of a cliff about a mile upstream from the new road bridge over the Fraser River near Tête Jaune Cache. The most readily accessible section is, however, on the lower railway track between Tête Jaune Cache and Rearguard Station.

Unit E 2,000'

Unit E is uniformly arenaceous. The sediments are coarse and poorly bedded. Graded bedding is rare and the succession contains few argillaceous interbeds.

Unit E crops out in the Fraser Canyon near the Robson Ranch

Fault and is exposed upstream from this locality. Exposure is also found on the upper railway track, northeast of Emperor Station.

Unit F 6,500'

A thick sequence of interbedded shales and siltstones makes up the bulk of Unit F. Rare arenaceous interbeds are found at the base of the unit which is conformable with Unit E. There are a few argillaceous sandstone layers similar to those found in the underlying unit. The shales are slaty, black and pyritic, and the siltstones are flaggy in appearance. Small interbeds of carbonate and carbonate-rich shale are found locally, mid-way through the section.

Good exposure is found along Highway 16 and up the slopes of a small wooded knoll at the northwest extremity of the Rainbow Range. A good section through the lower part of the unit is exposed in the Fraser River from this locality downstream to the contact with Unit E. The top of the unit is not exposed.

Unit G 2,500'

Unit G consists of thinly bedded arenaceous and argillaceous beds. Feldspathic sandstones and conglomerates are interbedded with shales and siltstones. The base of the section is not seen and outcrop is restricted to the uppermost part of the unit.

Unit H

The youngest unit in the map area consists of a sequence of quartzites and feldspathic sandstones. The sediment is well sorted and cross-bedded. The bedding tends to be thick and uniform.

Unit H is exposed in the Robson River and passes to the northeast out of the map area.

Correlation

Stratigraphic units A-H may be correlated on a lithologic basis with equivalent strata at Jasper (Table 1). The feldspathic sandstones and quartzites of Unit H almost certainly belong to the Lower Cambrian Gog Group. The quartzites are not fossiliferous, but pass upward into limestones with archaeocyathids and olenellids belonging to the Lower Cambrian Mural Formation. The Mural Formation crops out at Kinney Lake, just outside the map area to the northeast (Mountjoy, 1970). Unit G has also been assigned to the Lower Cambrian Gog Group by correlation with the Jasper Formation of Charlesworth et al. (1967). Units A-F belong to the Precambrian Miette Group. The equivalent strata west of the Trench belong to the Isaac Formation of the Cariboo Group and the Kaza Group in the Cariboo Mountains (Campbell, 1970).

TABLE 1. Precambrian and Lower Cambrian stratigraphic successions in the Cariboo Mountains and in the Mount Robson and Jasper areas of the Rocky Mountains. The more important lithologies are underlined (cg - conglomerate, ss - sandstone, sh - shale, slt - siltstone, ls - limestone, dol - dolomite, qt - quartzite).

AGE	GROUP	Cariboo Mountains Campbell 1970		Map Area Mount Robson		Jasper Charlesworth 1967		AGE	GROUP
		Formation	Lithology	Formation	Lithology	Formation	Lithology		
LOWER CAMBRIAN	CARIBOO	Mural 750'	ls, sh	H 500'+	ss qt, sh	"A" 700'+	qt cg gt, sh	GOG	LOWER CAMBRIAN
		Midas 500'	slt, sh, qt						
		Yanks Peak 1,200'	qt, sh						
		Yankee Belle 2,500'	sh, slt, ls	Jasper 1,600'	at, gt cg, sh				
		Cunningham 1,300'	ls, dol, sh			Upper Wynd 1,600'	sh, slt dol		
PRECAMBRIAN	KAZA	Isaac 3,000- 5,000'	sh, ls, ss qt	F 6,500'	sh, slt ls, ss	Lower Wynd 2,400'	qt, slt sh, cg		
		10,000'+	sh, slt, ss qt	E 2,000'	ss, qt slt, sh sh, slt gt ss, slt sh ss, slt sh cg, ss slt, sh	Old Fort Point 1,200'	sh, slt dol	MIETTE	PRECAMBRIAN
				D 1,000'		Meadow Creek 130'+	cg, gt slt, sh		
				C 1,700'					
				B 1,300'					
		A 300'+							

Discussion

Although the stratigraphy at Mount Robson was not examined in detail, it would appear to be similar to that at Jasper, and the sediments themselves closely resemble their Jasper counterparts (Charlesworth et al., 1967). No major tectonic break separates the two localities, although Price and Mountjoy (1970) have mapped a few relatively minor thrust faults.

The mixed argillaceous-arenaceous sequence of the Miette Group at Mount Robson differs in certain respects from the better known easterly facies. The westerly facies is in general more homogeneous on a mesoscopic scale so that individual map units are less easily defined.

Correlation is necessarily lithologic and in a monotonous sequence tends to be hazardous. However, within the framework developed for the Miette Group at Jasper, individual units at Mount Robson would appear to be substantially thicker. Unit F in particular is exceedingly thick; this may in part be a result of faulty estimation across imperfectly known structures. Unit G at Mount Robson appears to be less well sorted than the equivalent Jasper Formation.

The Old Fort Point Formation at Jasper is acknowledged to be one of the few reliable marker horizons in the Miette Group and may be correlated with the lower Hector Formation at Lake Louise. Correlation with Unit B is by no means certain because of the apparent lack of distinctive limestones, limestone-breccias and purple shales.

The occurrence of a characteristic "chessboard" albite was noted by workers in the Jasper area, together with a lack of detrital potash

feldspar. Both these findings are upheld by the present study and are discussed later.

Heavy mineral studies at Jasper show that both tourmaline and zircon are common in the Miette Group; there they are equated with an igneous and high-grade metamorphic source terrain. The same minerals noted at Mount Robson are presumably derived from the same source.

Sedimentary structures in the Miette Group at Mount Robson are indicative of turbidite type deposition. Scour-and-fill structures, flame structures and graded bedding all suggest deposition in an offshore marine environment. Cross-bedding is largely absent, except in the quartzites and feldspathic sandstones of Unit H. Cross-bedding in the Miette Group farther east is more common. This may be the result of deeper water deposition in the west.

The direction of current flow in the Lower Wynd at Jasper indicates a northeasterly source with a current flow direction of 240° . The result is similar to that found by Mountjoy and Aitken (1963) in a study of cross-bedding along the Snake Indian River, 40 miles northwest of Jasper. They reported current directions of 225° for the upper part of the Miette Group and 235° for the lower part of the Gog Group.

The Precambrian Miette and Cambrian Gog Groups are thought to overlie a westward extension of the Canadian Shield. This extension is known to slope beneath the western plains (Burwash, 1964), and is thought to continue under the Rocky Mountains (Bally et al., 1966).

Clastic sediment derived from the craton was deposited along the continental margin, and with the passing of time is presumed to have 'onlapped' onto the craton.

The nature of the sediments suggest a high-grade mixed igneous

and metamorphic source area compatible with the Churchill Province of the Canadian Shield. This finding is corroborated by radiometric ages on detrital "muscovites" by Charlesworth et al. (1970) at Jasper.

The enormous thickness and areal distribution of the Miette Group, combined with its uniform nature, are difficult to account for on the basis of its having a near-shore deltaic environment. In light of the sedimentary structures observed it is inferred that the sediments were "slumped" into their present stratigraphic position. The occurrence of mud-flake conglomerates suggests disruption and mass flow out of the deltaic environment which, by latest Precambrian time, must have been far to the northeast. For the sediment to remain unsorted and relatively fresh, deposition must have been rapid.

The Isaac Formation of the Cariboo Mountains correlates readily with Unit F which in turn is equivalent to the upper Wynd Formation at Jasper.

The nature of the sub-Cambrian boundary is poorly understood. Aitken (1969) drew attention to the magnitude of the unconformity found beneath the Cambrian at Lake Louise. The monotony of the late Precambrian strata and the nature of the basal Cambrian make it hard to document. The unconformity at Lake Louise appears to decrease in magnitude to the north and northwest. According to Charlesworth et al. (1967) there is no visible stratigraphic break at Jasper.

The lack of critical exposure at Mount Robson leaves the question of a sub-Cambrian unconformity unresolved. There is, however, a suggestion that Unit G at Mount Robson and the Jasper Formation at Jasper are transitional between and conformable with Upper Miette shales, sediments and lower Gog quartzites.

Chapter III

STRUCTURE

Introduction

Structurally the map area can be divided into the Western, Central, and Eastern zones. The Central Zone is bounded on the northeast by the Robson Ranch Fault and in the southwest by a shear zone.

The degree of metamorphism and deformation increases from northeast to southwest. The folds become more ductile and the schistosity more intense in the vicinity of the Trench. Although there is a pronounced change in structural style across the area, the geometry of the folds and their structural interpretation suggest only one main period of deformation.

Western Zone

The Western Zone is bounded on the southwest by a downfaulted block of carbonate which crops out in the floor of the Trench south of the map area; this carbonate may be Middle Cambrian or Late Precambrian in age.

The northeast contact with the Central Zone is exposed above the new road bridge across the Fraser River near Tête Jaune Cache. At this locality the contact would appear to be a zone of shearing and crumpling.

In the Western Zone, Units A, B and C are deformed into a series of tight, upright folds which plunge gently west northwest. The folds have a pronounced axial plane schistosity which dips steeply to the south southwest and steepens to nearly vertical in the vicinity of the sheared contact with the Central Zone. Arenaceous units in the limbs of the folds retain their sedimentary structures although there has been considerable ductile flow on a mesoscopic scale - contraction normal to and extension parallel to the axial plane. Schistosity development is less evident in the limbs of folds, although the rock fabric appears to have been orientated with regard to the fold axes.

Two major anticlines separated by a syncline are outlined by a distinctive pebble-conglomerate belonging to Unit A. These folds and a few mesoscopic folds are all that can readily be identified in the Western Zone.

Minor folds are very evident in the shear zone separating the Western and Central Zones. The shear zone, which is approximately 50 feet wide, separates two regions with different fold styles and the same geometric orientation. Minor folds in the shear zone are asymmetric and serve to illustrate the nature of the zonal contact (Plate I, #5).

Within the shear zone, different lithologic units have responded in different ways. Isolated beds of quartzose sandstone, usually competent, are here set in an argillaceous matrix and have acted in a ductile manner.

In response to the same stress conditions that gave rise to an axial plane schistosity in the fine-grained matrix, the quartzose layer has been compressed into bulbous knots and has been stretched by

shearing along the plane of schistosity parallel to the fold-axes B (Plate I, #5). The orientations of the fold-axes and schistosity planes are similar to those found in the Western Zone. The Western Zone has overridden the Central Zone causing the sediments to crumple within the zone of shear. The shear zone has the form of a reverse fault which probably has a stratigraphic displacement of 100-150 feet. This couple on the shear zone is reflected in the stratigraphy which indicates that the older Units A, B and C crop out to the west.

The shear zone is unlikely to be post orogenic and is probably a local readjustment in what is otherwise a zone of transition. Mountjoy (1970) considered that a transition occurs between the structural styles here attributed to the Western and Central Zones when examined further south in the main body of the Selwyn Ranges. A transition zone is thus probably the norm, with local crumpling and slippage where particularly argillaceous units are involved.

Central Zone

The Central Zone extends from the above shear zone in the southwest to the Robson Ranch Fault in the northeast. The zone is approximately eight miles wide and makes up the bulk of the Selwyn Range. The structure of the Central Zone is dominated by an anticline whose axial trace crosses the Robson Ranch. This anticline is overturned to the northeast, and the lower limb is cut by the Robson Ranch Fault.

The Central Zone may be subdivided into the Rearguard, Swiftwater and Emperor subdivisions which are separated by the Swiftwater thrust and the trace of the Robson Ranch anticline respectively.

Rearguard Subdivision

The Rearguard subdivision extends from the eastern limit of the Western Zone to the level of the Swiftwater thrust east of Rearguard Station.

Units A, B, C and D have been deformed into a series of folds. The phyllites of Unit B can be traced through a series of major anticlines and synclines with an axial separation of 700 feet. Both deformation and metamorphism increase southwestwards across the subdivision. The northeast boundary marks the approximate position of the biotite isograd. In the southwest deformation is complex, especially in Unit D, and the major anticlines and synclines begin to resemble anticlinoria and synclinoria.

The fold axes B plunge at shallow angles to the west northwest. The schistosity is essentially parallel to the axial planes, although in quartzose units the schistosity tends to fan out around the fold axes. The schistosity dips predominantly to the south southwest and ranges from 70°-90°. Dips to the north northeast are found locally and are invariably steep.

During folding the rocks in this region tended to be less ductile than those in the Western Zone. Parasitic folds tend to be asymmetric, inclined towards the northeast (Plate III, #2).

On a regional scale the Swiftwater thrust sheet contains an anticline-syncline pair. These folds are represented by the folds of the Rearguard subdivision. The Swiftwater thrust is thought to die out in the cliff face above Swiftwater Station (Campbell, 1970). If this is the case, then a transition occurs between the Rearguard and Swiftwater subdivisions.

Swiftwater Subdivision

The Swiftwater subdivision extends from the Swiftwater thrust to the axial trace of the Robson Ranch anticline. The strata belonging to Units A, B and C young progressively to the southwest. The whole subdivision essentially belongs to the upper limb of one major anticline, and deformation within the limb itself is restricted to relatively minor folds and flexures. Only one anticline-syncline pair of any regional significance was found in the subdivision.

The dip of the strata throughout the subdivision is relatively constant at about 40° south southwest and the fold axes of minor folds in the area, like those in the Rearguard subdivision, plunge at a shallow angle to the west northwest.

Minor parasitic folds on this major anticlinal limb tend to be asymmetric and have a steeper northeasterly limb. Schistosity tends to be poorly to moderately well developed in the Swiftwater sub-zone, depending on the lithologic nature of the unit. Schistosity parallels the axial planes of minor folds although it has a tendency to fan around fold axes in arenaceous units. The schistosity almost invariably dips to the south southwest and tends to be shallower than in the Rearguard subdivision.

Phyllitic interbeds within this subdivision display two schistosities: an early schistosity subparallel to bedding and a later axial-plane schistosity related to the minor folds in the area. The second schistosity is regional in extent.

The sediments have been metamorphosed to within the chlorite grade of regional metamorphism, with the sporadic occurrence of biotite in rocks of suitable composition in the southwest. The rock fabric is

less well imprinted with the regional schistosity and arenaceous rocks may show only a slight tendency towards micaceous foliation.

Emperor Subdivision

The Emperor subdivision extends from the axial trace of the Robson Ranch anticline to the Robson Ranch fault. The subdivision comprises the northeasterly, inverted limb of the Robson Ranch anticline. Inversion is indicated by cleavage-bedding relationships, graded bedding, and scour-and-fill sedimentary structures.

The internal structure of the inverted limb is locally complex, e.g. in the core of the anticline exposed in the cliff face above Emperor Station and near the Robson Ranch fault. In a general sense the bedding tends to be steep and the schistosity moderately shallow. Both dip to the south southwest.

Units A, B and C which underlie the subdivision are metamorphosed to within the chlorite metamorphic grade. Argillaceous units are slaty and less phyllitic. Schistosity is generally poorly developed and restricted to the more argillaceous rocks.

The Robson Ranch fault which separates the Central and Eastern Zones has been correlated with the Moose Lake thrust of Mountjoy (1970). The thrust appears to die out to the northwest and stratigraphic discordance becomes more evident as one traces the thrust along the western slope of the Moose Lake valley out of the map area. Campbell (1970) estimated that the stratigraphic throw across the fault about 6 miles upstream from the junction of the Robson and Fraser Rivers along Highway 16 is 5,000 feet or more.

Eastern Zone

The Eastern Zone extends from the Robson Ranch fault north-eastward into the Rainbow Range and out of the map area southwest of Kinney Lake.

The bedding dips steeply to the north northeast and forms a relatively structureless sequence. Where found, minor folds tend to be restricted to relatively incompetent horizons and internal structures tend to die out stratigraphically. Schistosity development is poor and is restricted to the more argillaceous sediments. The sediments are compacted and have been recrystallised within the chlorite metamorphic grade. Argillaceous rocks are now slates and no phyllites were found in this zone. The slates are cleaved or else show signs of incipient schistosity.

Fold axes again plunge to the south southeast and appear to have a slightly steeper plunge. Both deformation and metamorphism are at their lowest in the Eastern Zone, which is the stratigraphic top of the section, including Units E, F, G, and H.

Chapter IV

FOLIATION AND LINEATION

Foliation

Apart from bedding which is discernable throughout the map area, although indistinct in some of the more phyllitic schists, there are three distinct structural foliations. The earliest schistosity, S_1 , is restricted to the Swiftwater subdivision of the Central Zone. Its occurrence is restricted to argillaceous rocks and its orientation is subparallel to bedding. The second schistosity, S_2 , is the main regional schistosity associated with the period of folding. It is found throughout the area as an axial plane schistosity and becomes increasingly more evident in the more highly deformed western part of the map area. The third schistosity, S_3 , is restricted to the vicinity of the Trench and appears to be a "crenulation cleavage" associated with a late-tectonic period of crenulation.

Schistosity - S_1

The S_1 schistosity is defined by the orientation of chlorite and a phengitic muscovite. In view of the fact that chloritoid porphyroblasts have grown in the plane of the S_1 schistosity, in rocks of suitable composition, it is thought that the schistosity is the result of recrystallisation of chlorite grade micas within the stress field, along with, or followed by the formation of chloritoid (Plate V, #1).

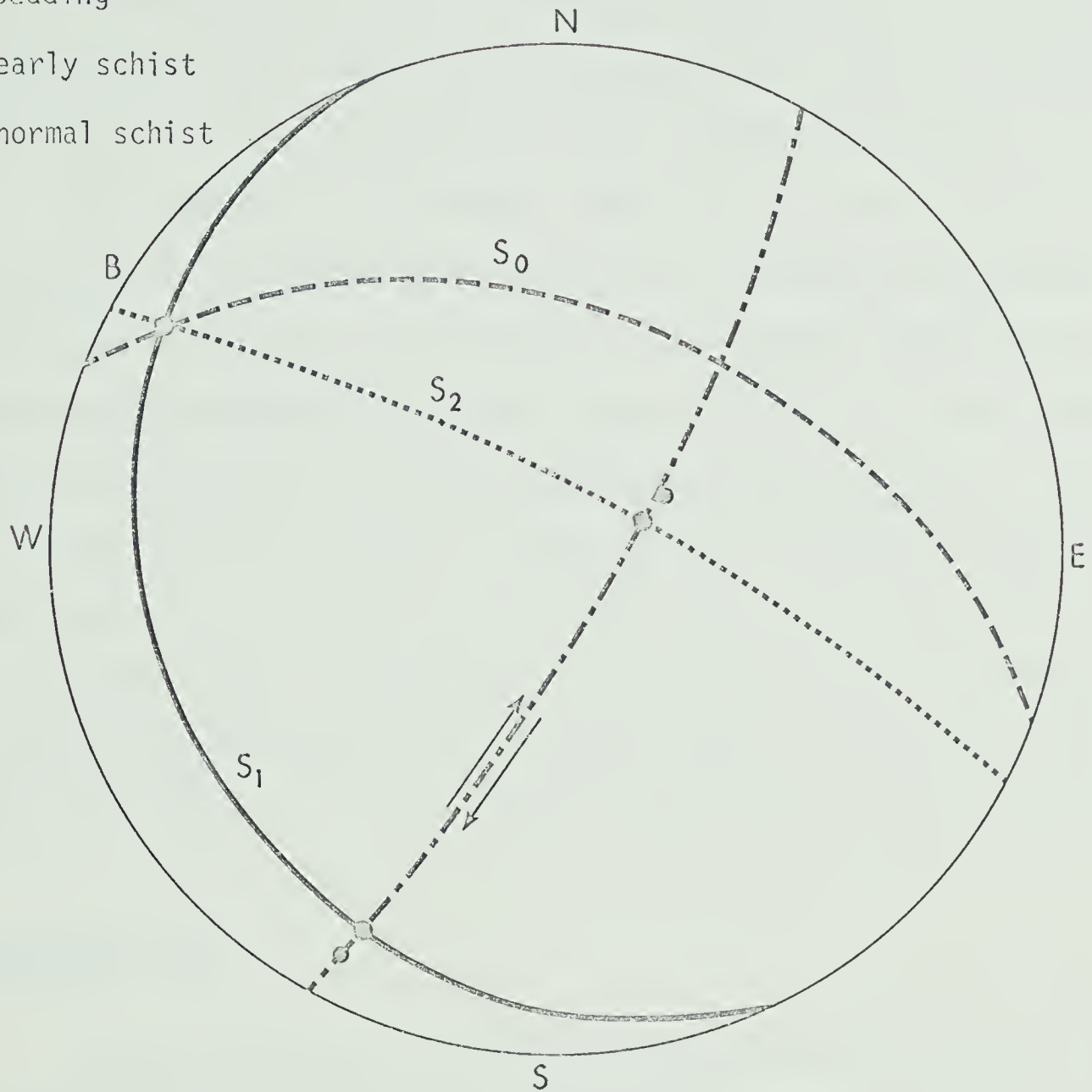
Figure 1

An example of the relationship between S_1 and S_2 Schistositities
in the Swiftwater Subzone

S_0 = Bedding

S_1 = early schist

S_2 = normal schist



The S_1 schistosity is restricted to a few outcrops of phyllite in the vicinity of Swiftwater Station. In every case the S_1 schistosity was disrupted and rotated by movement along the superimposed S_2 schistosity. Both S_1 and S_2 schistosity-bedding intercepts define the axis of the regional fold trend and can be related to it (Fig. 1). In the case of S_1 this may be a secondary effect induced by rotation.

The origin of S_1 is unknown. With the occurrence of chloritoid it is the only evidence of an early period of deformation and metamorphism found in the area. The fact that S_1 is generally subparallel to bedding and was subsequently folded suggests that it is an axial plane cleavage associated with an early period of recumbent folding. There is, however, little evidence to support this and the scale of folding would require that the whole of the Selwyn Range lies on the upper limb of a recumbent fold. Alternatively, the schistosity might be related to some form of "frictional drag" folding related to the underlying Robson Ranch fault. The implications of this will be discussed below.

Schistosity - S_2

The S_2 schistosity is defined in phyllites by the parallel faces of micaceous minerals, muscovite-chlorite and locally, biotite. It forms a 'slaty cleavage' parallel or subparallel to the axial plane of minor and major folds formed during the main period of deformation. In schistose arenaceous rocks, the schistosity is defined by alternating layers rich in quartz and mica. The orientation is partly the result of neocrystallisation of micas, orientated such that the laths parallel to the axial planes of folds are elongated parallel to the fold-axes.

Physical rotation of previously existing micas may also be involved in the western part of the map area and the predominant mechanism in the eastern part. Where the phyllitic rocks of the Swiftwater subdivision display S_1 , mechanical rotation is very obviously responsible in large part for S_2 . With increase in deformation and the onset of biotite formation in certain horizons, the amount of recrystallisation increases to a maximum in the Western Zone.

It should be noted that biotite and chlorite porphyroblasts usually post date the main period of S_2 formation and define it less than the chlorite grade mineralogy. There are, however, exceptions: certain rocks in the western zone developed synkinematic biotite.

In the Western Zone the S_2 schistosity is clearly related to the axial planes of the folds. In the Central Zone there is a greater tendency for the foliation to 'fan' about the fold axis. The schistosity in the Central Zone shows obvious signs of "refraction" in graded beds and its orientation is partially controlled by the lithology.

Schistosity - S_3

The S_3 schistosity is formed by the mechanical rotation of micas which define the S_2 schistosity. There is no suggestion of neocrystallisation. The schistosity is largely incipient and only one occurrence of S_3 foliation was found in which the S_3 translation had obliterated the S_2 schistosity. This occurrence (Plate III, #8) lies on the north bank of the Fraser River, just upstream from the old road bridge at Tête Jaune Cache.

The distribution of this S_3 "crenulation-cleavage" is usually inferred from the presence of crenulation on the earlier S_2 foliation.

It has a relatively constant orientation, dipping at 73° in a direction of 72° and is essentially an axial plane cleavage for the crenulation "folds" (Plate III, #6). The crenulations and hence schistosity, die out away from the Trench and the schistosity does not correspond to the axial plane of a major fold system. Only one minor fold was found with an orientation analogous to an S_2 cleavage crenulation (Plate III, #7).

Lineations

Four lineations which can be correlated with two separate events were recognised in the map area. All are mesoscopically penetrative and are best developed in the western part of the map area. They are defined by:

1. Preferred orientation of the long axes of mica grains,
2. Preferred orientation of elongated quartz pebbles and boudinage of feldspar clasts,
3. The intercept of one 'S' plane on another, e.g. bedding and schistosity, and
4. Crenulation of an 'S' plane.

Lineations 1-3 parallel the regional orientation of fold axes, F_1 , and are associated with the formation of the S_2 schistosity. Lineation 4 parallels the fold axes of microfolds imposed on S_2 schistosity, F_2 , and marks the trace of S_3 on S_2 .

Lineation 1

Muscovite, chlorite and, locally, biotite lie in the axial plane of F_1 folds. The crystal laths are both rotated about the S_2 schistosity and have crystallised within it, such that individual

crystals are elongated parallel to the fold axes. This feature gives a textural grain to the schistosity face, a grain best displayed in schists containing biotite which stands out against a background of muscovite and chlorite.

Lineation 2

Quartz grains and pebbles in the western part of the map area tend to be elongated parallel to the F_1 fold-axes. The grains are compressed within the axial planes of the folds and are deformed into ellipses. This feature is best developed in a pebble conglomerate within Unit A. The extreme elongation of some of the "pebbles" (15 x 4 x 2 cm) suggests that solution and accretion may have been involved. Pebbles of feldspar have fractured and exhibit boudinage parallel to the long axes of quartz particles.

Lineation 3

Except in the northeast, S_2 -bedding intersections are conspicuous in most outcrops throughout the map area. The intersections parallel F_1 fold-axes. Similarly the trace of S_3 on S_2 defines the orientation of the fold-axes of the late-tectonic crenulations F_2 .

Lineation 4

The crenulations noted on the S_2 surfaces are in fact F_2 micro-folds. These folds are best developed on phyllitic surfaces and die out away from the Trench into the Central Zone. Well defined crenulations in the western part of the area become kinks and are less well orientated away from the Trench.

Chapter V

FOLDS

The F_1 folds described for the various structural zones differ in style yet belong to one period of orogenesis and are related to the formation of one axial plane schistosity, S_2 . The folds are predominantly "buckle folds": within them the thicknesses of folded layers remain essentially constant. In the vicinity of the Trench the folded layers have experienced considerable ductile deformation on a mesoscopic scale.

The F_2 microfolds are a type of "buckle fold". They are late-tectonic, but have a distinct axial plane schistosity and they are treated as a genuine fold system.

F_1 Folds

Because of the progressive change in fold style from northeast to southwest, no one description is adequate to describe the nature of the folds in the area. Details concerning the shape and style are given for each of the structural zones separately. The geometry of the folds is, however, defined by the orientation of the F_1 fold-axes and the S_2 schistositities. These orientations vary slightly from southwest to northeast in a manner unrelated to the style of the folds involved.

Orientation diagrams based on the poles to all bedding and schistosity measurements in the map area do bring out many of the features observed in the field, although they must be used with caution

in interpreting fold styles.

A density plot for 540 bedding poles defines a girdle about a fold-axis with a trend and plunge of 296° and 5° , respectively (Fig. 2). The girdle gives pronounced maxima which may reflect various geometries across the map-area.

Similarly a pole density plot for 404 schistosity measurements taken across the area is summarised in Figure 4. The girdle defined by the poles straddles the vertical plane; however, it is strongly weighted to indicate an east southeasterly plunging fold-axis. The trend and plunge of this "mean" axis is 118° - 4° . The mean orientation of schistosity has a strike of 116° and a dip of 85° SW. This fits well with the bedding pole minimum observed in the bedding pole density plot. Schistosity values indicate a steep to shallow southwest dip with only a minor steep northeasterly dipping component.

It is interesting to note that, although both bedding and schistosity poles lie on great circles, indicating cylindrical folding, the fold-axes are about 9° apart. In view of the known shift in the F_1 fold axis from west northwest to east southeast this may be significant.

The S_2 schistosity was observed in the field to flatten slightly from southwest to northeast. The area was thus subdivided into seven strips parallel to the regional trend.

In Strips 1-3, from the Trench to Morey Station, the schistosity is steep and may even dip northeast. The fold-axes as defined by the schistosity density plots (Fig. 3) are essentially horizontal. Strips 4-7 have shallower schistosity dips and no northeasterly component. All seven maxima when plotted on a stereonet define a girdle equivalent to that noted for the total schistosity density plot (Fig. 4).

It would appear that the shallow schistosities northeast of Morey Station are related to the east southeasterly fold axis found to predominate in the Emperor subdivision to the northeast. It also appears that bedding relates to the west northwest plunging axis. Clearly the two are not "ideally" orientated with regard to each other and the two processes of F_1 folding and S_2 schistosity development are not perfectly related.

The map-area was further subdivided into 25 minor domains using geographic and, where possible, structural criteria. The domains are subparallel to the regional strike and may be grouped into subzones and zones reflecting the structural pattern across the strike. (Structural data were processed by means of the IBM 367/67 computer using programmes written in Fortran and APL). Fold axes were calculated using the APL programme "FOLD" and pole density distribution plots were prepared using a FORTRAN programme based on one developed by Muecke (1966).

A mean fold axis was calculated for each of the minor domains from bedding-schistosity intersections, found either from the line of intersection of the two planes (using the APL program LIN) or from the pitch of one plane on another (by means of the APL programme PLUN). The net total derived from all sources was reduced to a mean value (using the APL programme MEANSURF) and the resultant values are given in Table 3.

Minor fold axes plunge both to the NW and the SE. Plunges are shallow, yet there is a significant difference in direction of plunge between folds Sw of the Robson Ranch axial trace and those NE of it. The difference in plunge is only a matter of a few degrees. As can be seen from Table 3 there is a general increase in the incidence of SE-

TABLE 2

Schistosity Pole Maxima

	# obs	Pole to NE	Pole to SW	Fold Axis	Domains
1	118	31-8	212-2	302-0	1,2,3,4,5,6,7,9
2	134	29-5	209-0	299-0	8,10,11,12
3	63	25-10	204-2	294-10	13,14
4	13	26-33	-	-	15,17
5	7	26-24	-	-	16
6	30	21-52	-	-	18,19,25
7	39	13-45	-	118-14	20,21,22,23,24

1 + 2 = Western Structural Zone + Rearguard Subzone of
Central Division

3 = West Swiftwater Subzone

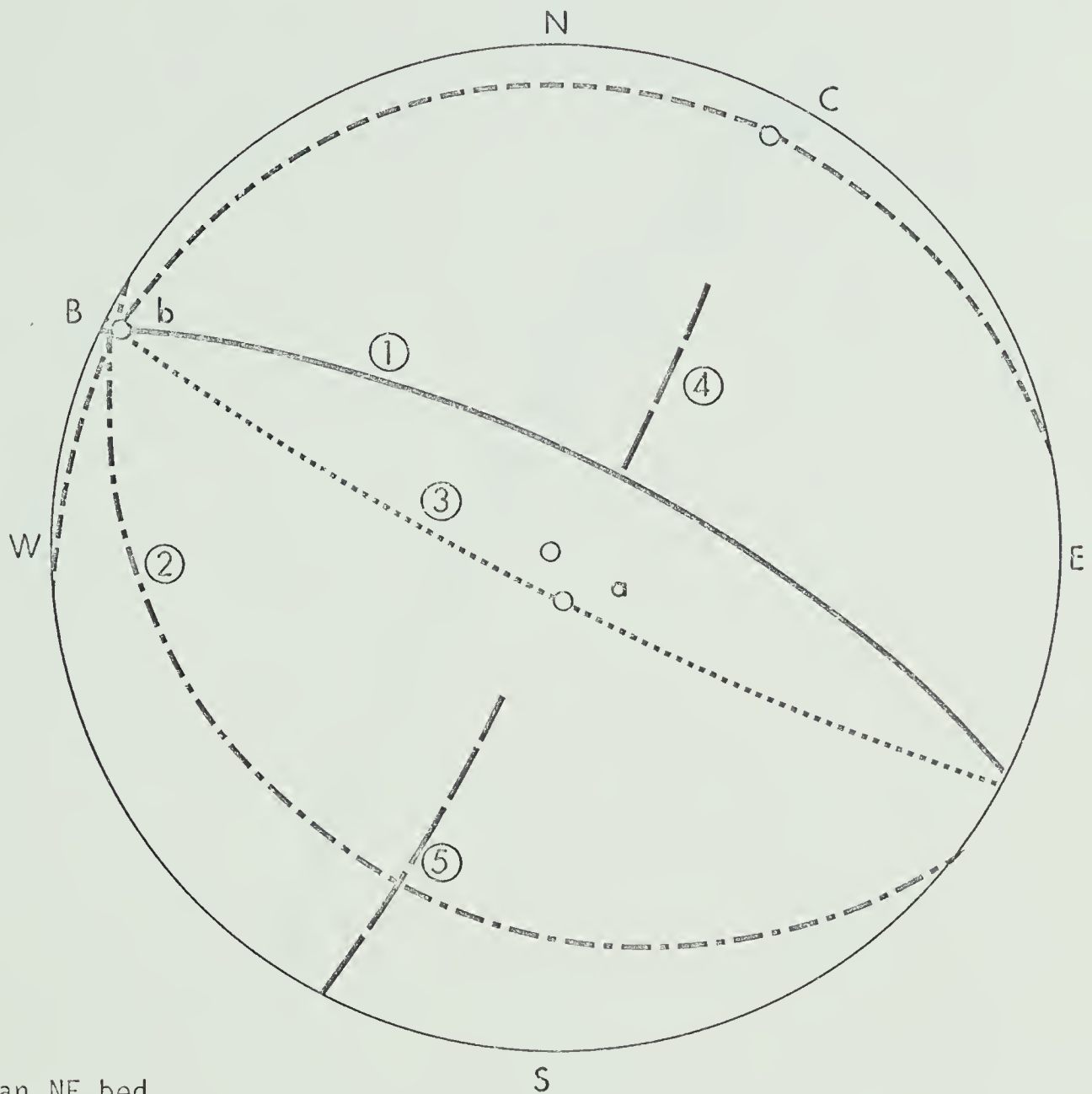
4 + 5 = East Swiftwater Subzone Central Zone

6 = Emperor Subzone

7 = Eastern Structural Zone

Figure 2

Fold Synopsis - Bedding Total



1) Mean NE bed

2) Mean SW bed

4) Poles to SW beds

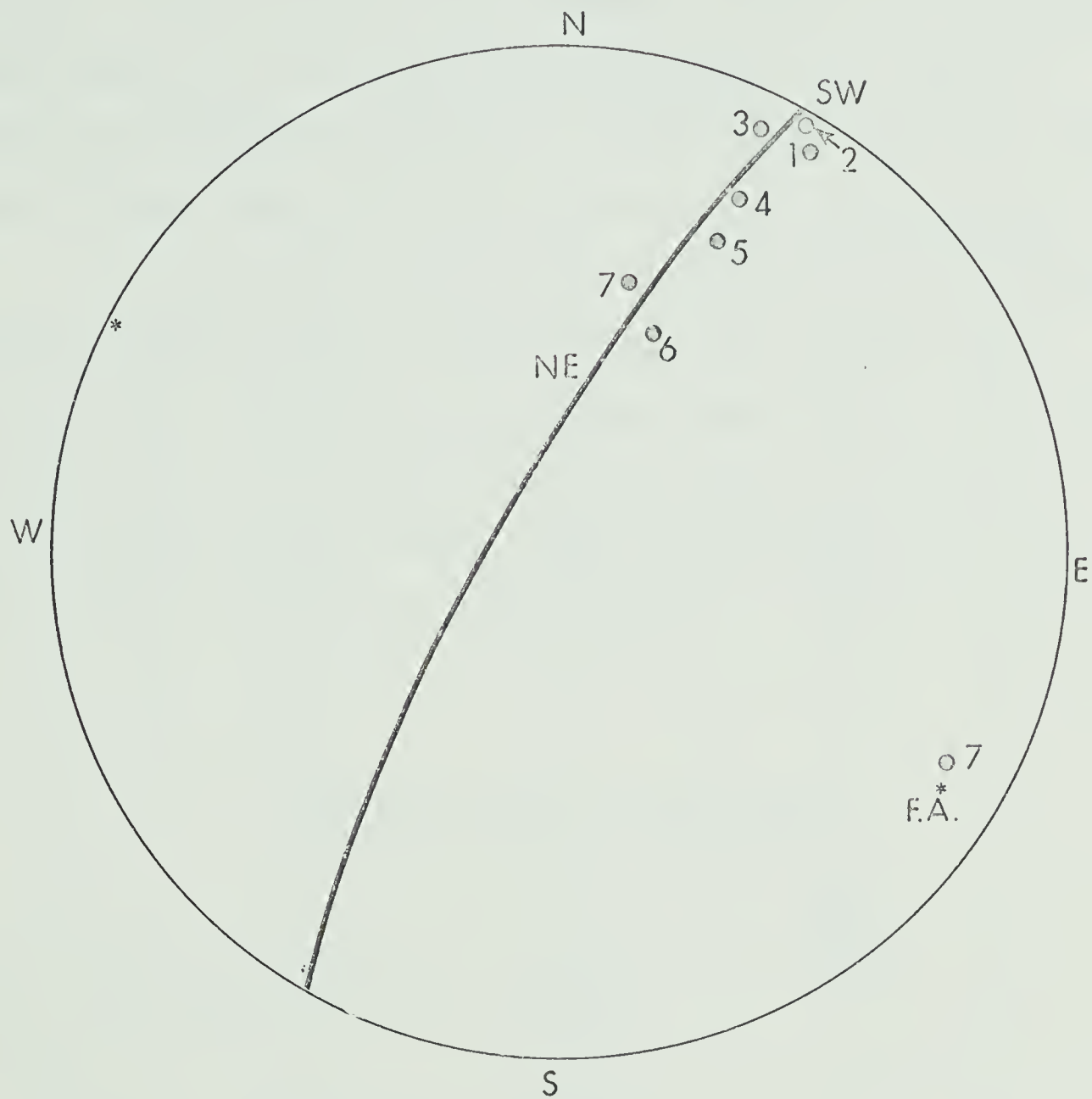
5) Poles to NE beds

Apical Angle -21°

3) Mean Schistosity
Axial Plane

FIGURE 3

Schistosity Pole Maxima in Grouped Domains from SW — NE



Axial Plunge

* = $118^{\circ}-10^{\circ}-(NE)$

= $298^{\circ}-3^{\circ}-(SW)$

plunging fold-axes as one progresses towards the NE, and within the Eastern Structural Zone they predominate.

The trend of the fold axis across the map-area is remarkably constant. Folds plunge at a shallow angle to the NW, at an angle of approximately 10° in the Western and West Central Zones, with an increasing incidence of anomalous SE plunging folds. NE of the axial trace of Robson Ranch anticline the regional plunge is to the SE.

The trends and plunges of folds as calculated from schistosity-bedding intercepts, (1) calculated directly, and (2) derived from lineations on a single plane, were plotted separately on an equal area stereonet. The fold axes have a remarkably constant orientation as calculated using the two methods. Both show pronounced WNW plunging maxima, with a significant pole group plunging in the reverse direction, ESE.

Trend and Plunge of Minor Folds

			WNW
(1)	208 LIN derived Axis	= $301^{\circ}-2^{\circ}$	Maxima
(2)	138 PLUN derived Axis	= $300^{\circ}-6^{\circ}$	
<hr/>		<hr/>	
346	Total Axis	= $299^{\circ}-5^{\circ}$	

The indirect bedding-schistosity intercept value appears to be as reliable as the directly measured lineation of one plane on another.

TABLE 3

Mean Trend and Plunge of Fold Axes

within Subdomains 1-25

The precision parameter is defined in Fisher (1953)

	#	WNW	#	ESE	#	Total Mean	Precision Parameter
1	* 5	296-2	3	125-3	8	212-0	471
2	* 16	303-12	1	118-3	17	303-11	192
3	# 16	303-10	1	126-5	17	303-9	121
4	* 11	298-16	3	121-3	14	297-12	45
5	# 13	297-14	4	124-2	17	296-10	40
6	# 12	300-14	-	-	12	300-14	243
7	# 13	298-8	2	122-5	15	298-7	191
8	# 15	300-10	1	130-4	16	300-9	211
9	# 6	299-5	2	119-1	8	300-4	263
10	# 45	299-11	12	119-7	57	298-7	75
11	# 6	294-10	1	131-6	7	292-8	131
12	# 27	295-12	6	121-5	33	294-9	110
13	# 13	293-7	2	109-2	15	293-6	169
14	# 18	284-10	6	118-3	24	283-7	76
15	# 5	298-9	-	-	5	298-9	253
16	+ 3	290-5	4	125-17	7	129-8	38
17	# 2	312-10	2	119-2	4	315-4	73
18	+ 2	288-3	7	116-13	9	117-10	85
19	+ 2	303-3	13	119-13	15	119-11	111
20	° 3	288-8	9	123-14	12	127-9	26
21	° -	-	9	113-15	9	113-15	125
22	° -	-	9	111-14	9	111-14	122
23	° 2	292-7	8	107-24	10	106-18	13
24	° 2	289-8	1	105-19	3	82-1	26
25	+ -	-	-	-	-	-	-

* Western Zone subdomains

° Eastern Zone subdomains

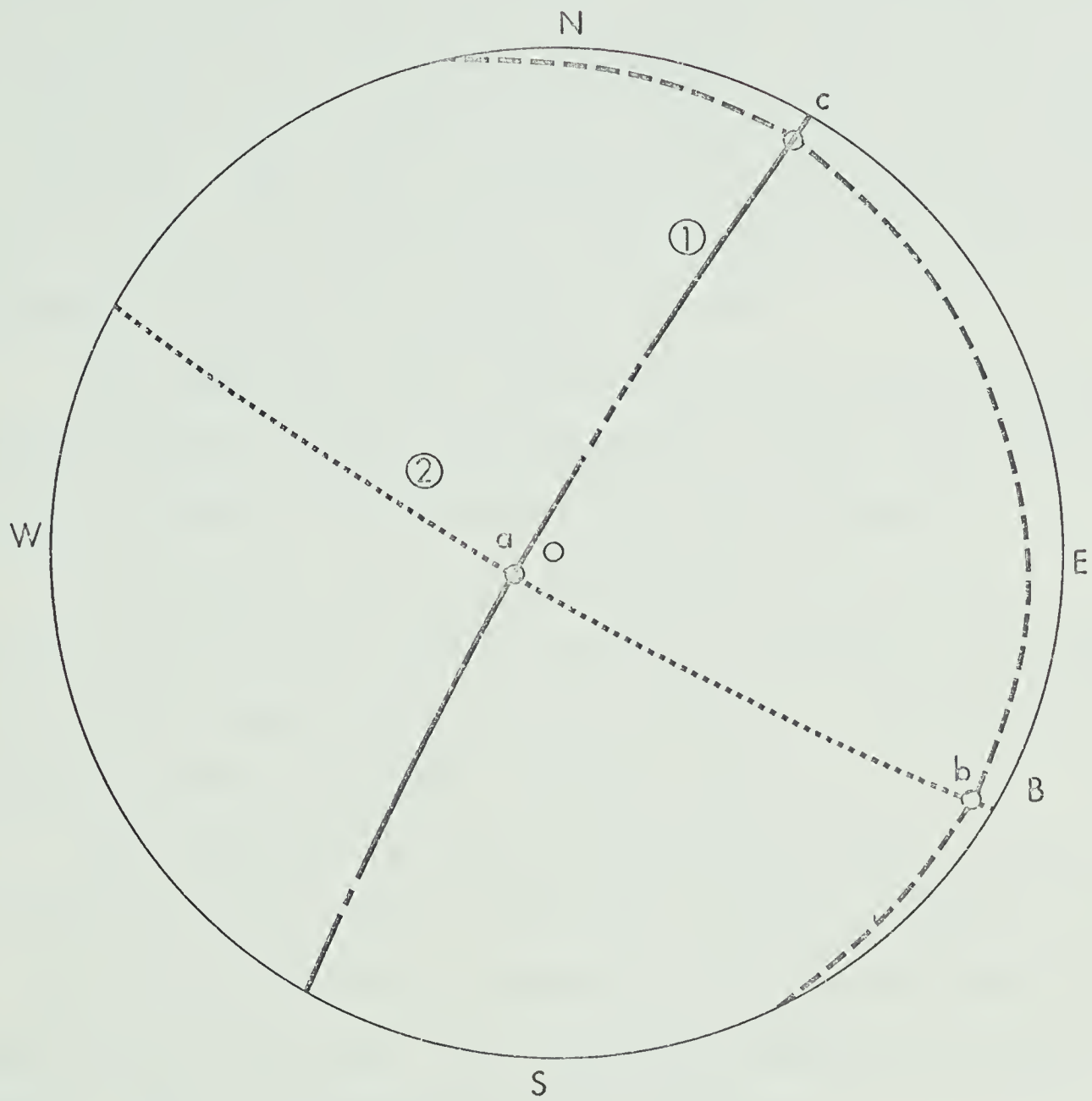
Central Zone Swiftwater and Rearguard Subdivisions

+ Central Zone Emperor Subdivision

Figure 4

Fold Synopsis

Total Schistosity



1) SW schistosity Poles

2) Mean schistosity

F₂ Folds

The crenulations or F₂ microfolds are best developed on S₂ surfaces in the vicinity of the Trench. The trend and plunge of the mean F₂ fold-axes are 108° and 70°, respectively. The microfolds are post-metamorphic, late-tectonic, and are "buckle folds" distorting the S₂ schistosity. They tend to be symmetrical and of limited areal extent (Plate III, #6). The microfolds are locally asymmetrical, with shallow southeasterly limbs, on northeast-facing S₂ planes.

The crenulations would indicate compression and possibly slip movement along the S₂ plane, the northeasterly, Central Zone, moving relatively northwest, and the Western Zone moving southeast.

In the Western Zone where bedding and schistosity S₂ are parallel to the F₂ axis orientation and the S₃ orientation can be shown to be related to the original F₁ and S₂ orientation. Orientations taken from one such outcrop are shown in Figure 5 and Plate III, #6.

The average pitch of the F₂ crenulation microfolds on the original S₂ schistosity faces, which are essentially parallel to bedding, is 70° SE. This is very close to being parallel to the F₁ axial planes and normal to the F₁ fold-axes. This relationship appears to be fairly general. Kinks on S₂ plunge in the same direction

The principal stress-axis orientation postulated for F₁ and F₂ folding in domain 2 are shown in Figure 5. The following angular relationships may be observed on this diagram: $\delta_1 \wedge \delta_1' = 45^\circ$, $\delta_2 \wedge \delta_3' = 45^\circ$, and $\delta_3 \wedge \delta_2 = 0^\circ$.

δ_1 , δ_1' , δ_2 , δ_3' all lie in the same plane which has a dip and strike of 16°-20°W. After the main orogenic event there was a

rotation of 45° in the plane 16° - 20° W, a reversal of the δ_2 and δ_3 positions, and the instigation of a "strike-slip" type of stress axis orientation. The axes δ_1' , δ_2' , δ_3' might be expected to cause faulting or movement about one of the two planes shown, symmetrical about the δ_1' , δ_2' plane. These two planes, orientated 47° - 72° NE, and 106° - 90° do not in fact define the limits of the Rocky Mountain Trench, but the 106° - 90° plane does parallel the break through channel taken by the Fraser River from Rearguard through to the Trench; no faults are known but it may well be a zone of weakness.

The S_3 schistosity and F_2 folds thus relate to a period of potential strike slip faulting, subparallel to the Rocky Mountain Trench.

Structural Assessment

A. Brown (1967) undertook a mesoscopic-scale structural fabric analysis in the McBride map area, to the northeast of the present study area. His findings which relate to a regional assessment both sides of the Trench are summarised thus:

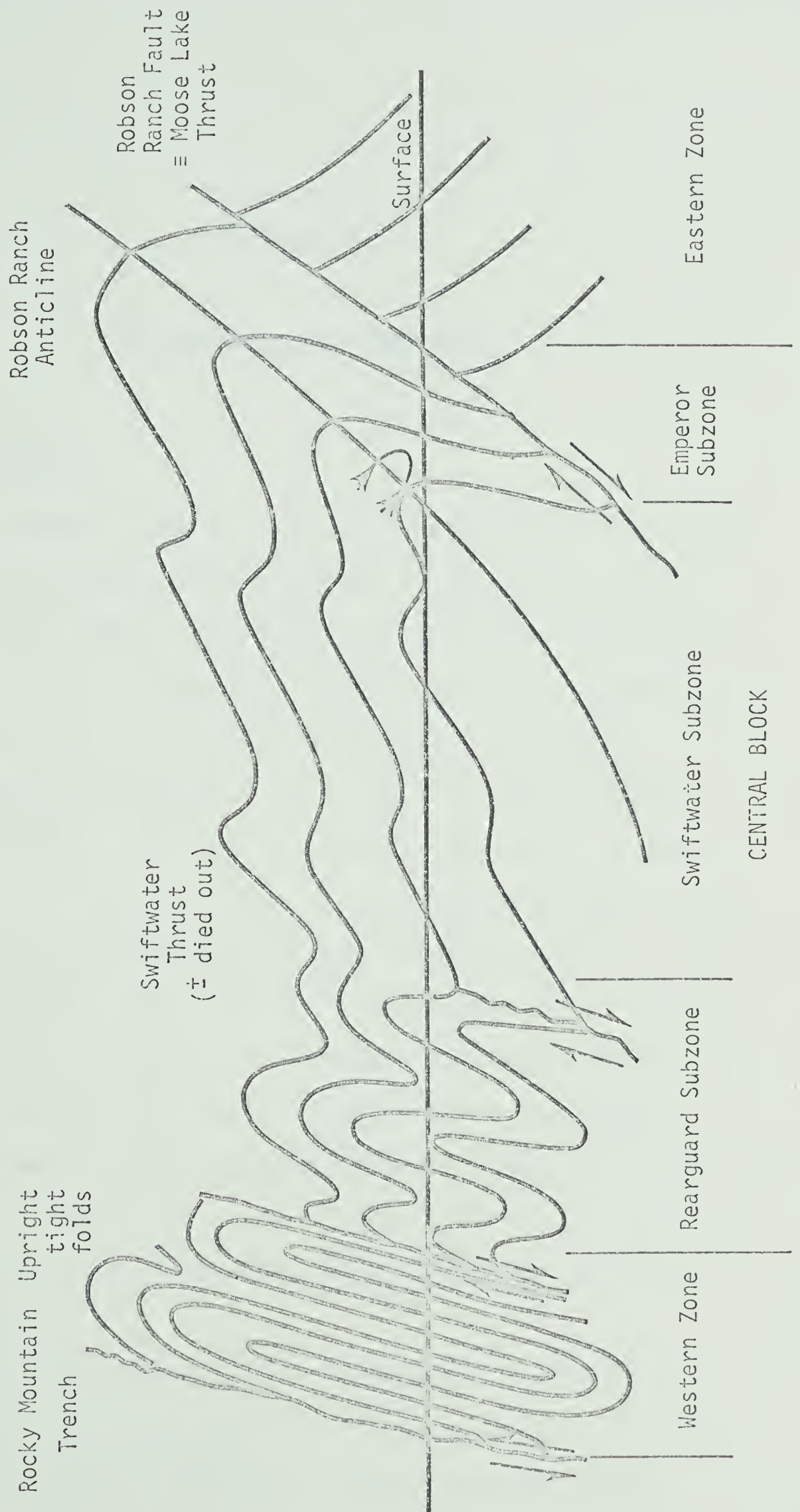
"In the southern two-thirds of the map-sheet an early slip folding (F_1), on a west northwesterly axis, has been rotated by a later composite folding (F_2) on a northwesterly axis; a third set of folds (F_3), generated by movement on a plane perpendicular to the F_2 axis, is thought to be due to squeezing and extension of the rocks due to differential uplift on the F_2 axis. The F_1 folding has a very local distribution, even in areas where it is most commonly observed."

By correlation with the structures in the present map area, the F_3 described by Brown would appear to relate to the crenulation folding, F_2 , defined for Mount Robson. Similarly his F_2 "composite" folds correlate with the here defined F_1 folds, although their orientation is to the west northwest. The early "slip folding" of Brown may equate with the early period of S_1 schistosity development at Mount Robson, in which case there may be an early F_0 period of folding in the map area, which is now obliterated by the subsequent events.

Campbell (1967) notes that folds equivalent to the F_1 at Mount Robson plunge to the northwest, and have a northeasterly dipping axial schistosity. These apparently steepen to vertical tight isoclines in the vicinity of the Trench, and overturn producing a southwesterly dipping schistosity northeast of the Trench. The section examined at Mount Robson is thus the northeasterly limb of an anticlinorium, integrally related to the structural style of the Cariboo Mountains (Fig. 6).

Figure 6

Schematic View of the Section between Mount Robson and Tête Jaune Cache



Chapter VI

METAMORPHISM AND PETROGRAPHY

Metamorphic Setting

The sedimentary rocks in the map area show signs of increased deformation and metamorphism from northeast to southwest. In the Eastern Structural Zone, and the Emperor and Swiftwater subdivisions of the Central block, the sediments belong to the chlorite grade of regional metamorphism. The incoming of biotite as a prograde regional metamorphic indicator occurs in the more highly deformed Rearguard subdivision. The biotite isograd is defined by the formation of biotite in rocks of greywacke composition, and appears to be a function of the rock chemistry and phase content, as well as of increased metamorphic grade. In argillaceous sandstones and pelitic units the isograd is a function of the whole-rock Al/Mg and Fe ratio, and cannot be defined in the field. Particularly Al-rich pelitic units, such as Unit B, remain below the "biotite isograd" (for their particular bulk chemistry) until well into the Western Structural Zone. The nature of the isograd will be discussed more fully elsewhere (p. 153).

The chlorite grade mineralogy is syntectonic with biotite formation late to post syntectonic. The formation of biotite at the expense of the original, schistosity-orientated chlorite grade

mineralogy generated a porphyroblastic biotite and chlorite pair which is only weakly subparallel to the original muscovite defined schistosity. This would suggest a late to post tectonic metamorphic event.

In some of the biotite-bearing phyllites of the Western Structural Zone the biotite-muscovite-chlorite assemblage is undoubtedly syntectonic. Either movement continued late in the Western Structural Zone, or else biotite formation was initiated early. The latter would perhaps seem to be more likely.

The high clay fraction has a pronounced effect on the physical properties of the rock (Charlesworth et al. 1967). Clay and/or metamorphic mica is usually sufficient to isolate individual clasts of quartz and feldspar, and acts as a 'lubricant' during deformation. This gives the rocks increased ductility during deformation, and inhibits the destruction of individual clasts. This itself may have important implications during low-grade regional metamorphism.

Metamorphism is thought to have been associated with the emplacement of the Shuswap metamorphic complex in the Cariboo Mountains. This in turn is thought to represent one stage in the northeasterly tectonic movement of material out of the Cordilleran Geosyncline onto the North American Craton. Tectonic readjustments of isotherms is consistent with post tectonic metamorphism in the lower metamorphic grades.

The age of metamorphism would appear to be late Cretaceous or early Tertiary. A K^{40}/Ar^{40} radiometric age on a phyllite taken by Weiner (1966) from the biotite grade of regional metamorphism, near the Trench at Tête Jaune Cache, yielded an age of 69 m.y. This date is the nearest to complete updating known at present.

Petrography

The rocks at Mount Robson may be classified in both sedimentary and metamorphic terms. The transition from relatively unaltered sediment in the northeast, to more highly deformed metasediments in the vicinity of the Trench, involved progressive recrystallization of the original mineralogy, and the imprinting of a fabric orientation. In the northeast where the chlorite grade sediments are comparatively undeformed the detrital grain outlines remain distinct (Plate IV #1) and the argillaceous material in shales, siltstones and sandstones is recrystallised to a chlorite-phengitic muscovite assemblage, with only a trace of fabric orientation in the finer grained sediments.

The effect of progressive metamorphism across the area has been to break down the primary clastic grain outlines, recrystallise the chlorite grade matrix mineralogy, and generate a biotite grade mineralogy. The sedimentary lithology is discernable throughout, largely because of the resistant and inert nature of the larger grains of quartz and feldspar. These remain suspended in a mica rich matrix, which reacts around them.

In Unit F argillite has recrystallised to slate with a fine aggregate of intimately intermixed chlorite, and phengitic muscovite. Randomly orientated blades of chloritoid may be superimposed on this assemblage, where the rocks are of suitable composition. Poikiloblastic porphyroblasts of sideritic carbonate are thought to predate the chlorite grade mineralogy orientation, although whether they are pre or early chlorite grade metamorphism is not known. They also occur in fine arenaceous sediments, and enclose fine detrital sand grains.

The incipient schistosity found in the Eastern Zone becomes a

pronounced slaty cleavage in Unit B below Emperor Station, and a well defined phyllitic schist southwest of Morey Station. With increase in metamorphic grade sedimentary features in argillaceous beds become indistinct. Two schistotities are commonly found in the Central Zone. The original chlorite grade mineralogy, with chloritoid porphyroblasts superimposed defines the S_1 schistosity. The S_1 schistosity is kinked and rotation has occurred into the S_2 schistosity plane. The early carbonate, and the later chloritoid porphyroblasts have both been rotated into the new schistosity. In the southwest, phyllitic schists are markedly coarser grained, and there is much evidence for shearing and "flowage" along the S_2 schistosity.

The transition from slate to phyllitic schist is accompanied by a coarsening of individual mica grain sizes, and a separation into distinct phases. Intergrowths of phengitic-muscovite and chlorite are not common in the higher metamorphic grades. The chlorite-phengitic muscovite assemblage continues well into the biotite zone.

In arenaceous rocks the larger quartz and feldspar grains become strained, and elongate in the plane of the S_2 schistosity, parallel to the F_1 fold axis. This tendency is hardly noticeable in the northeast; however, it becomes very evident in the western part of the map-area. The quartz grains are also flattened into the S_2 plane by pressure solution, and appear to have elongated by quartz accretion along the grain axis parallel to the F_1 fold axis. The quartz grains in the Western Zone, in particular those associated with a conglomeratic horizon in Unit A may become extremely elongated by this method (Plate II #7). Grains of feldspar are deformed by stress alone, and shatter rather than grow by accretion. There is a marked modal reduction in fine quartz and feldspar

with grade increase, and a corresponding increase in mica content. Detrital outlines become blurred and the sediments become schistose.

At low metamorphic grades the chlorite-phengitic-muscovite assemblage is mixed, with books of mica consisting of interleaved chlorite and phengite (Plate IV #1). This feature, characteristic of low grades, is gradually lost by recrystallisation of the two phases. The common origin of the two phases is thus evident. Both chlorite and phengite help define the S_2 schistosity plane until the onset of biotite formation in the southwest.

In rocks bearing microcline the formation of biotite totally removes the chlorite phase, and porphyroblasts of biotite, only weakly orientated parallel to S_2 coexist with the strongly orientated phengitic muscovite. In rocks free of microcline, in which biotite and chlorite porphyroblasts have been generated either parallel or weakly subparallel to the S_2 schistosity, all the early chlorite phase is lost, and phengitic muscovite alone defines the S_2 plane.

The sideritic carbonate noted earlier is bedding controlled, it would appear to recrystallise with increase in metamorphic grade, although it retains its inner poikiloblastic core (Plate IV, #7). The new carbonate is noticeably less rusty, and is found to be ankerite. In the chlorite grade assemblage the original carbonate may be seen to be replaced by a younger phase. In the biotite zone this has gone to completion. Large "augen" of carbonate elongated parallel to the schistosity, with a core of poikiloblastically enclosed quartz grains, and pressure shadows of quartz are characteristic of the more highly deformed biotite grade argillaceous sandstones. The "augen" are enveloped by chlorite and biotite, and only rarely does muscovite come in contact with the

carbonate phase (Plate IV, #6).

Detrital grains of feldspar retain their identity in all but the most schistose sandstones. The feldspar is albite in all but a few conglomeritic feldspar-rich horizons. The great predominance of albite in the relatively unaltered sediments in the northeast is inconsistent with the postulated source area, and a period of post depositional ionic diffusion at the onset of chlorite grade metamorphic conditions is thought to have converted detrital clasts of plagioclase and microcline into an albite detrital "pseudomorph". This process is touched on elsewhere. Albite from a plagioclase host may retain the original polysynthetic twinning, or else it may develop the characteristic chessboard pattern, noted by workers at Jasper. Carbonate is often found to be associated with these albites, and microlites of white mica are found in the cores of some "detrital" albites thought to have been derived from a potash feldspar source. Both microcline and plagioclase may give rise to chessboard albite. The chessboard pattern is found within the biotite metamorphic grade, although in highly schistose grits where detrital outlines are lost, albite generally appears to be optically structureless.

Chapter VII

GEOCHEMISTRY AND MINERALOGY

Samples

A suite of eight Middle Miette Group samples were collected during a two mile traverse along the lower of the two Canadian National Railway Lines, between Rearguard Station and the Level Crossing at Tête Jaune Cache. Samples #1-4 were taken within the "Central" Structural Zone, in an area of relatively minor structural deformation. Samples # 5-8 come from within the "Western" Structural Zone, where deformation is much more evident. An overall metamorphic grade increase might be expected from Sample # 1 in the northeast, to Sample # 8 in the southwest; also, a small grade increase might be anticipated between Samples # 4-5 (Map 4).

The samples fall in the "biotite-muscovite-chlorite-quartz-albite" subfacies of the green schist facies of prograde regional metamorphism.

The sampling traverse starts above the biotite isograd, as defined for rocks of greywacke composition, and extends towards the eastern limit of Miette Group outcrop. The traverse is essentially perpendicular to the biotite isograd, in terms of the regional geology. The eight samples analysed range in composition from argillite to quartz pebble conglomerate. They were picked for their varied lithology, and with the exception of Sample # 8, a calcareous schist, all fall within

a lithologic series based on the relative proportions of clay matrix and quartz clast content.

Samples #4, 3, 7, are phyllitic, and contain little free detrital quartz, they are true meta-argillites, whereas Samples #1, 5, 6, 2, are progressively more quartzose.

The main purpose of this part of the study, which included the determination of whole-rock chemical analyses by classical wet chemical methods, and the chemical analyses of coexisting mineral phases by means of the Electron Microprobe, was to examine the rocks in the light of an "equilibrium" assemblage.

If one accepts that the basic mineralogy is compositionally controlled, then within a given assemblage there is still the potential for "buffering" due to physical and chemical considerations, such as temperature, pressure and fugacity.

Whole-rock Chemistry

The bulk chemistry of any rock is dependent on the proportions of its constituents. In Samples #1-7 the sediment consisted of varying proportions of pebble and sand sized grains of detrital quartz and feldspar, mixed with remnant ferromagnesian minerals, and set in a matrix of one or more clay minerals. To these one should add sulphides, oxides, and relatively inert heavy minerals as minor constituents.

Any sample thus has an extremely wide range of possible composition, and in any rock series the bulk rock compositions will depend on the most important variables in the system. As previously stated Samples #1-7 show an inverse relation between detrital quartz, plus feldspar, and clay matrix. The chemical effect of this is shown in Table 4, 5, and Figures 7, 8.

In Table 4 the chemical analyses are listed in order of decreasing Si content. The oxide percentages of Al, Fe, Mg, K, Ti, increase with clay content at the expense of Si. Both Ca and Na tend to decrease along with Si, although the total alkali content rises markedly with increase in clay content. The content of Mn appears to remain constant throughout.

Figures 7, 8 bring out the systematic nature of the inverse relationship. The distribution of Al, Si, and FeMgMnTi components are plotted in Figure 8. It would appear that the Al/Mg + Fe ratio of the rock increases as the clay content rises, and the free quartz content drops. Sample # 7, which is a phyllite which probably contained little free quartz, thus has a markedly higher Al/Mg + Fe ratio than Sample # 2, a highly quartzose pebble conglomerate.

TABLE 4

Whole-Rock Chemical Analyses

	2	6	5	1	4 [*]	3	7	8 [*]
SiO ₂	78.18	75.40	67.91	64.90	61.06	58.56	48.84	34.99
TiO ₂	0.23	0.42	0.58	0.85	0.82	0.96	1.17	0.38
Al ₂ O ₃	8.94	10.91	14.50	15.42	17.20	18.52	22.80	8.95
Fe ₂ O ₃	0.71	0.23	0.75	1.13	1.54	1.43	3.09	1.12
FeO	2.34	2.75	3.02	5.06	5.60	5.51	5.12	1.97
MnO	0.06	0.06	0.07	0.04	0.07	0.09	0.08	0.18
MgO	0.94	1.25	1.24	2.12	2.08	2.19	3.12	1.86
CaO	1.98	1.14	1.72	0.53	0.02	0.65	1.15	24.65
Na ₂ O	1.30	1.79	2.42	0.92	0.48	1.69	0.68	0.46
K ₂ O	1.48	2.89	3.32	5.46	5.60	4.96	8.00	2.40
H ₂ O ⁻	0.09	0.10	0.08	0.04	0.18	0.05	0.13	0.15
H ₂ O ⁺	1.68	1.42	1.93	2.42	3.06	2.65	4.09	1.34
P ₂ O ₅	0.61	0.14	0.14	0.11	0.10	0.10	0.25	0.27
CO ₂	1.90	1.87	2.32	0.84	1.93	2.96	1.59	21.47
S					0.21			
	100.44	100.39	100.00	99.85	99.87	100.22	100.11	100.19
Oxidation Ratio	37.76	14.33	33.18	30.83	35.48	34.69	54.69	53.20

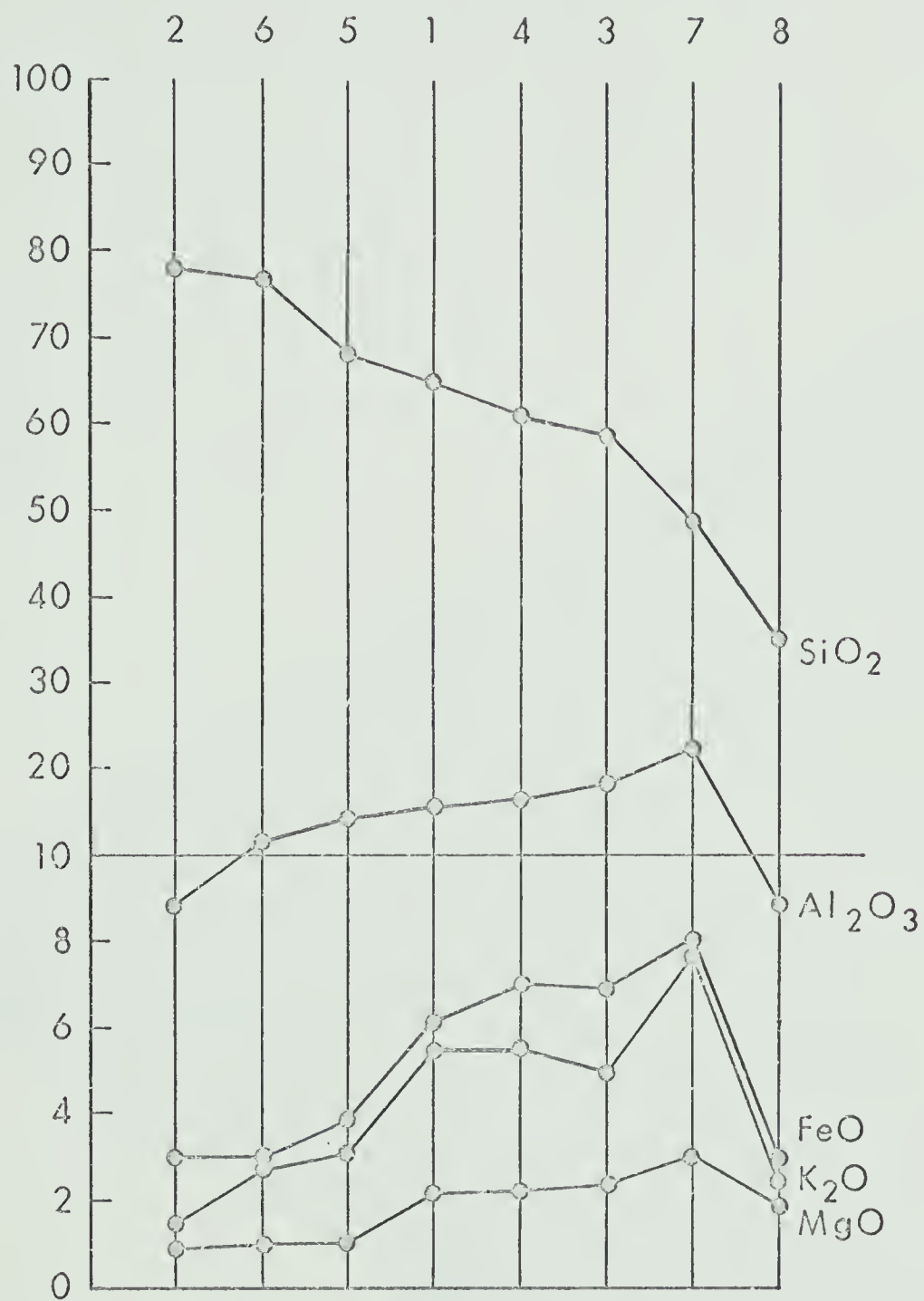
* Analyses by A. Stelmach, Department of Geology, University of Alberta, 1970

TABLE 5

Whole-Rock Chemical Analyses

	1	2	3	4	5	6	7	8
SiO ₂	64.90	78.18	58.56	61.06	67.91	75.40	48.84	34.99
TiO ₂	0.85	0.23	0.96	0.82	0.58	0.42	1.17	0.38
Al ₂ O ₃	15.42	8.94	18.52	17.20	14.50	10.91	22.80	8.95
Fe ₂ O ₃	1.13	0.71	1.43	1.54	0.75	0.23	3.09	1.12
FeO	5.07	2.34	5.51	5.60	3.02	2.75	5.12	1.97
MnO	0.04	0.06	0.09	0.07	0.07	0.06	0.08	0.18
MgO	2.12	0.94	2.19	2.09	1.24	1.25	3.12	1.86
CaO	0.53	1.98	0.65	0.02	1.72	1.14	1.15	24.65
Na ₂ O	0.92	1.30	1.69	0.48	2.42	1.79	0.68	0.46
K ₂ O	5.46	1.48	4.96	5.60	3.32	2.89	8.00	2.40
H ₂ O ⁻	0.04	0.09	0.05	0.18	0.08	0.10	0.13	0.15
H ₂ O ⁺	2.42	1.68	2.65	3.06	1.93	1.42	4.09	1.34
P ₂ O ₅	0.11	0.61	0.10	0.10	0.14	0.14	0.25	0.27
CO ₂	0.84	1.90	2.96	1.93	2.32	1.87	1.59	21.47
S				0.21				
				S=0				
	99.85	100.44	100.22	99.87	100.00	100.39	100.11	100.19
Mg/Mg+Fe	.3852	.3621	.3669	.6504	.3767	.4315	.4155	.5099
Al/Mg+Fe	1.0867	1.3335	1.2035	1.1157	1.7081	1.4727	1.1665	0.9829

Figure 7

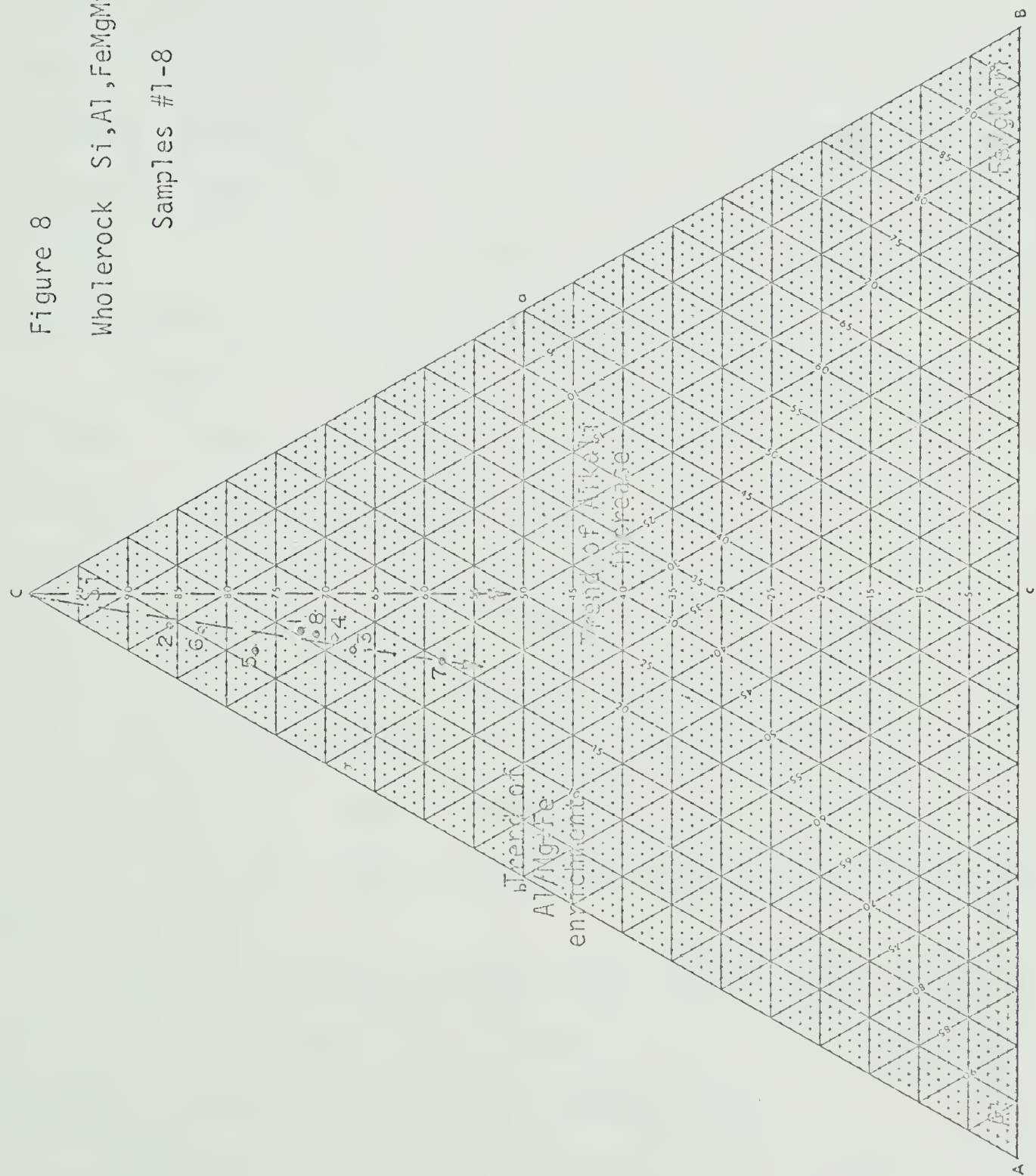


Whole-rock Chemical Distribution of
Major Elements
Samples #1-8

Figure 8

Whole-rock Si, Al, FeMgMnTi Plot

Samples #1-8



The same trend is followed by the total alkali content, which increases in proportion to the clay content of Samples #1-7. Sample #8 is a calc-argillite, and thus has an anomalously high Ca content. Interestingly enough the clay component contains the same proportions of Si, Al, FeMgMnTi as the more phyllitic Samples #1, 3, 4.

The systematic, almost linear relationship found between quartz-rich and quartz-poor samples in Figure 8 is confused by the presence of feldspar in the original detrital material. The presence of feldspar in the coarser sediments, Samples #2, 6, 5, must increase the Al/Mg + Fe ratio of the rock, which will thus deviate from the "ideal" clay mineralogy Al/Mg + Fe ratio. This deviation should itself decrease with the feldspar content of the more argillaceous sediments.

In Figure 9 oxide percentages of Al, plotted against KNaCa and FeMgTi illustrate the remarkably restricted field of the clay mineralogy, in terms of these end members. The spread of points is towards the compositional limits of feldspar. The more argillaceous Samples #1, 3, 4, 7, and Sample #2, which, although a conglomerate, has little feldspar, plot within the compositional range of the clay mineral illite. The distribution appears to bear little relationship to the smectite compositional range, also plotted on the same figure, and feldspar contamination alone can account for the apparent spread in clay matrix composition.

The "average pelite" of Shaw (1956) plotted on the same figure falls close to the composition of Sample #7, and differs little from the clay matrix compositions found in the present study.

Sample #3 in Table 6 correlates well with a standard illite analysis quoted by Deer, Howie and Zussman (1962), and also the "average

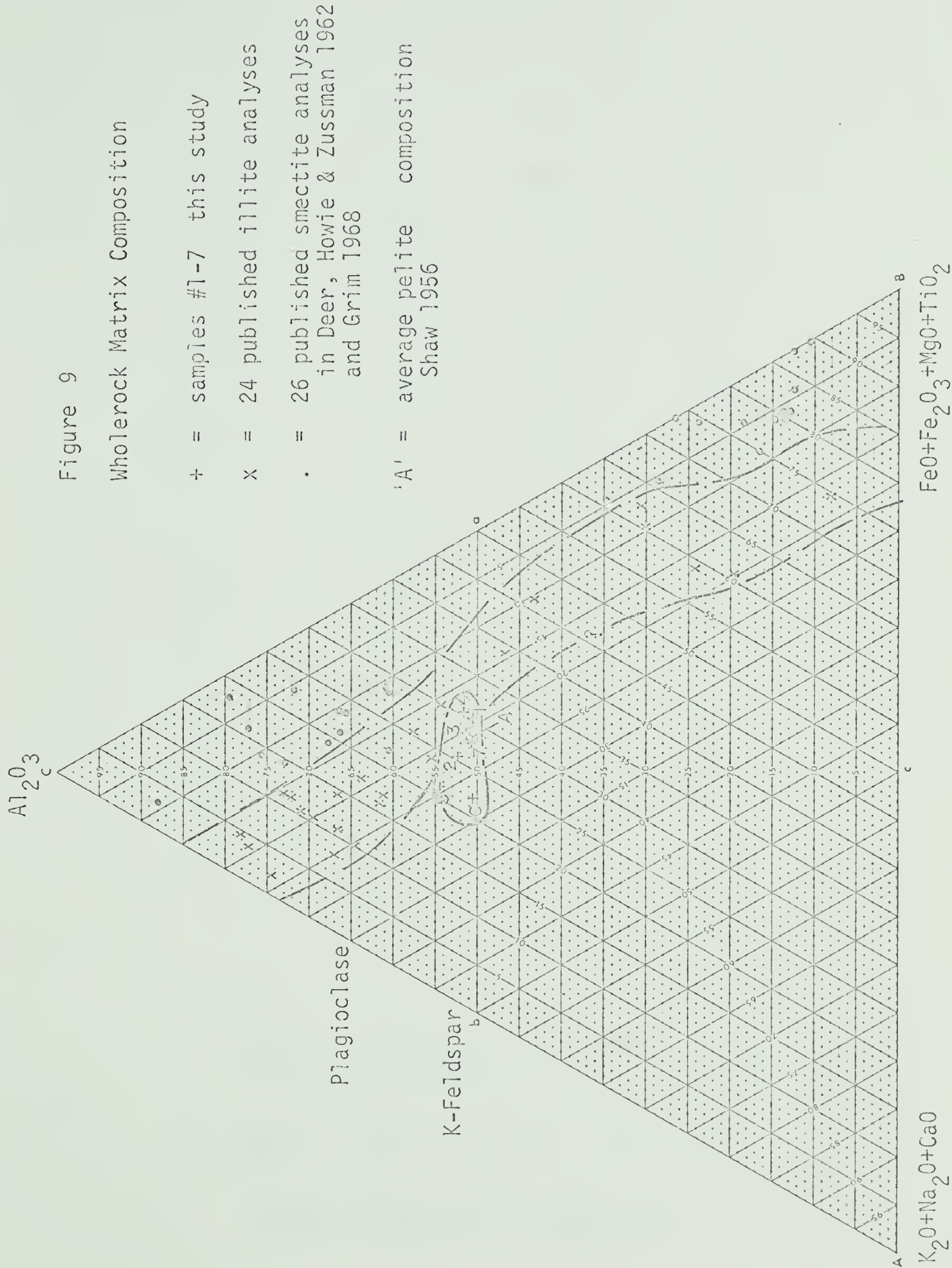


TABLE 6

	A	B	C
SiO_2	61.54	58.56	56.91
TiO_2	0.82	0.96	0.81
Al_2O_3	16.95	18.52	18.50
Fe_2O_3	2.36	1.43	4.99
FeO	3.90	5.51	0.26
MnO	-	0.09	-
MgO	2.52	2.19	2.07
CaO	1.76	0.65	1.59
Na_2O	1.84	1.69	0.43
K_2O	3.45	4.96	5.10
H_2O^+	3.47	2.65	5.98
H_2O^-	-	0.05	2.86
P_2O_5	-	0.10	-
CO_2	1.67	2.96	-
	100.28	100.22	99.50

A = Average composition of 129 "pelitic" rocks
Shaw, D.M. (1956)

B = Sample #3 Tête Jaune Cache - this study

C = Illite, Fithian Illinois (Kerr et al. 1950)
in Deer, Howie and Zussman, 1962

pelite" analysis given by Shaw.

Illite on deposition tends to be oxidised and the $\text{Fe}^{++}/\text{Fe}^{+++}$ ratio has obviously been affected by a redox reaction, altering it to the reduced state. The amount of reduction is in fact large compared with the "average pelite". Albite present in Sample #3 will account for the slight excess of Na over that of true illite.

Within the above framework it is possible to detect certain chemical characteristics, peculiar to individual samples or groups of samples, which reflect the nature of the original sediment.

Samples #2, 6, 5, are quartz-rich, coarse, and have a high Al/Mg + Fe ratio. Sample #2 is low in alkali content and relatively feldspar free, whereas Samples #6, 5 are comparatively rich in Ca and Na, a function of plagioclase content.

Samples #1, 8, 4, 3 are less siliceous, and petrographically contain little or no feldspar. They have a lower Al/Mg + Fe ratio, which tends to increase with Si decrease.

Sample #8, the calcareous schist, is very low in Na and K, and very high in Ca.

Sample #7 is very low in Si. It is, however, very high in Fe, Mg, K.

Other notable occurrences include the exceedingly low Ca content in Sample #4, the high P content of Sample #2 and the low K content of Sample #3. The distribution of Mn would appear to be consistent, and a little low in Sample #1.

Discussion

The roughly linear distribution in Figure 8 indicates that reduction in quartz content is accompanied either by a systematic increase in one clay mineral species, or else a delicate balance of more than one clay mineral. In the light of the obvious similarity of the sediment matrix composition to that of a published illite, in the case of Sample #3, and the illite composition field in Figure 9, it seems reasonable to assume that the clay content was essentially monomineralic, and composed of illite. Illite may itself cover a wide compositional range, and it is interesting to note that the matrix composition closely resembles that of Shaw's "average pelite".

The illite was almost certainly contaminated by ferromagnesian minerals and detrital chlorite and biotite were noted in the sediments at Jasper (Charlesworth et al., 1967). The composition of the clay material at Jasper was also inferred to be illite.

Feldspar is a major contaminant in some of the coarser sandstones. Samples #6, 5 probably reflect this in their high Na and Ca contents. Microcline is less easily detected than plagioclase, as the K increase associated with it is masked by a general increase associated with the clay. A high feldspar content would increase the Al/Mg + Fe ratio of the rock for low levels of Mg and Fe.

In the more argillaceous sediments there would also appear to be a tendency to increase the Al/Mg + Fe ratio with Si decrease. In this case Al substitution for Si in the illite itself may be responsible.

The significance of the detrital sediment may not be restricted to its bulk chemistry. Not only is the presence of feldspar as detrital

clasts important to the distribution of alkali cations, a process discussed later (p.137), but it may also influence the Al/Mg + Fe ratios of the phyllosilicate phases. The effect of "fixing" Al in an albite may serve to reduce the Al readily available for the formation of mica, thus in Sample #5, although the Al content of the rock appears to be normal or high, much is taken up by albite, and the mica is MgFe rich.

The whole-rock analyses were plotted on an A K F diagram, along with the analysed mineral phases (Fig.10). Two samples deviate slightly from their mineralogically defined bulk compositional fields. Sample #2 is probably slightly low in total alkali content, and Sample #8 was not observed to contain chloritoid. In the latter case the rock is inhomogenous, and the composition may be slightly averaged.

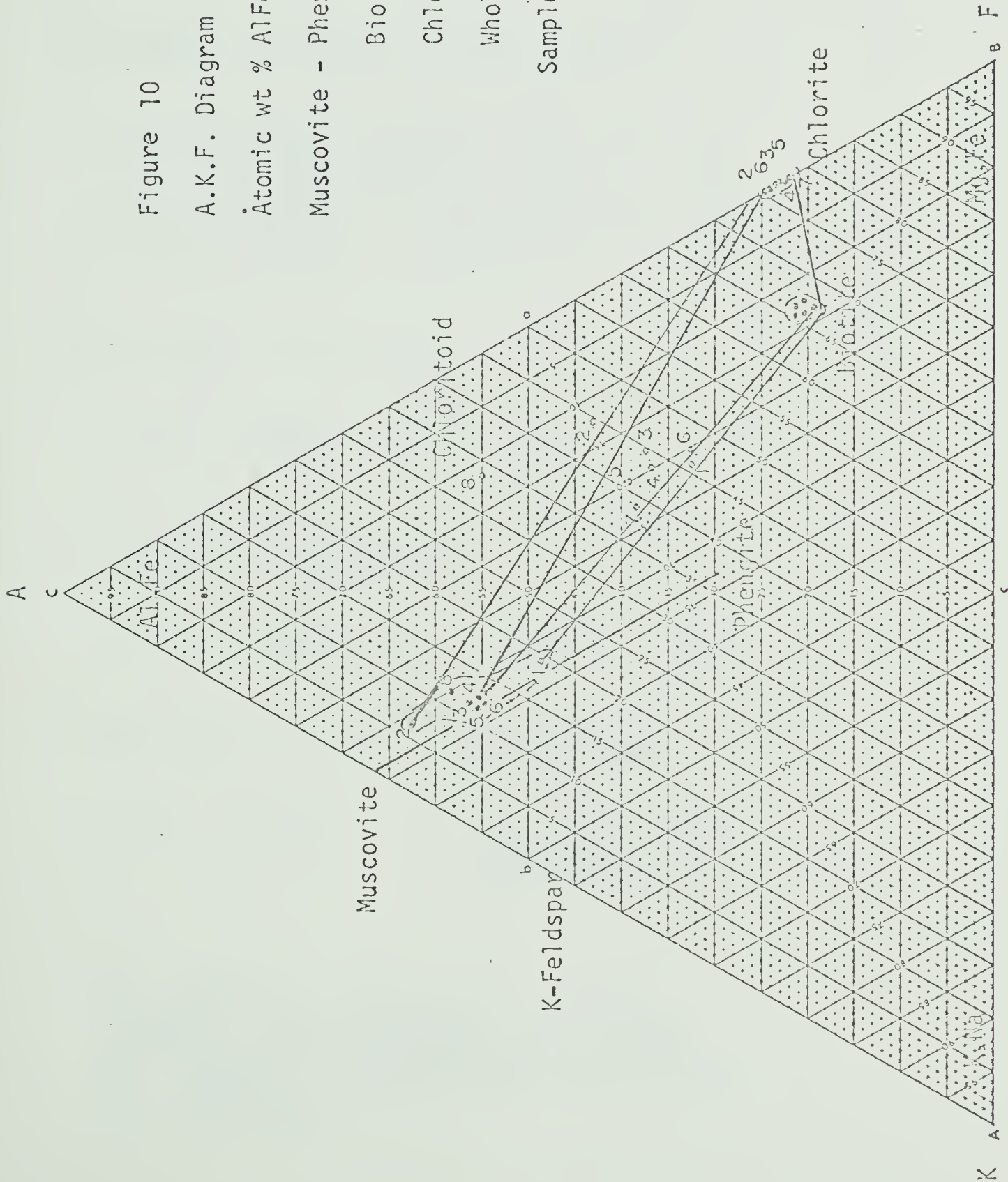


Figure 10

A.K.F. Diagram

Atomic wt % AlFe⁺⁺⁺, K Na, MgFe⁺⁺

Muscovite - Phengite_{ss} Fe as Fe⁺⁺

Biotite_{ss} Fe as Fe⁺⁺

Chlorite_{ss} Fe as Fe⁺⁺

Wholerock Fe as Fe⁺⁺ & Fe⁺⁺⁺

Samples #1-8

TABLE 7
Mineral Assemblages
in relation to an A.K.F. diagram
(Figure 19)

1. Muscovite - biotite - chlorite field

Q, M, C, FeMgCarb, Ab, Bi, Il, Mg, Po	#5
Q, M, C, FeMgCarb, Ab, Bi, - Mg, Py	#6
Q, M, C, FeMgCarb, Ab, Bi, Il, Mg	#3
Q, M, C, FeMgCarb, - Bi, Il, Mg, Po	#4
Q, M, C, FeMgCarb, - Bi, Il, -	#7

2. Muscovite - biotite join

Q, M, -, FeMgCarb, Ab, Bi, Il, Mg	#1
-----------------------------------	----

3. Muscovite - chlorite join

Q, M, C, FeMgCarb, Ab, - Il, Mg	#2
---------------------------------	----

4. Muscovite - chlorite - chloritoid field

Q, M, -, FeMgCarb, - - Hm, CaCarb Rutile, Py	#8
---	----

Q = quartz; M = muscovite; C = chlorite;
FeMgCarb = ankerite/siderite; Ab = albite;
Bi = biotite; Il = ilmenite; Mg = magnetite;
Hm = hematite; CaCarb = calcite; Py = pyrite;
Po = pyrrhotite.

TABLE 8

Muscovite Chemical Analyses

	1	2	3	4	5	6	7	8
SiO ₂	47.00	46.78	46.90	47.27	46.30	45.40	47.55	46.02
TiO ₂	0.71	0.27	0.38	0.36	0.36	0.37	0.40	0.34
Al ₂ O ₃	28.48	34.97	32.35	32.35	31.88	31.31	31.66	32.83
FeO	4.31	1.32	2.33	2.52	2.75	2.65	2.67	2.97
MgO	2.02	0.68	1.39	1.37	1.12	1.35	1.51	0.93
CaO	0.00	0.03	0.00	0.00	0.04	0.01	0.00	0.08
Na ₂ O	0.17	1.16	0.61	0.65	0.67	0.66	0.49	1.75
K ₂ O	10.44	9.22	10.04	10.10	10.27	10.11	9.91	9.12
SrO	0.03	0.04	0.04	0.03	0.04	0.04	0.03	0.06
BaO	0.74	0.70	0.76	0.54	0.91	0.68	0.81	1.11
F	0.22	0.17	0.00	0.11	0.00	0.00	0.00	0.38
H ₂ O	5.23	4.11	4.63	4.43	5.03	6.50	4.43	3.95
	99.35	99.45	98.71	99.44	99.37	99.08	99.46	99.54
Mg/Mg+Fe	.4551	.4797	.5156	.4924	.4209	.4761	.4986	.3587
Al/Mg+Fe	2.6324	9.7167	4.7429	4.5499	4.7307	4.3622	4.1566	5.0000

Muscovite Chemistry

A dioctahedral mica intermediate in composition between true muscovite and phengite is found in all eight of the samples analysed.

The chemical analyses shown in Table 8 and displayed diagrammatically in Figure 10, 20, indicate that there are two muscovites of extreme composition, and a group intermediate between the above in terms of celadonite solid solution and phengite content.

From A.K.F. diagram (Fig. 10) the mica composition varies systematically across the three phase position, from the muscovite-chlorite case with a high Al/Mg + Fe ratio, through the intermediate three-phase muscovite-biotite-chlorite position, to the muscovite biotite join which marks the minimum Al/Mg + Fe ratio found in the analysed muscovite-phengite series.

The muscovites are plotted on a modified A.K.F. diagram (Fig. 20 Winkler 1962). $A = Al_2O_3 - (K_2O + Na_2O)$; $K = K_2O + Na_2O$, and $F = FeO + MgO + TiO_2 + MnO$. They fall close to the muscovite-ferri muscovite join of Butler (1967) and may be grouped distinctly with increase in their Al/Mg + Fe ratios. The analyses are compared to equivalent plots of analysed muscovites on subsequent figures (Butler, 1967; Lambert, 1959; Mather, 1970; Smith, 1963; Guidotti, 1970. Fig. 20, 21, 22).

The muscovite from Sample #8 has a composition similar to that of the main three-phase group of muscovites, although it is anomalous in some respects.

Samples # 1, 2 define the measured end-points between a phengite-rich, and a phengite-poor "muscovite-like" white mica. From Table 8 it is apparent that the first is low in Al, and correspondingly high in

Fe, Mg, and Ti. The whole-rock composition (Fig.10), although similar to that of Sample #6, is low in Al and high in alkalis. In the absence of chlorite the high whole-rock Mg, Fe, Ti must necessarily be reflected in the remaining phases which are thus Al-poor and Mg- Fe- Ti-rich.

Sample #2 at the other extreme has an Al-rich, alkali-poor, whole-rock chemistry, biotite is absent and the coexisting micas are Al-rich and Mg- Fe- Ti-poor.

The above muscovites both have their chemistry controlled by the critical nature of the whole-rock chemistry, which lies outside the main three-phase triangle on an A.K.F. diagram (Fig.10). The width of these critical two-phase bands is not known. The amount of compositional tolerance found in the three-phase muscovites is small, and restricts the range of phengite substitution compatible within each of the two-phase bands.

The normal three-phase muscovites are intermediate between the above in terms of Al/Mg + Fe ratios and plot closely, regardless of a spread of whole-rock values which lie within the three phase field. Samples #3, 4, 5, 6, 7 are all very similar in muscovite chemistry (Table 8), slight differences do occur in one or more which reflect the nature of the original sediment.

Samples #5, 6 from quartzose rocks are slightly low in Si relative to Samples #3, 4, 7, the more argillaceous sediments. Sample #5 is low in Mg, and Sample #7 is low in both Na and K. Sample #5 contains a slight excess of Ba, and a trace of Ca.

From Table 8 Sample #8 is low in Si and K, yet is high in Na, Ca, Ba, reflecting the alkali-rich environment of the rock.

The presence of Ba in these muscovites is noticeable and allowance has been made for Ba in calculating the Modified A.K.F. diagram

TABLE 9

Muscovite Structural Formulae*

based on 14 cations



1. $K_{1.83}Na_{0.04}Al^{VI}_{4.08}[Si_{6.48}Al^{IV}_{1.52}_{20}](OHF)_4$
2. $K_{1.58}Na_{0.30}Al^{VI}_{4.08}[Si_{6.25}Al^{IV}_{1.75}_{20}](OHF)_4$
3. $K_{1.72}Na_{0.16}Al^{VI}_{4.06}[Si_{6.33}Al^{IV}_{1.67}_{20}](OHF)_4$
4. $K_{1.74}Na_{0.17}Al^{VI}_{4.05}[Si_{6.37}Al^{IV}_{1.63}_{20}](OHF)_4$
5. $K_{1.78}Na_{0.17}Al^{VI}_{3.98}[Si_{6.29}Al^{IV}_{1.71}_{20}](OHF)_4$
6. $K_{1.78}Na_{0.18}Al^{VI}_{4.01}[Si_{6.28}Al^{IV}_{1.72}_{20}](OHF)_4$
7. $K_{1.71}Na_{0.13}Al^{VI}_{3.94}[Si_{6.26}Al^{IV}_{1.74}_{20}](OHF)_4$
8. $K_{1.56}Na_{0.49}Al^{VI}_{3.92}[Si_{6.17}Al^{IV}_{1.83}_{20}](OHF)_4$

Al^{VI} = Total Y site content

*For detailed structural formulae see
Table 10

TABLE 10

Muscovite Structural Formulae

on basis of 14 cations

	1	2	3	4	5	6	7	8
Si ⁺	6.48	6.25	6.33	6.37	6.29	6.28	6.26	6.17
Al ^{IV}	1.52	1.75	1.67	1.63	1.71	1.72	1.74	1.83
Al ^{VI}	3.11	3.77	3.48	3.46	3.40	3.39	3.30	3.37
Ti	0.07	0.03	0.04	0.04	0.04	0.04	0.04	0.03
Fe	0.49	0.15	0.26	0.28	0.32	0.31	0.30	0.33
Mg	0.41	0.13	0.28	0.27	0.22	0.27	0.30	0.19
Ca	0.00	0.00	0.00	0.00	0.01	0.00	0.00	0.01
Na	0.04	0.30	0.16	0.17	0.17	0.18	0.13	0.49
K	1.83	1.58	1.72	1.74	1.78	1.78	1.71	1.56
Ba	0.04	0.04	0.04	0.03	0.05	0.03	0.04	0.06
F								
OH	4.0	4.0	4.0	4.0	4.0	4.0	4.0	4.0
"X"	1.91	1.92	1.92	1.94	2.01	1.99	1.88	2.12
"Y"	4.08	4.08	4.06	4.05	3.98	4.01	3.94	3.92
"Z"	8.00	8.00	8.00	8.00	8.00	8.00	8.00	8.00
%Al ^{IV} *	19.00	21.87	20.87	20.37	21.37	21.50	21.75	22.87

* Average Al^{IV} content in tetrahedral site = 21.2%

+ Average Si^{IV} cation content = 6.31

(Fig. 20).

Muscovite Structural Formulae

The muscovite structural formulae in Tables 9, 10, calculated on the basis of 14 cations, reflect some of the mineralogical differences mentioned earlier.

Muscovite 'X' site cations are deficient in all cases, excepting in Samples #5, 8, the deficiency is usually slight, and is compensated by an excess in 'Y' site divalent cations. The formulae shown are calculated relative to an ideal cation content, there is, however, a possibility that there is a genuine cation deficiency in the muscovites as suggested by calculating the formulae relative to 24 (OOHF). The excess water and cation deficiency found may indicate the presence of the hydroxonium ion. The deficiency is, however, probably better expressed in terms of ideal total cation content.

The alkali cation content is predominately K, with minor Na and Ba. As shown in Figure 11 the majority of the samples contain approximately 10% paragonite molecule in solid solution. Sample #8 contains over 20% paragonite in solid solution, close to the maximum postulated by Eugster and Yoder (1955).

Samples #1, 2, 3, 5, 6 contain albite, which does not appear to influence the partitioning of Na between muscovite and biotite. Muscovite takes nearly all the Na in excess of that required to form albite. Muscovite and biotite partition their alkali cations preferentially (Fig. 12), yet attain a fairly even cation distribution (Fig. 13). Muscovite shows a greater tolerance in terms of alkali cation contents,

Figure 11

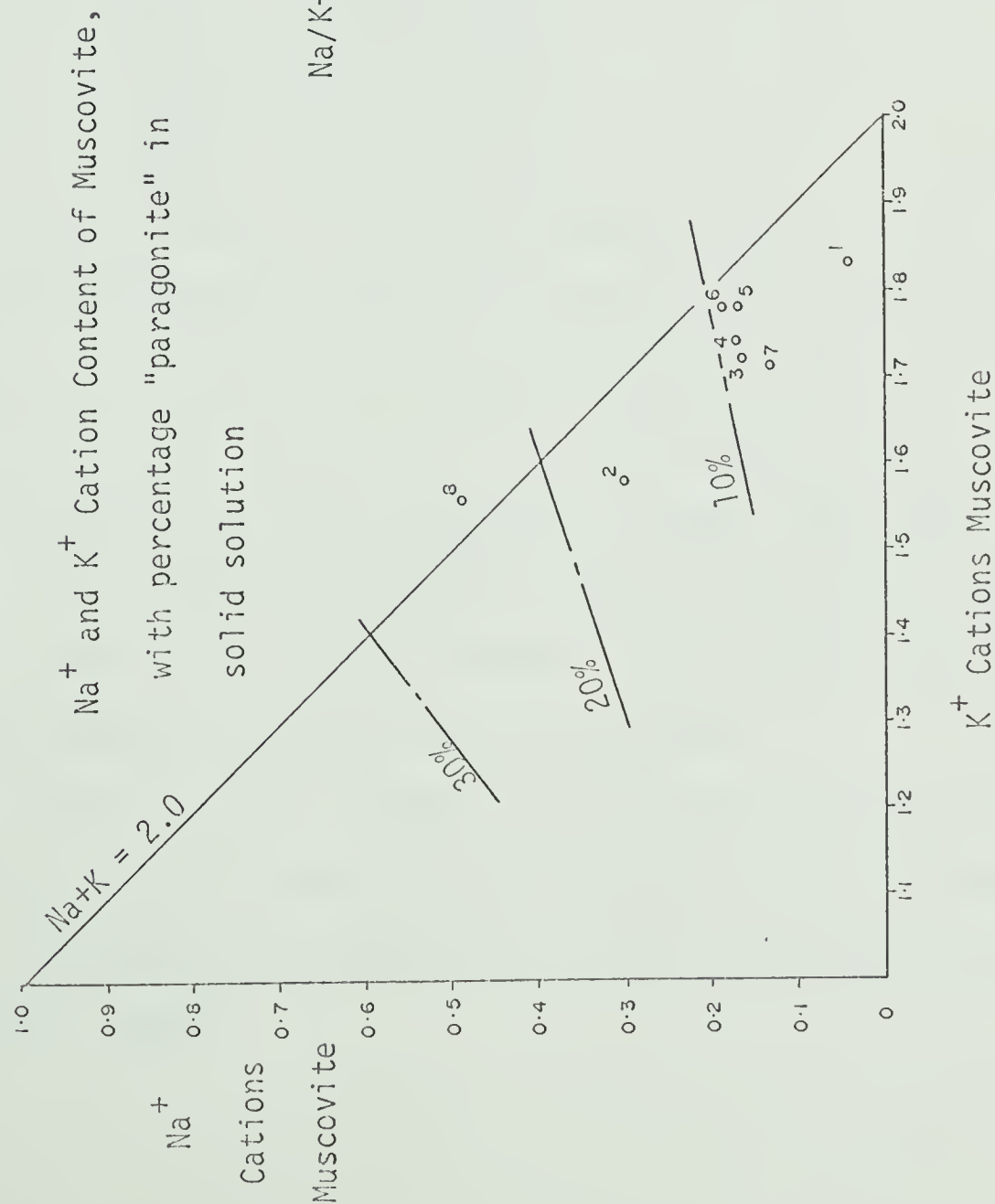
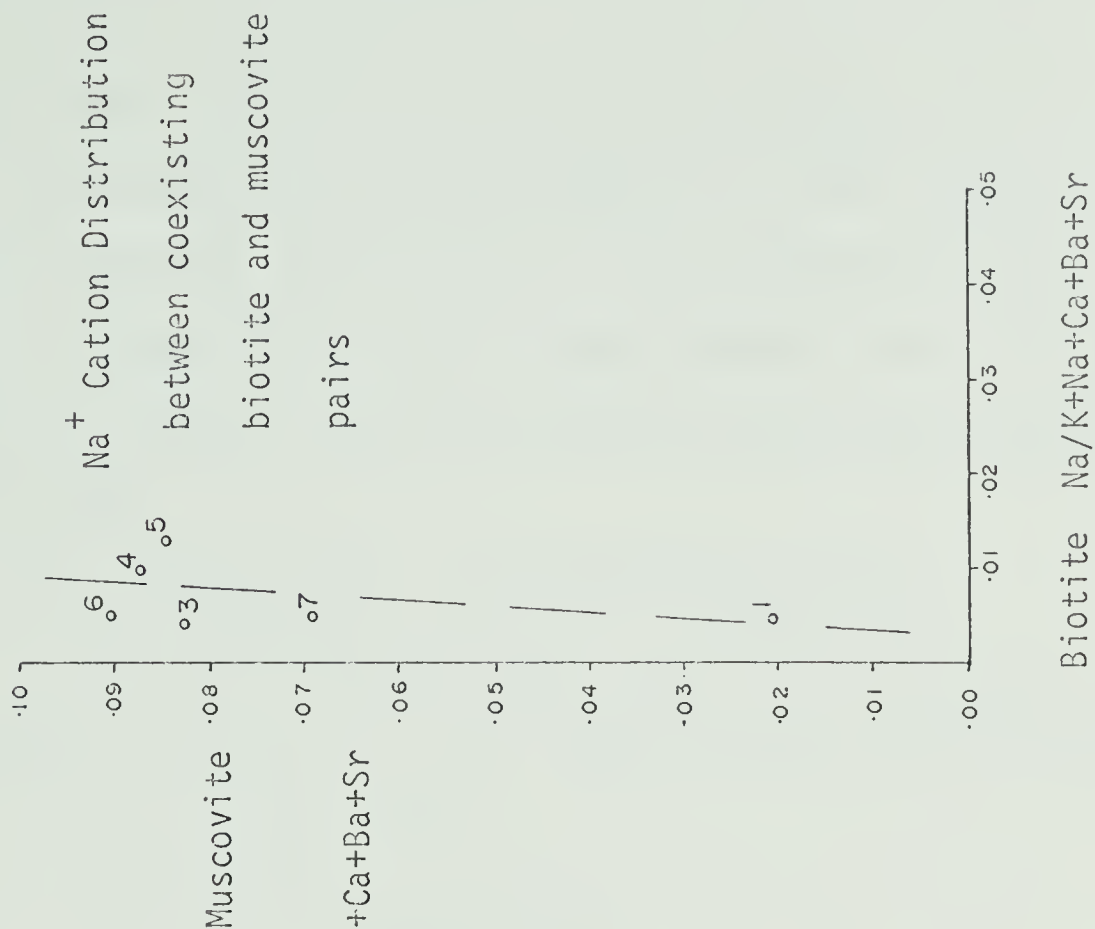
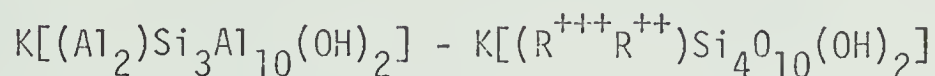


Figure 12

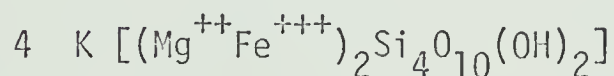
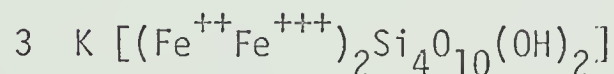
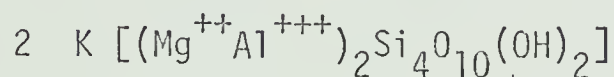
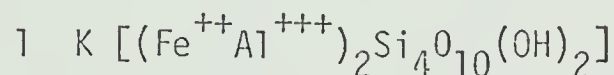


but near "ideal" partitioning is displayed by Samples #3, 4, 6.

True muscovite has one tetrahedral Si in four replaced by Al. Phengitic micas have an excess of Si in the tetrahedral site, balanced by Mg and Al substitution for Al in the octahedral sites. The analysed muscovites are phengitic and fall within the muscovite-celadonite system of Velde (1965)



In order to balance the Si-Al ratio in the tetrahedral sites, the octahedral ions Mg, Fe^{++} , Fe^{+++} have to substitute accordingly, giving four possible end members.

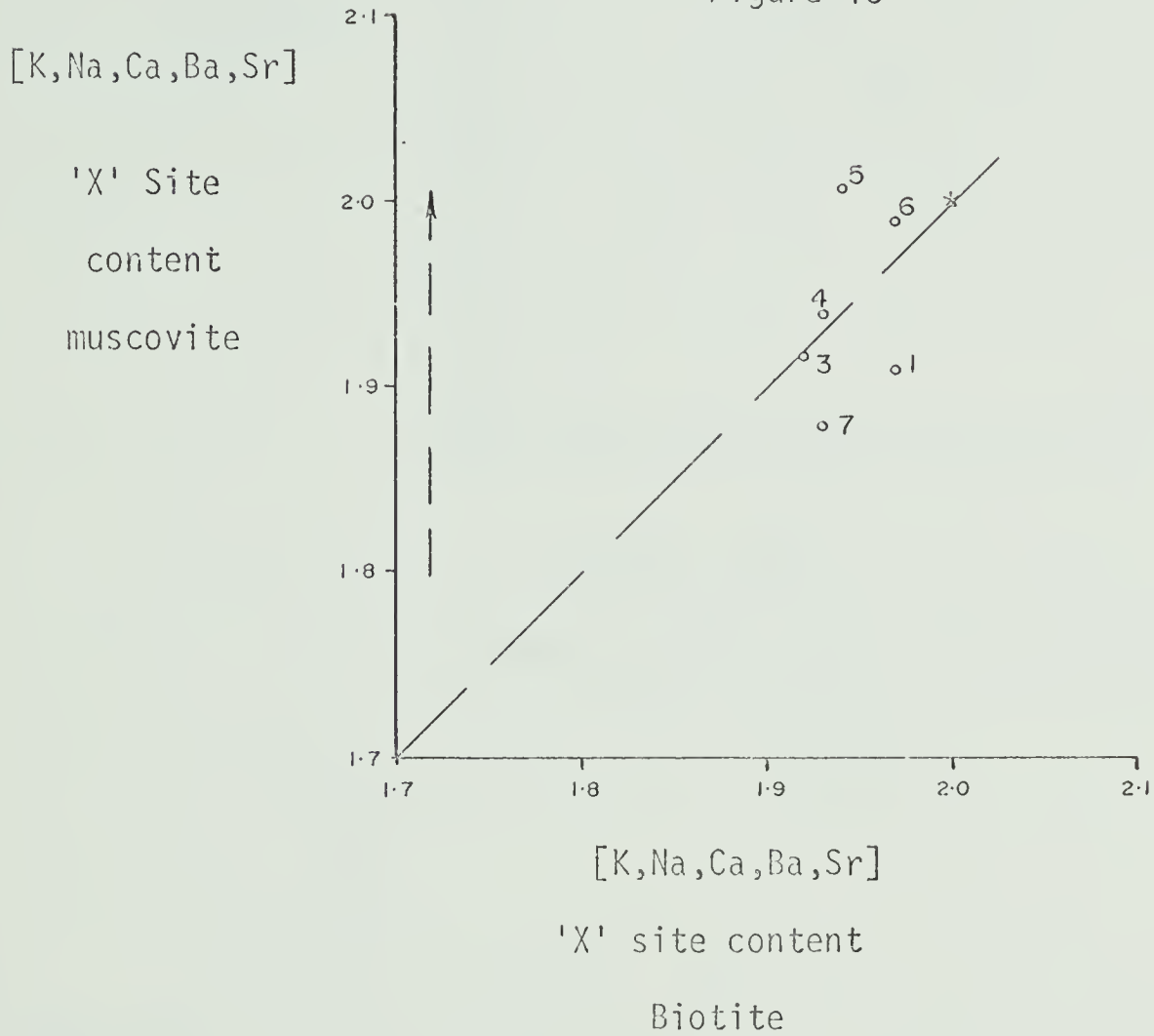


Mg and Fe appear to substitute equally (Table 10) and it seems likely that the phengite contains equal parts of Type 1 and Type 2 celadonite. By nature of the Electron Microprobe analysis, it is not possible to determine the Fe^{++}/Fe^{+++} ratio, and Types 3 and 4 substitution are also possible (see data on phengites in Brown, 1967; Mather, 1970).

All the samples are phengitic, with an average Al^{IV} content in the 'Z' position of 21.2 atomic percent. They thus fall short of the Al^{IV} requirement of true muscovite by 3.8 percent.

The Al^{VI} and Al^{IV} contents of coexisting muscovite and biotite pairs (Figs. 14, 15) suggest an equilibrium distribution, however, small errors in the analysis of either Si or Al will substantially effect both Al^{IV} and Al^{VI} values.

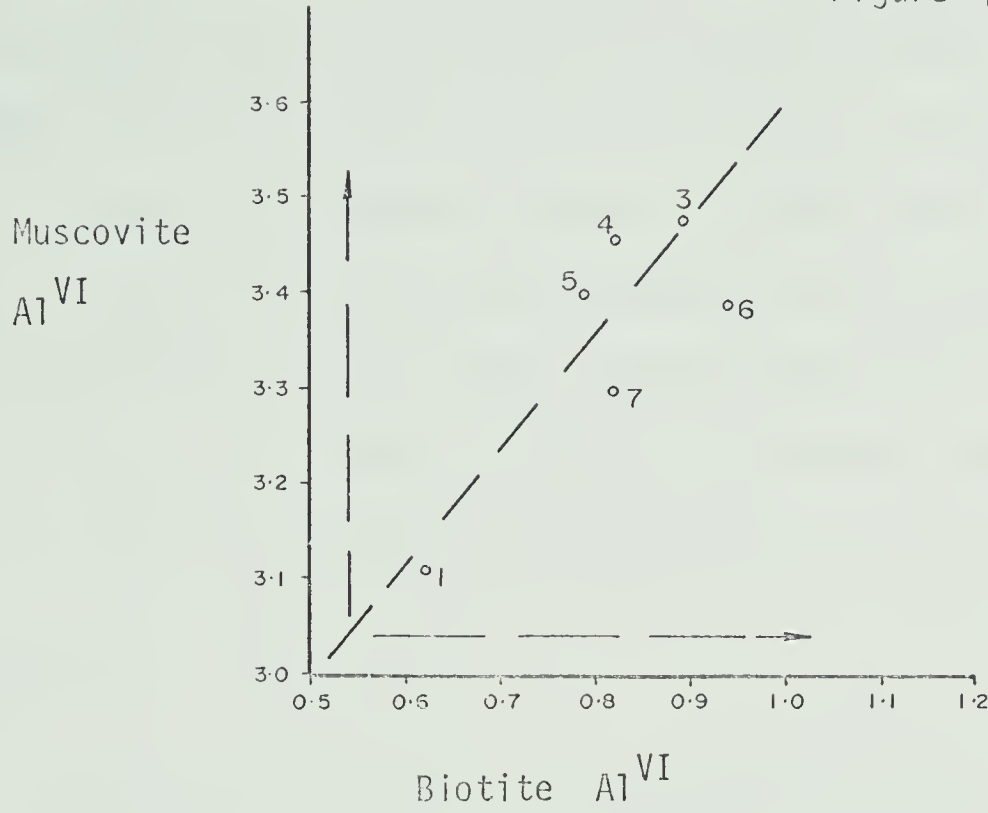
Figure 13



Distribution of large cations in coexisting muscovite and biotite pairs

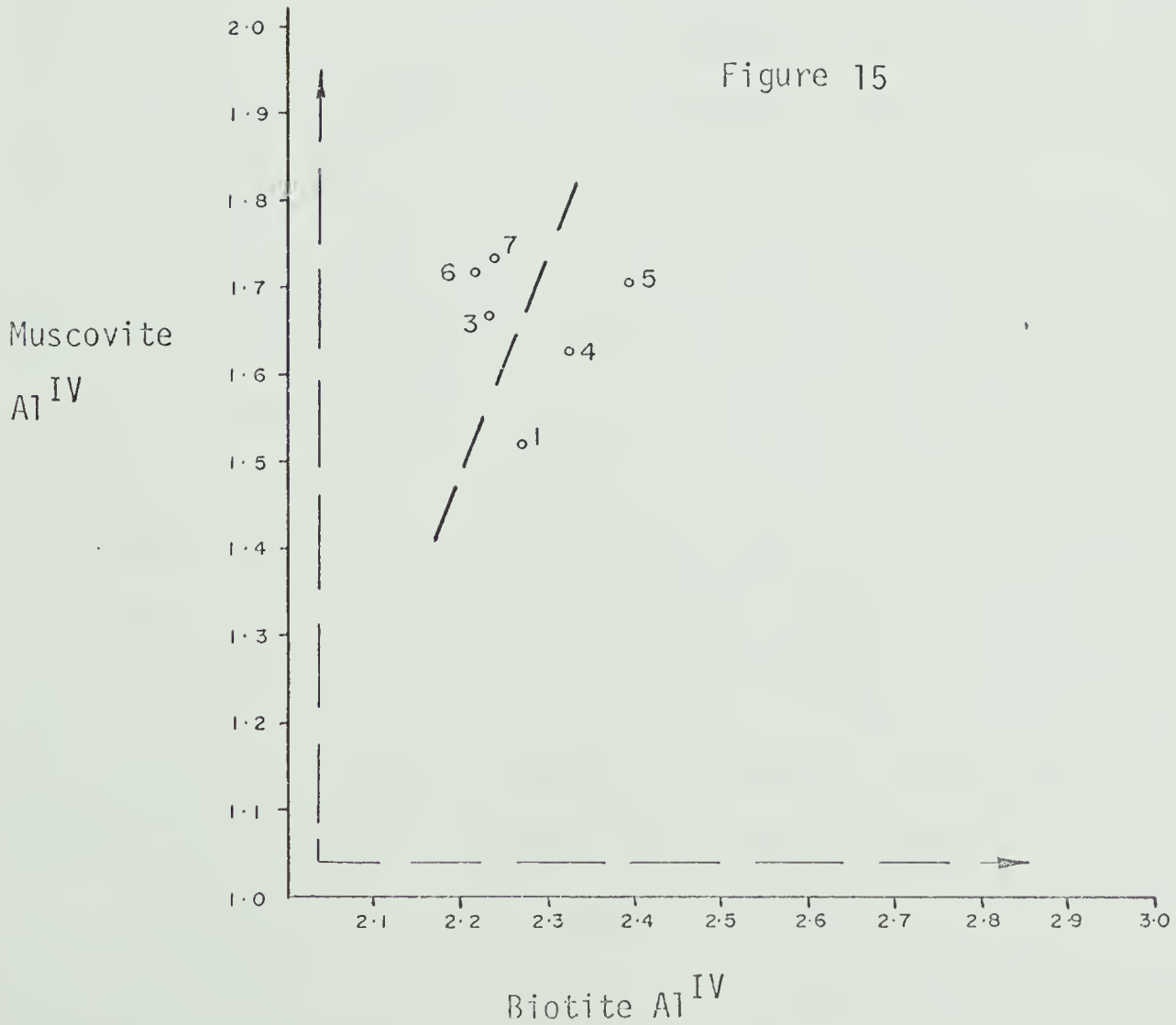
* = 'ideal' partitioning between 'X' saturated micas

Figure 14



Octahedral Al^{VI} Content in Coexisting Mica Pairs

Figure 15



Tetrahedral Al^{IV} Content in Coexisting Mica Pairs

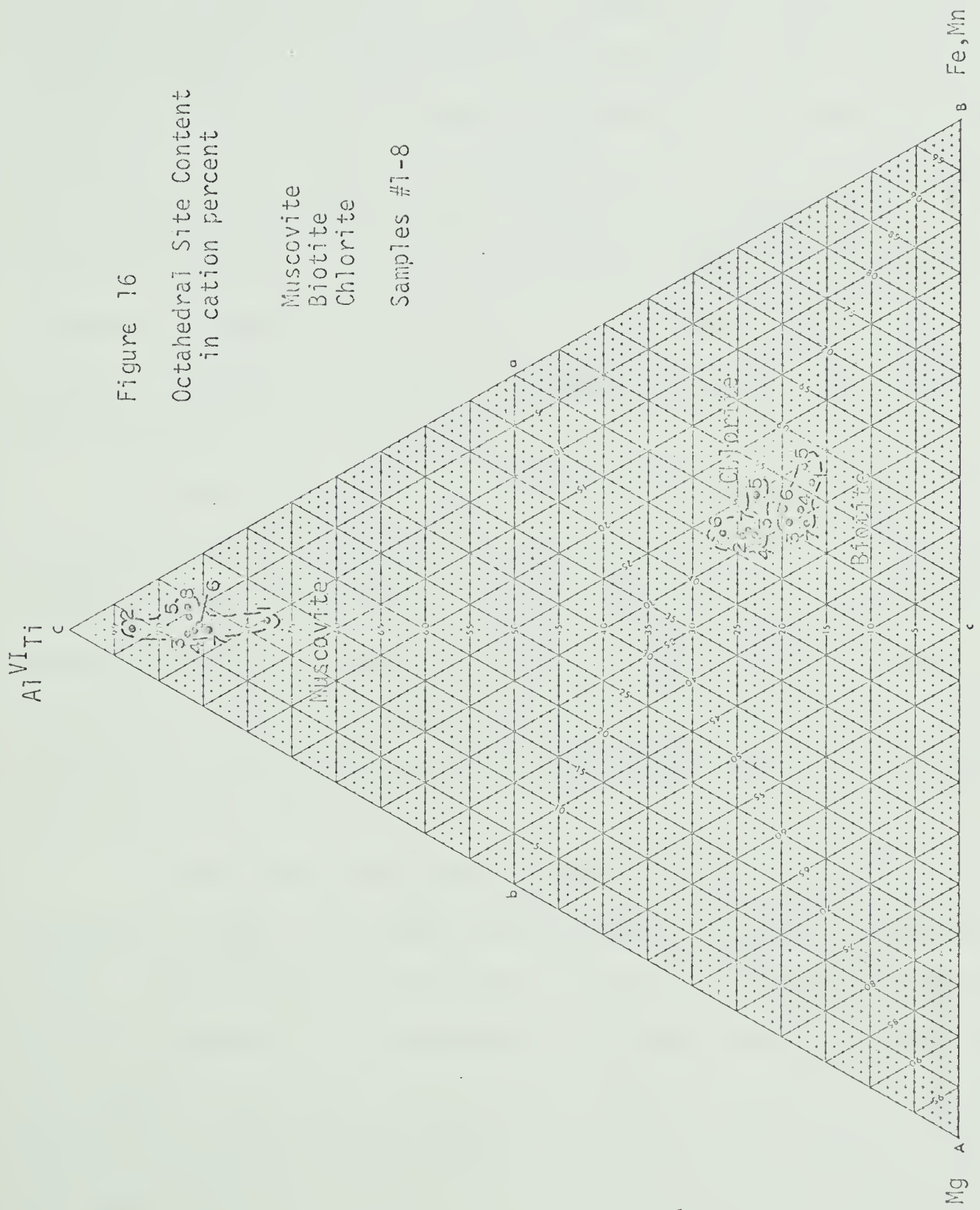
The octahedral cations (Fig.16) show that Mg and FeMn divalent cations substitute equally as the $Al^{VI}Ti$ content decreases. The Mg/Mg + Fe ratio should thus remain constant, regardless of the Al/Mg + Fe ratio, and phengite content. It would appear that the Mg/Mg + Fe ratio in the three-phase muscovites may deviate from this equal partitioning of Mg and FeMn, and may become more Fe-rich as in Samples #5, 6, 8. The Mg/Mg + Fe ratio is extremely important in the rocks, and will be discussed in a later section (p.115).

Discussion

The muscovite analyses are remarkable for their clear cut and systematic differences. They appear to have attained a high degree of equilibrium, and to have had their chemical contents very clearly defined by a combination of whole-rock composition, coexisting phases and physical environment.

As illustrated by Brown (1967), coexisting chlorites and muscovites from the chlorite metamorphic grade have no compositional controls imposed upon them, other than the effect of the whole-rock chemistry. In natural sediments it is possible to get a range of celadonite solid solution in muscovite from pure muscovite to phengite, depending on the Al/Mg + Fe ratio of the sediment (Fig.10). The addition of biotite as a third phase will restrict the composition of the muscovite to the most phengitic acceptable, and the three coexisting phases will cease to be entirely whole-rock dependent.

The effect of adding ankerite, an MgFe phase alone cannot alter the Al/Mg + Fe ratio, but may, like the oxides and sulphides, help buffer the Mg/Mg + Fe ratio of each phase.

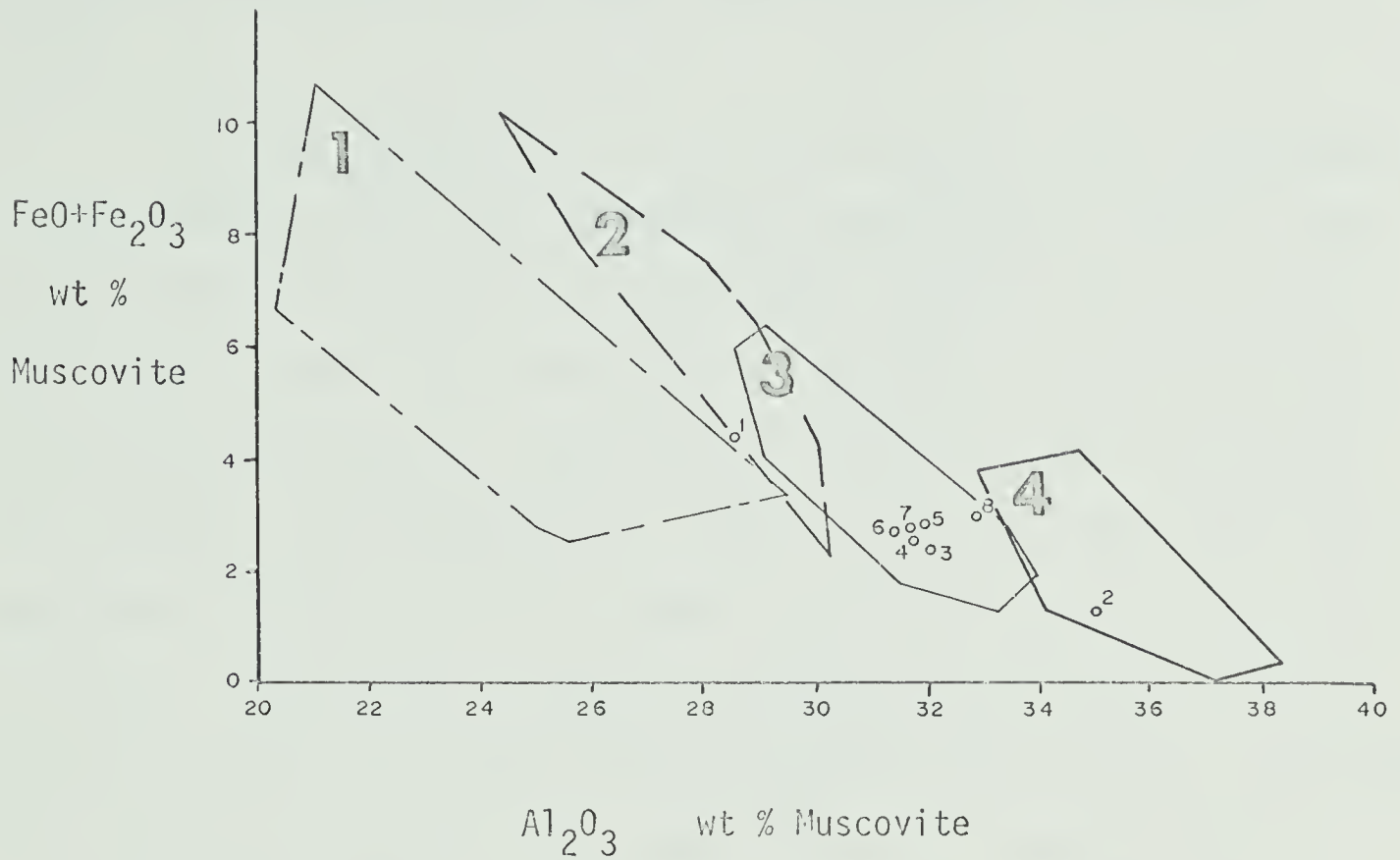


Velde (1965) indicates that Mg and Fe-rich phengites are stable at low temperatures and pressures, based on experimental work in the muscovite-celadonite system, and in fact pure muscovite is rarely found in low grade metamorphic rocks. Muscovite ought to be stable at low metamorphic grades, and Butler (1967) attributes its scarcity to the rarity of high Al, low MgFe-rich sediments in nature. Most pelitic and semipelitic rocks contain a phengitic muscovite at low metamorphic grades. According to Butler, these are celadonite-rich by default, because there are no other ferromagnesian phases to take up the Mg and Fe. The addition of biotite, almandine, and staurolite allows the muscovite to reduce its celadonite content, and the phengite thus becomes progressively closer to muscovite with increase in metamorphic grade. This concept will be discussed more fully later.

In view of the above, Butler (1967) found that variations in Al_2O_3 and total $FeO + Fe_2O_3$ may be used to define fields of celadonite content, based on the $Al_2O_3/FeO + Fe_2O_3$ ratio, these he correlated with metamorphic grade. His data, in addition to that of other published analyses up to 1967, illustrates and supports his contention (Fig.17). It should be noted that the coexisting mineralogy is of major importance, and governs the actual ratio.

The three-phase muscovites from Mount Robson cluster about an $Al_2O_3 / FeO + Fe_2O_3$ ratio normally attributable to Almandine zone muscovites. They are thus very 'pure' and contain far less celadonite than might be expected close to, and above the biotite isograd. In comparison with Mather's muscovites from the biotite isograd they are low in phengite (Figure 20). Relative to the phengite suites reported by Lambert (1959) and Butler (1967), the analysed muscovites are equivalent to muscovites

Figure 17



Samples #1-8 Fe total as FeO

Distribution of FeO+Fe₂O₃ and Al₂O₃ in
phengitic muscovites as a function of
metamorphic grade. After Butler 1967

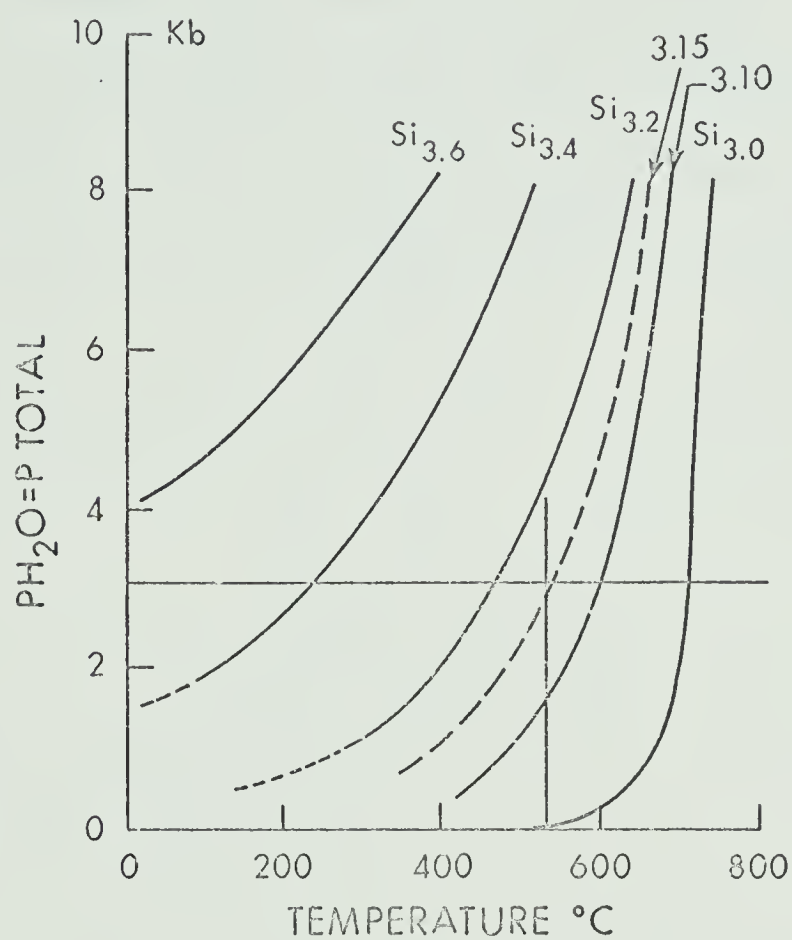
- 1 = Blueschist Facies
- * 2 = Chlorite and Biotite Zones
- * 3 = Almandine Zone
- * 4 = Staurolite and Higher Zones
- * = Greenschist Facies

from much higher metamorphic grades (Fig.21,22). The phengites quoted by Smith (1963) are mostly from chlorite-muscovite pairs, and thus like Sample #2, have their compositions fixed by the whole-rock Al/Mg + Fe ratio.

An obvious explanation for the low phengite content encountered is the addition of the new ferromagnesian phase ankerite, which at low levels serves the same function as almandine and staurolite at higher metamorphic grades. This bears out the suggestion by Butler that the coexisting phases tend to reduce the celadonite content of a phengite. This concept is a refinement of an original idea by Lambert (1959) that phengites tend to approach the composition of pure muscovite with grade increase. Four analyses from the sillimanite zone are shown in Fig. 21. These are taken from Guidotti (1970) and would agree with this supposition. The three-phase muscovites thus appear to have the composition of a muscovite attributable to the almandine zone of regional metamorphism.

According to Velde (1967) the Si^{IV} content of a phengitic muscovite, here averaging 6.3 cations (Table 10), is independent of whole-rock chemistry, and ferromagnesian substitution. His work on synthetic material suggests that low temperatures and high water pressures favour the phengitic end member. This has been disputed by Brown (1967) who feels that the bulk composition is the overriding control. The temperature of formation of the phengite, as estimated from Velde's geothermometer (Fig. 18) is around 500°C. This value is high and probably unrealistic; it does, however, fit with the "apparent" high grade nature of the muscovites. According to Velde (1967) high water pressures increase the Mg, Fe and Al substitution, and temperature controls Al^{IV} content. The two are, however, interrelated, and it is difficult to apply them to

Figure 18



After Velde B. 1967

Stability Curves for Phengitic Micas in the
Series $K[Al_2Si_3AlO_{10}(OH)_3]-K[MgAlSi_4O_{10}(OH)_2]$

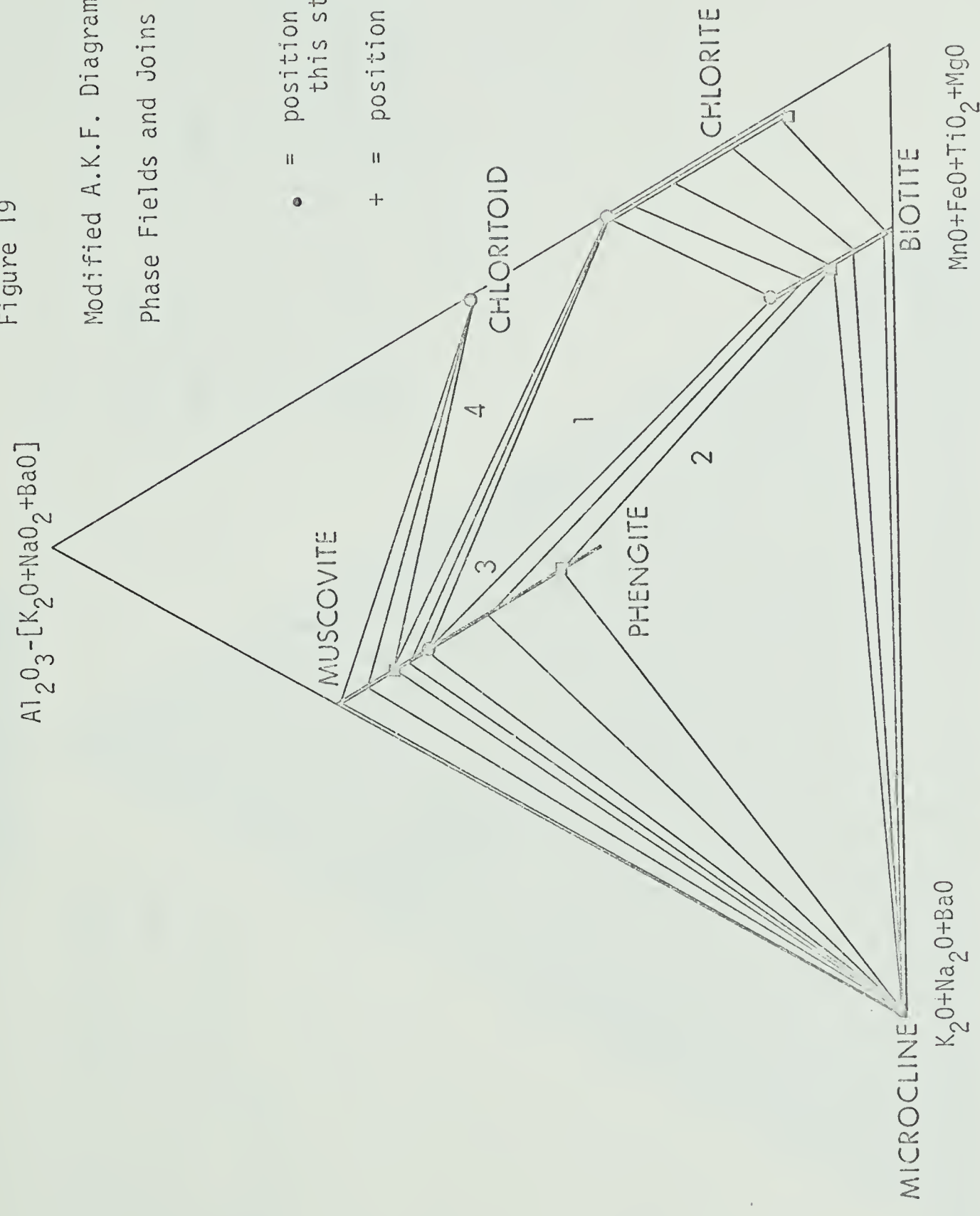
At 3 Kbars the temperature of formation of a
muscovite whose Si^{IV} content = 3.15 cations
would be 500°C ±

[Si^{IV} in terms of maximum 4.0 cations]

natural systems.

Another interesting feature of the Mount Robson muscovites is that they plot closer to the muscovite-phengite join on a modified A.K.F. diagram than the phengite suites reported by Lambert (1959), Butler (1967), Mather (1970), Smith (1963) (Fig. 20). They would thus appear to be less deficient in coarse alkali cations than most analysed phengites. The reason for this is not known; however, it is in accordance with the very high degree of equilibrium attained in the rocks.

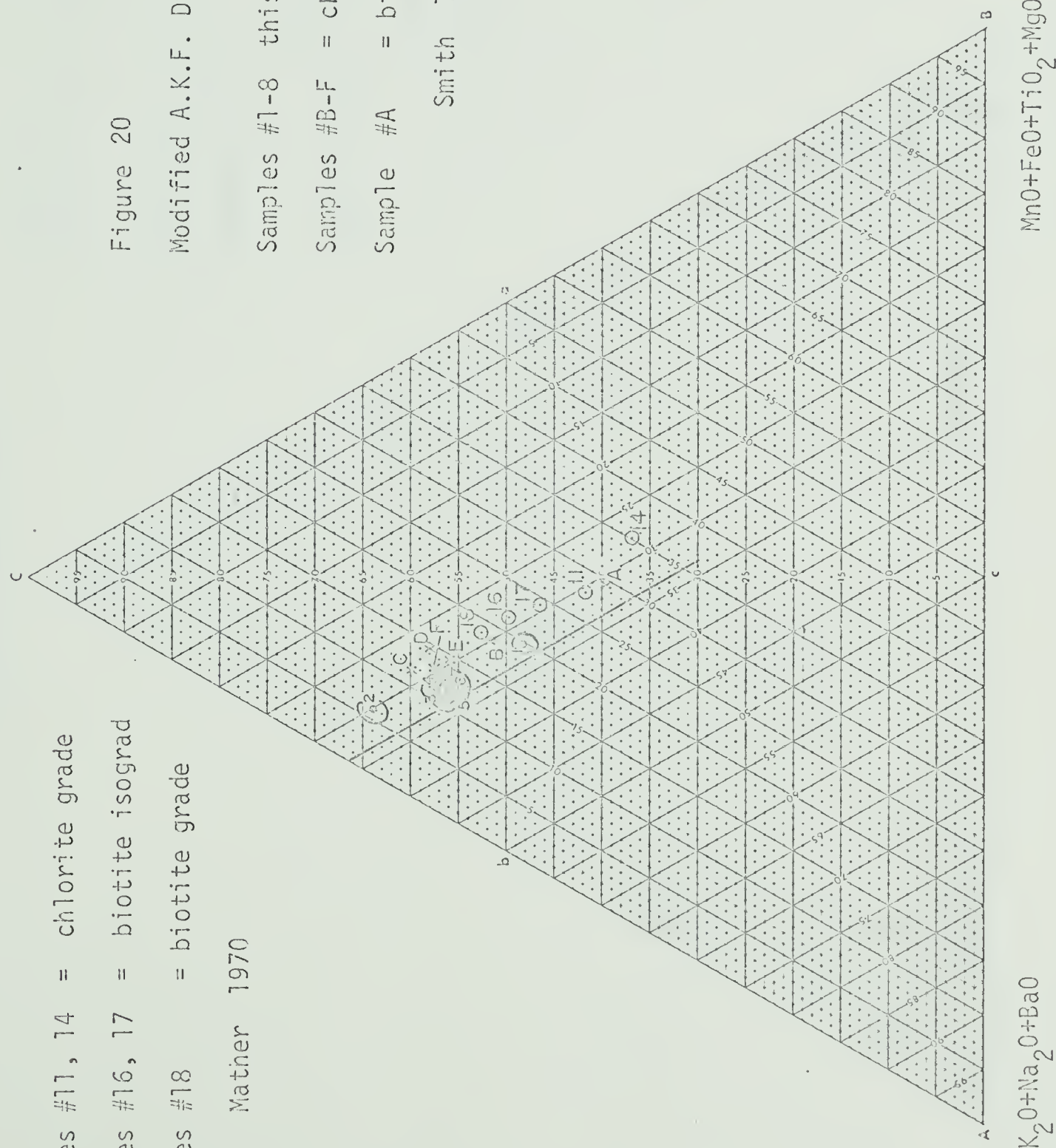
Figure 19
Modified A.K.F. Diagram Stylized
Phase Fields and Joins



$$\text{Al}_2\text{O}_3 - [\text{K}_2\text{O} + \text{Na}_2\text{O} + \text{BaO}]$$

Samples #11, 14 = chlorite grade
 Samples #16, 17 = biotite isograd
 Samples #18 = biotite grade

Matner 1970



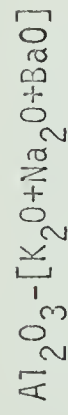


Figure 27

Modified A.K.F. Diagram

Samples #41, 44 = Lower Sillimanite Grade

Samples #13, 17 = Upper Sillimanite Grade

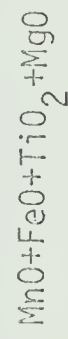
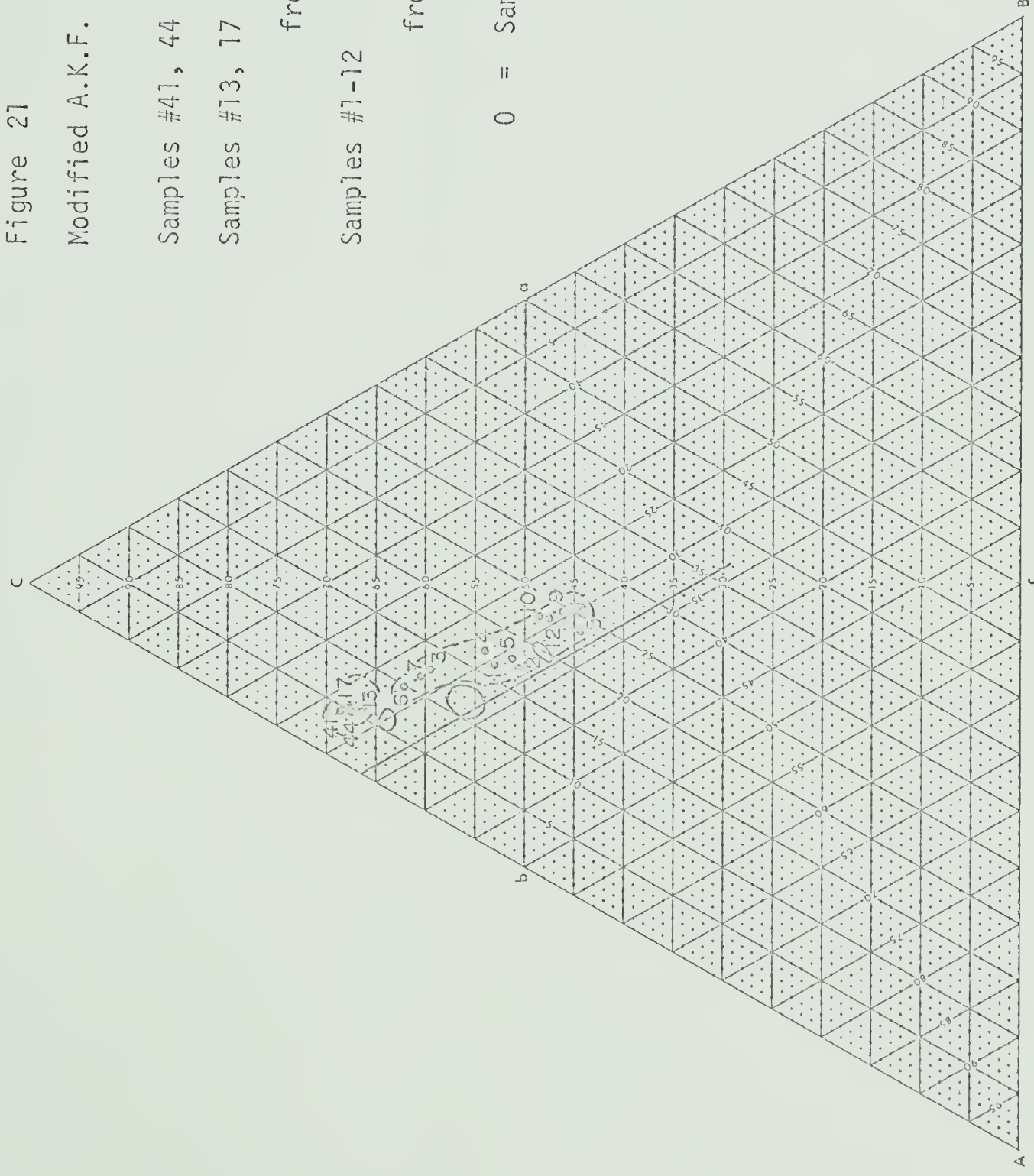
from Guidotti 1970

Samples #1-12 = Upper Greenschist Facies

from Lambert 1959

0 = Sample point(s) this study

see Figure 20



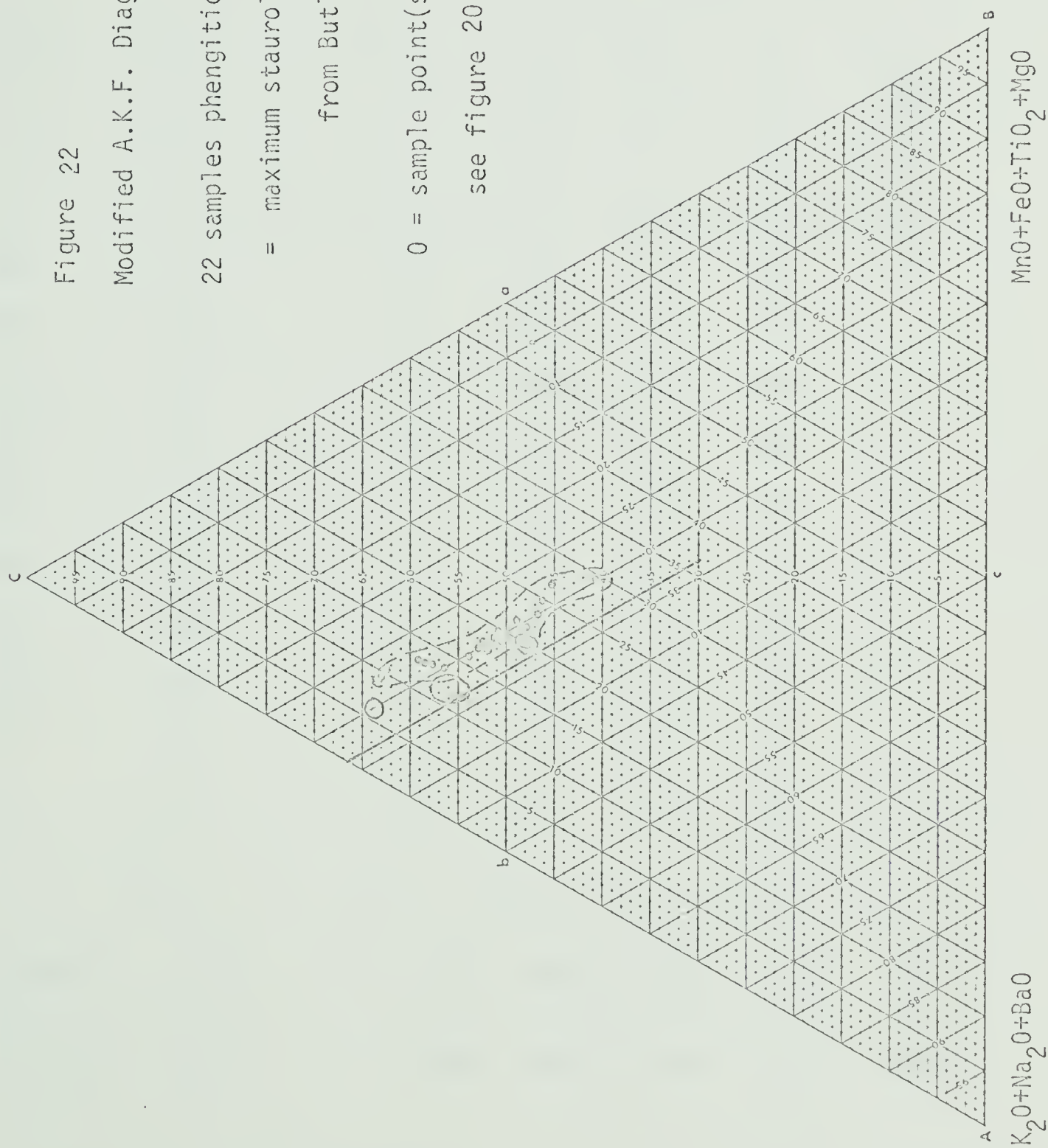
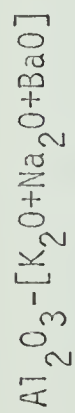


Figure 22

Modified A.K.F. Diagram

22 samples phengitic-muscovite

= maximum staurolite metamorphic grade
from Butler 1967

0 = sample point(s) this study
see figure 20

TABLE 11

Biotite Chemical Analyses

	1	2	3	4	5	6	7	8
SiO ₂	35.77		36.51	36.03	34.75	36.01	36.43	
TiO ₂	3.27		2.19	2.22	2.15	2.10	2.25	
Al ₂ O ₃	15.28		16.73	16.91	16.72	16.63	16.35	
FeO	25.31		23.58	24.51	25.68	23.38	23.86	
MnO	0.06		0.00	0.05	0.03	0.02	0.05	
MgO	6.79		7.72	7.48	6.33	7.19	8.04	
Na ₂ O	0.04		0.05	0.06	0.07	0.05	0.05	
K ₂ O	9.50		9.38	9.41	9.27	9.49	9.51	
SrO	0.03		0.02	0.03	0.03	0.02	0.04	
BaO	0.22		0.14	0.13	0.24	0.13	0.17	
H ₂ O	3.69		3.52	2.98	4.67	4.81	3.21	
P ₂ O ₅	0.05		0.04	0.03	0.01	0.03	0.03	
Cl'	0.00		0.01	0.01	0.02	0.01	0.00	
F'	0.15		0.22	0.27	0.18	0.20	0.12	
	100.16		100.11	100.12	100.15	100.07	100.11	
Mg/Mg+Fe	.3234		.3685	.3524	.3052	.3541	.3752	
Al/Fe+Mg	.2879		.3158	.3148	.3188	.3237	.3018	

Biotite Chemistry

The trioctahedral mica, biotite, was found in six of the samples analyses; in all cases it coexists with a phengitic muscovite, and with the exception of Sample #1, a chlorite.

The chemical compositions of the analysed biotites are shown in Table 11, and are illustrated on the A.K.F. diagram (Fig. 10), and the A.F.M. diagram (Fig. 23).

The population shows an overall consistency in its composition. As a group the biotites are very low in Na, Al, and high in Fe, a characteristic normally associated with low-grade metamorphic biotites, such as those reported by Lambert (1959).

By inspection Samples # 1, 5 are low in Si, and have a reduced Mg/Mg + Fe ratio. This is caused by an excess of Fe, which in Sample #1 is accompanied by a high Ti value, and a reduction in Al content. These two samples are more femic in composition, a characteristic displayed by the other, coexisting ferromagnesian phases. In whole-rock terms, the first is Al-poor and contains no chlorite. The biotite formed is thus acceptable in terms of its bulk composition.

The A.F.M. plot (Fig. 23) with total Fe as FeO, illustrates the Fe-rich nature of the biotites, and shows the close relationship between the coexisting biotite and chlorite pairs. This relationship is in accordance with the clear cut equilibrium textures found in the analysed samples. Similar tie-lines are found in the A.K.F. diagram (Fig. 10). Sample #1 does not differ substantially from the normal three-phase biotites.

Appreciable amounts of Ba are found in Samples #1, 5, although what association Ba has with the femic nature of these samples is not

Figure 23
A.F.M. Diagram after Winkler 1967
Total Fe as FeO
Assemblage + Quartz + Muscovite
Samples #1-7

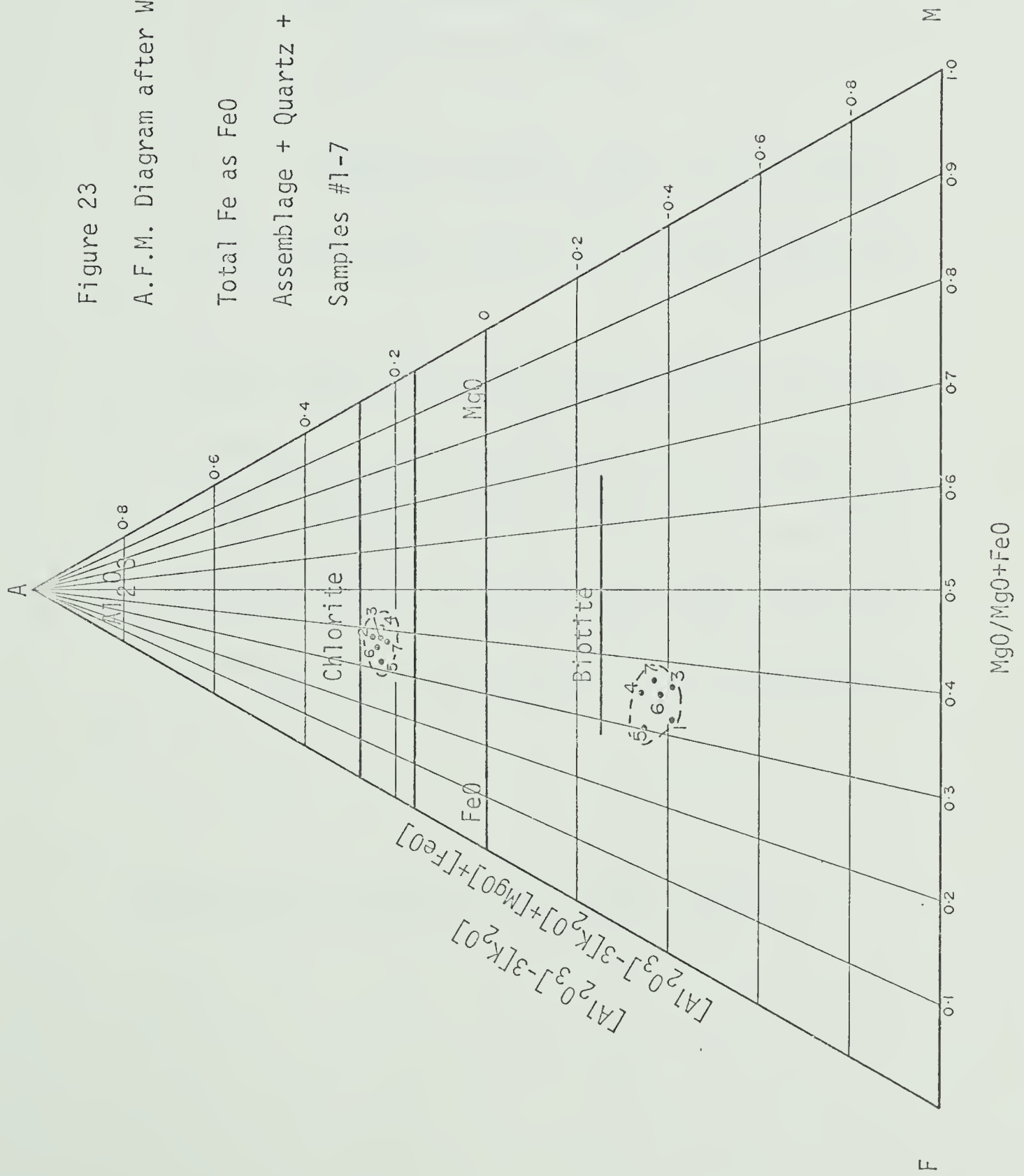
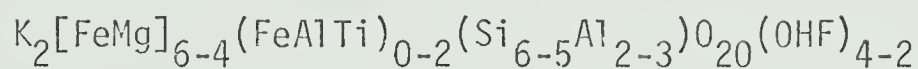


TABLE 12

Biotite Structural Formulae*

based on 16 cations



1. $K_{1.94}Na_{0.01}[Mg_{1.62}Fe_{3.39}Al_{0.62}][Si_{5.73}Al_{2.27}O_{20}](OHF)_4$
- 2.
3. $K_{1.89}Na_{0.01}[Mg_{1.82}Fe_{3.12}Al_{0.89}][Si_{5.77}Al_{2.23}O_{20}](OHF)_4$
4. $K_{1.90}Na_{0.02}[Mg_{1.76}Fe_{3.23}Al_{0.82}][Si_{5.68}Al_{2.32}O_{20}](OHF)_4$
5. $K_{1.91}Na_{0.02}[Mg_{1.52}Fe_{3.48}Al_{0.79}][Si_{5.61}Al_{2.39}O_{20}](OHF)_4$
6. $K_{1.95}Na_{0.01}[Mg_{1.72}Fe_{3.14}Al_{0.94}][Si_{5.79}Al_{2.21}O_{20}](OHF)_4$
7. $K_{1.92}Na_{0.01}[Mg_{1.90}Fe_{3.16}Al_{0.82}][Si_{5.77}Al_{2.23}O_{20}](OHF)_4$
- 8.

*For detailed structural formulae see Table 13

TABLE 13

Biotite Structural Formulae
based on 16 cations

	1	2	3	4	5	6	7	8
Si	5.73		5.77	5.68	5.61	5.79	5.77	
Al ^{IV}	2.27		2.23	2.32	2.39	2.21	2.23	
Al ^{VI}	0.62		0.89	0.82	0.79	0.94	0.82	
Ti	0.39		0.26	0.26	0.26	0.25	0.26	
Fe	3.39		3.12	3.23	3.48	3.14	3.16	
Mg	1.62		1.82	1.76	1.52	1.72	1.90	
Mn	0.01		0.00	0.01	0.00	0.00	0.01	
Na	0.01		0.01	0.02	0.02	0.01	0.01	
K	1.94		1.89	1.90	1.91	1.95	1.92	
Ba	0.01		0.01	0.01	0.01	0.01	0.01	
P	0.01		0.01	0.00	0.00	0.00	0.00	
F								
OH	4.00		4.00	4.00	4.00	4.00	4.00	
"X"	1.97		1.92	1.93	1.94	1.97	1.93	
"Y"	6.03		6.09	6.08	6.05	6.05	6.15	
"Z"	8.00		8.00	8.00	8.00	8.00	8.00	

known. Sample #7 would appear to be particularly rich in Mg. It would also seem to have a slightly reduced Al/Mg + Fe ratio.

In general the Al/Mg + Fe ratio appears to be constant and reduced for Sample #1. The Mg/Mg + Fe ratio is also constant, it is reduced in Samples #1, 5.

Biotite Structural Formulae

The structural formulae of the biotites as shown in Tables 12, 13, were calculated on the basis of an "ideal" 16 cation content.

The 'X' sites are all deficient in large alkali cations (Fig.13), a deficiency made up by an excess of smaller divalent cations. Biotite and muscovite partition the available cations, and some appear to approach ideal 1:1 partitioning. The range of cation content tolerated by biotite is less than that of muscovite. The biotite contains very little Na, which is preferentially taken up by muscovite in the form of paragonite solid solution (Fig. 12). Muscovite also concentrates Ba, leaving biotite with K, and little else. The low Na content in biotite may be a factor inherited from the chlorite grade mineralogy, in which Na preferentially entered albite, and left the phyllosilicate system.

All the biotite analyses indicate an excess of cations for the octahedral site, a feature which may cancel out the deficiency noted above. In the octahedral cation plot (Fig. 16) biotite shows a distinct scatter, with the octahedral FeMn content increasing at the expense of Mg, and to lesser extent Al^{VI} Ti. Any increase in the Mg/Mg + Fe ratio ought to be coupled with a slight increase in the Al/Mg + Fe ratio. Mg and Al^{VI} content have been cited as regional indicators in metamorphic grade.

There is thus an "apparent" grade increase from Sample #5 to Samples #3, 7. This same relationship is expressed elsewhere in studies concerning the coexisting ferromagnesian phases. The sequence does not reflect the sample grade increase sequence, but rather, appears to be a function of the original rock compositions (Fig. 9).

Biotite and muscovite approach equilibrium in their Al^{IV} and Al^{VI} cation distributions (Fig. 14, 15). The Al^{IV} plot suggests a low range of tolerance and little variation in each, a function of the relatively constant Si content. The Al^{IV} content of Sample #1 differs little from the three-phase biotite group; however, the Al^{VI} distribution shows both to be deficient.

Biotite and muscovite equilibrium is again suggested by their $Al/Mg + Fe$ plots (Fig. 24). The muscovite ratio is much more variable than for biotite, and the relationship is approximately linear. Some allowance has to be made for the possibility of analytical error, which would substantially influence the values shown.

Discussion

Wenk (1970) found that in the Alps the Al^{VI} content of both muscovite and biotite increase with grade increase, and that the effect on biotite is more than for muscovite. The ratio,

$$KD = Al^{VI}_{\text{musc}} / Al^{VI}_{\text{bio}}$$

decreases with metamorphic grade increase, from 14 at low metamorphic levels to 3 at high grades. The samples analysed give an average KD value of 4.18, a very low value for the lower biotite grade. The variation in metamorphic grade between Samples #1-8 is not large, and the figure is realistic, although compositionally controlled. Here again

the mineral chemistry is indicative of a higher metamorphic grade than the biotite grade mineralogy implies. In this case both muscovite and biotite appear to be anomalous. Sample #1 lacks biotite and is thus a "lower grade" mineralogy; it does, however, differ little in its ratio (Fig. 14).

According to Wenk the figure 1.61 is typical for the Al musc/Al bio ratio for the Greenschist metamorphic facies. The ratio for the Mount Robson samples is 1.63. The total Al content is thus evenly distributed, and complications only occur in distributing the Al between the Al^{IV} and Al^{VI} sites of the two minerals. The Al^{IV} content in each case is related to the Si^{IV} content. Whether this is controlled by the metamorphic grade directly (Velde, 1967; Snelling, 1957), or is controlled indirectly by the Al/Mg + Fe ratio of the whole-rock remains uncertain. The possibility exists that the Al^{VI} content is directly governed by Fe^{+++} content of the mineral, which in turn is a function of the oxygen fugacity. In this case Al^{VI} would control Al^{IV} , and Al^{IV} would make up any deficiency with the relatively mobile element Si. By this argument the Si^{IV} content is fixed by, and does not fix Al^{IV} .

TABLE 14

Chlorite Chemical Analyses

	1	2	3	4	5	6	7	8
SiO ₂		23.54	23.95	24.78	23.84	26.36	25.38	
TiO ₂		0.06	-	0.06	0.05	-	-	
Al ₂ O ₃		22.28	21.41	21.42	21.96	21.77	20.50	
FeO		30.39	31.01	31.45	34.14	30.41	30.91	
MnO		0.12	0.05	0.09	0.10	0.08	0.13	
MgO		10.55	10.66	11.27	9.32	10.08	10.48	
CaO		0.01	0.01	0.01	0.04	0.03	-	
K ₂ O		0.01	0.01	-	0.01	-	0.01	
SrO		-	0.02	0.01	0.02	0.07	0.01	
H ₂ O		12.03	11.89	11.03	10.75	11.46	11.96	
P ₂ O ₅		0.01	0.09	0.04	0.03	0.04	0.08	
		99.00	99.10	100.16	100.26	100.30	99.46	
Mg/Mg+Fe		.3822	.3799	.3898	.3273	.3714	.3767	
Al/Mg+Fe		.3190	.3017	.2929	.3049	.3170	.2914	

Chlorite Chemistry

The mineral chlorite is found in six of the analysed samples. In each case it coexists with a phengitic muscovite and, with the exception of Sample #2, a biotite.

The chlorite population is remarkably constant in its chemistry (Table 14, Figs. 10, 23). The chlorites have the composition of ripidolite in all cases, except Sample #6, which is brunsvigite (Deer, Howie and Zussman, 1962).

Variations in chemistry are slight, Si is high in Samples #6, 7. The Al content of Sample #2 is high, and in Sample #7 is low. The Mg content of Sample #4 is high, and in Sample #5 is low. These variations in Mg content reflect the $Mg/Mg + Fe$ ratio of the chlorite; this would appear to vary slightly, yet systematically, in line with other coexisting ferromagnesian phases. The exceedingly Fe-rich nature of Sample #5 has a marked affect on the $Mg/Mg + Fe$ ratio, but does not affect the $Al/Mg + Fe$ ratio, which is constant throughout, only slightly high in Sample #2.

The chlorites show a restricted plot on an A.F.M. diagram (Fig. 23). They appear to be in equilibrium with coexisting biotite, and their tie-lines are close to parallel. Samples #4, 7 do in fact cause the tie-lines to cross. A similar arrangement may be seen on an A.K.F. diagram (Fig. 10).

The chlorites are rich in Fe and Al, and are fairly typical metamorphic chlorites, similar to those described by Atherton (1964). They contain trace amounts of Mn and P and Sample #6 contains traces of Sr.

TABLE 15

Chlorite Structural Formulae*

based on 20 cations



- 1.
2. $[\text{Mg}_{3.43}\text{Al}_{8.89}\text{Fe}_{5.55}][(\text{Si}_{5.15}\text{Al}_{2.85})\text{O}_{20}](\text{OH})_{16}$
3. $[\text{Mg}_{3.48}\text{Al}_{2.80}\text{Fe}_{5.69}][(\text{Si}_{5.26}\text{Al}_{2.74})\text{O}_{20}](\text{OH})_{16}$
4. $[\text{Mg}_{3.59}\text{Al}_{2.70}\text{Fe}_{5.63}][(\text{Si}_{5.30}\text{Al}_{2.70})\text{O}_{20}](\text{OH})_{16}$
5. $[\text{Mg}_{3.01}\text{Al}_{2.76}\text{Fe}_{6.18}][(\text{Si}_{5.16}\text{Al}_{2.84})\text{O}_{20}](\text{OH})_{16}$
6. $[\text{Mg}_{3.24}\text{Al}_{3.22}\text{Fe}_{5.48}][(\text{Si}_{5.69}\text{Al}_{2.31})\text{O}_{20}](\text{OH})_{16}$
7. $[\text{Mg}_{3.43}\text{Al}_{2.87}\text{Fe}_{5.67}][(\text{Si}_{5.57}\text{Al}_{2.43})\text{O}_{20}](\text{OH})_{16}$
- 8.

* For detailed structural formulae see Table 16

TABLE 16

Chlorite Structural Formulae
based on 20 cations

	1	2	3	4	5	6	7	8
Si		5.15	5.26	5.30	5.16	5.69	5.57	
Al ^{IV}		2.85	2.74	2.70	2.84	2.31	2.43	
Al ^{VI}		2.89	2.80	2.70	2.76	3.22	2.87	
Ti		0.01	0.00	0.01	0.01	0.00	0.00	
Fe		5.55	5.69	5.63	6.18	5.48	5.67	
Mg		3.43	3.48	3.59	3.01	3.24	3.43	
Mn		0.02	0.01	0.02	0.02	0.02	0.02	
Ca		0.00	0.00	0.03	0.01	0.01	0.00	
Sr		0.00	0.00	0.00	0.00	0.01	0.00	
P		0.00	0.02	0.01	0.01	0.01	0.01	
F								
OH		16.00	16.00	16.00	16.00	16.00	16.00	
"Y"		11.90	12.00	11.99	12.00	11.99	12.00	
"Z"		8.00	8.00	8.00	8.00	8.00	8.00	

Structural Formulae

The structural formulae of chlorite has been calculated for an ideal cation content of 20 cations. The formulae are given in Tables 15, 16.

The octahedral cation plot (Fig. 16) shows the distribution of $\text{Al}^{\text{IV}}\text{Ti}$, FeMn , and Mg , in coexisting muscovite, biotite, and chlorite phases. The chlorites cluster with two exceptions: Sample #5 is FeMn -rich, and Sample #6 is $\text{Al}^{\text{VI}}\text{Ti}$ -rich. With the exception of Sample #5, which is anomalous in all the phyllosilicates, there is a constant $\text{Mg}/\text{Mg} + \text{Fe}$ ratio in terms of the octahedral cation content. The position of Sample #6 is interesting as it has a higher octahedral $\text{Al}^{\text{VI}}\text{Ti}$ content than Sample #2, which, on an A.K.F. (Fig. 10), is too Al -rich to form biotite. The position of this sample does, however, stress the importance of a constant $\text{Mg}/\text{Mg} + \text{Fe}$ ratio in the octahedral site. The $\text{Al}/\text{Mg} + \text{Fe}$ ratio appears to allow some flexibility. The significance of the $\text{Mg}/\text{Mg} + \text{Fe}$ ratio has been mentioned previously, and will be discussed at a later stage.

The chlorite and biotite $\text{Al}/\text{Mg} + \text{Fe}$ ratios suggest an equilibrium assemblage, although Sample #4 would appear to be high in biotite, and low in chlorite (Fig. 15). By comparison with the muscovite-biotite plot (Fig. 16) biotite ought to be normal, in which case the chlorite value is very low indeed.

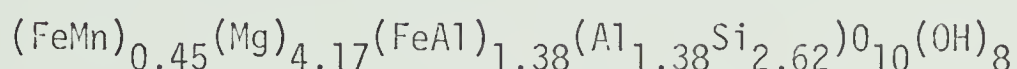
The Al content is distributed between Al^{IV} and Al^{VI} sites. The Al^{IV} content is a control on the amount of Si^{IV} present, and in Samples #5, 6 this is fairly high. Conversely, Sample #2 is lower in Si^{IV} and higher in Al^{IV} .

Discussion

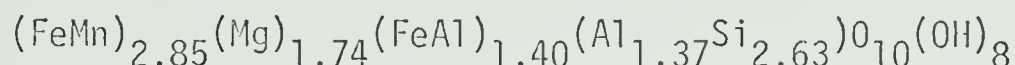
The equilibrium textures observed for chlorite are reflected in the mineral chemistry. The chlorites are extremely uniform in composition and appear to belong to an equilibrium assemblage. Apart from some slight variation in Si content and a small range in the $Al/Mg + Fe$ and $Mg/Mg + Fe$ values there is little observed variation. This is significant because Sample #2 lacks a coexisting biotite phase, and presumably has not been involved in a biotite-producing reaction. The composition of the coexisting muscovite and chlorite phases in this sample are in part fixed by the whole-rock chemistry. The $Al/Mg + Fe$ ratio of the muscovite is high and the ratio for the chlorite is very slightly higher than for the normal three-phase chlorites. Because of its critical composition, Sample #2 did not react to form a biotite phase, and presumably any rocks having a chlorite with a higher $Al/Mg + Fe$ ratio would also have remained unaltered. Sample #2 therefore is above the highest $Al/Mg + Fe$ chlorite ratio possible to produce biotite under the present metamorphic conditions. The chlorite texture in Sample #2 is similar to that of muscovite, and it appears to be formed syn-tectonically. The three-phase chlorites are all porphyroblastic and syn- to post-tectonic in age. These chlorites have certainly been recrystallised and appear to have been crystallised with the maximum $Al/Mg + Fe$ ratio possible. The $Mg/Mg + Fe$ ratio of chlorite in this sample is essentially no different from that found for the three-phase chlorites, which suggests that recrystallisation of the mineral is not necessary in order to equilibrate Mg and Fe with the coexisting phases, and that the biotite producing reaction itself is not responsible for

fixing the Mg/Mg + Fe ratio.

The chlorite grade chlorite which reacted to form the biotite and chlorite porphyroblasts must have had a lower Al/Mg + Fe ratio than the resultant chlorite, and had an unknown Mg/Mg + Fe ratio. The only estimate available as to the composition of the chlorite grade chlorite is from X-ray diffraction work on samples at Jasper. The following composition was calculated by Evans (1961) using a method developed by Shirozu (1958); the technique is poor and the composition is admittedly suspect.



Sample #3 from Mount Robson in a similar format is:



According to Evans the Mg^{++} to Fe^{++} ratio of the chlorites is 3.67:1. Similar estimations by Stauffer (1961) give a ratio of 3.6:1, and by Weiner (1966) is 3.1:1. These values may also be rather unreliable.

The chlorites at Mount Robson give an average ratio of 0.61:1, and in Sample #5 it is as low as 0.48:1. The implication is that there is a six-fold decrease in Mg content as one increases the metamorphic grade. Rather ironically there is a substantial Fe increase with metamorphic grade, counter to the accepted partitioning trend. The reason for this, as for the anomalies encountered with the muscovite, is thought to be the formation of ankerite in place of the chlorite grade siderite and calcite reported from the sediments at Jasper (Charlesworth et al., 1967). The addition of ankerite as a fourth ferromagnesian phase greatly influences the distribution of Fe and Mg in the system.

If the (AlFe^{+++}) content of the chlorite given by Evans is completely made up of Al, and the amount of Fe^{+++} is likely to be small, then the total Al cation content in the structural formulae is equal to,

or less than any of the values at Mount Robson, with the exception of Sample #4 which is known to be Al/Mg + Fe deficient.

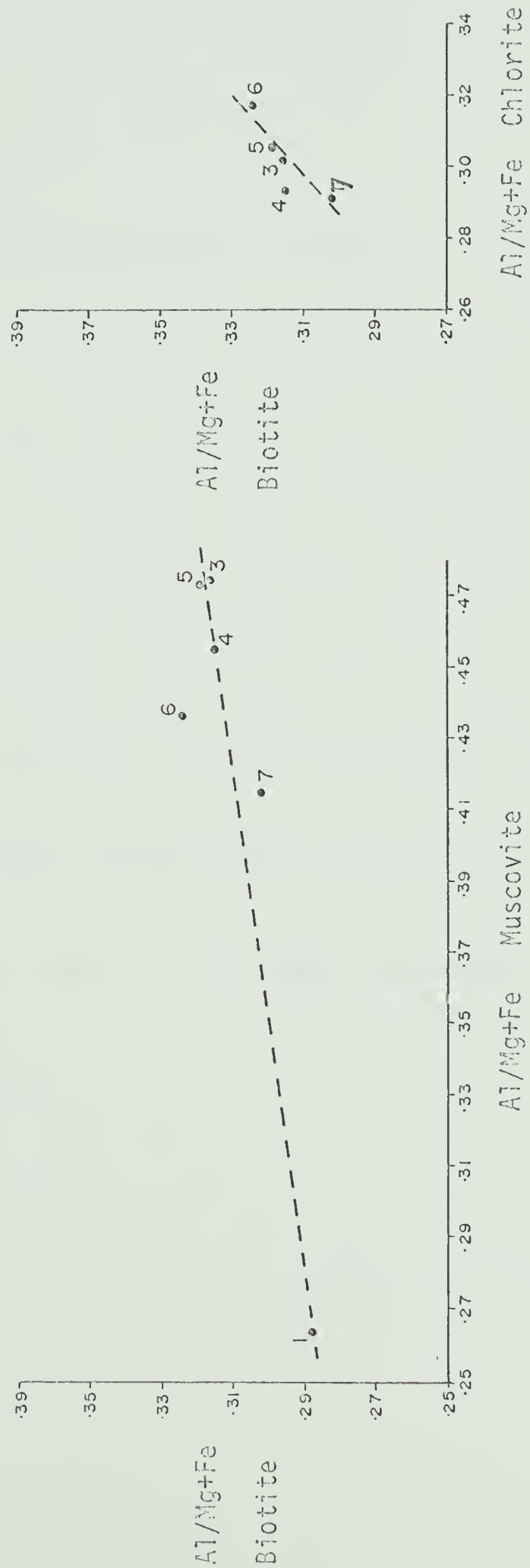


Figure 24

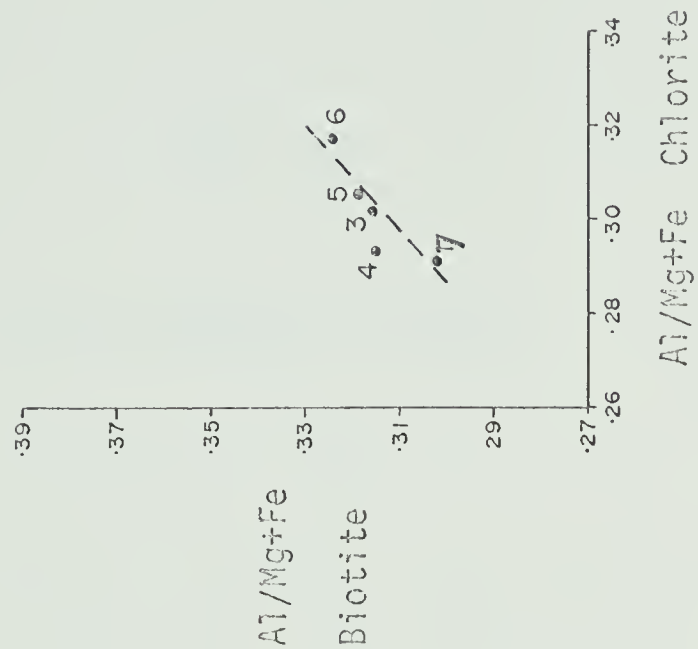


Figure 25

TABLE 17

Carbonate Chemical Analyses

	1	2	3	4	5	6	7	8A	8B
CaO	26.44	26.32	26.60	0.43	26.43	25.87	26.48	27.79	53.39
FeO	16.81	15.33	15.72	42.61	18.09	15.67	15.39	10.87	2.30
MgO	7.70	8.49	8.66	10.26	7.25	8.12	8.53	10.86	1.04
MnO	1.40	1.22	0.58	1.47	1.10	1.17	1.49	0.53	0.38
SrO	0.14	0.03	0.07	0.03	0.07	0.07	0.08	0.02	0.05
CO ₂	45.63	47.02	46.24	43.45	45.31	46.56	46.03	47.48	43.35
	98.12	98.41	97.87	98.25	98.25	97.46	98.00	97.55	100.51
Mg/Mg+Fe	.4520	.4992	.4979	.3023	.4191	.4826	.4994	.6426	.4490

Carbonate Chemistry

Carbonate is found in all of the samples analysed. In Samples #1-7 there is only one stable carbonate phase. However, in Sample #8 the calcareous schist, two carbonate species are present.

The carbonate analyses are shown in Table 17. In Samples #1, 2, 3, 5, 6, 7, the carbonate appears to be an ankerite, falling midway between the two end members, $\text{CaFe}(\text{CO}_3)_2$ - $\text{CaMg}(\text{CO}_3)_2$. The Mg/Mg + Fe ratio varies slightly, indicating enrichment towards the Fe-rich end member.

In Sample #4 there is a pronounced whole-rock Ca deficiency which prohibits the formation of ankerite. The carbonate found lies in the siderite-magnesite solid solution field, with the Mg content slightly in excess of that found in the ankeritic carbonates.

The calcareous schist recrystallised to form a relatively pure calcite and an anomalous "ankerite". The calcite phase contains only a minor amount of Fe and Mg in solid solution. The ankeritic carbonate phase contains less Fe and correspondingly more Mg than the others, in which the Mg content is approximately equal to that of Fe. The anomalous ankerite is also slightly richer in CaO content. The MnO content ranges from 0.5-1.5 percent in the ankeritic phases, and is less in pure calcite. A trace of Sr is found throughout, and is significantly above the average in Sample #1. The low totals are unlikely to indicate appreciable concentrations of any other element and they may in part be analytical error, resulting from the tendency for carbonates to burn and defocus the electron microprobe beam during analysis.

Structural Formulae

The carbonate structural formulae given in Table 18 are

TABLE 18

Carbonate Structural Formulae
based on 2 cations

	1	2	3	4	5	6	7	8A	8B
Ca	1.03	1.02	1.04	0.02	1.03	1.03	1.03	1.07	1.88
Fe	0.51	0.47	0.48	1.35	0.55	0.49	0.47	0.33	0.06
Mg	0.42	0.46	0.47	0.58	0.39	0.45	0.46	0.58	0.05
Mn	0.04	0.03	0.02	0.05	0.03	0.04	0.05	0.02	0.01
Sr	-	-	-	-	-	-	-	-	-
O	6.78	6.87	6.88	6.76	6.72	7.07	6.82	7.01	5.82
C	2.26	2.29	2.29	2.25	2.24	2.36	2.28	2.34	1.94

calculated on the basis of 2 cations. The carbon chemistry may be represented in terms of the three end members: calcite, siderite, and magnesite, and are shown in Fig. 26. From the figure it is apparent that the amount of calcite component in the ankerite is fixed at 53 cation percent Ca. The Mg/Mg + Fe ratio is variable, but tends to cluster at a maximum value which allows equal parts of magnesite and siderite into the structure at 24 catio percent.

In Sample #4 there is 30 cation percent Mg in the siderite solid solution. Similarly there is 30 cation percent Mg in the anomalous ankerite of Sample #8; this increase is off-set by a reduction to 16 cation percent of Fe content.

Discussion

In Sample #4 the obvious lack of Ca in the whole-rock content prohibits the formation of ankerite and requires Fe to substitute in the Ca position. The amount of excess Mg which goes into the Ca site is far less, and the resultant Mg/Mg + Fe content of the carbonate is thus very low. By restoring the "ideal" amount of Ca for an ankerite in place of Fe, the Mg/Mg + Fe ratio is slightly higher than normal.

The two phases in Sample #8 are the result of subsolidus immiscibility insofar as one carbonate could not take up the Ca, Fe and Mg available. The rock is low in free silica and the carbonate phase appears to have 'fixed' the Fe and Mg released by the clay component as it upgraded to a biotite grade muscovite. Muscovite is the most common silicate in the rock which contains traces of chlorite and presumably chloritoid, although it was not seen. The carbonate "sink" reduces the necessity for ferromagnesian silicates.

Rosenberg (1967) studied the subsolidus relationships between

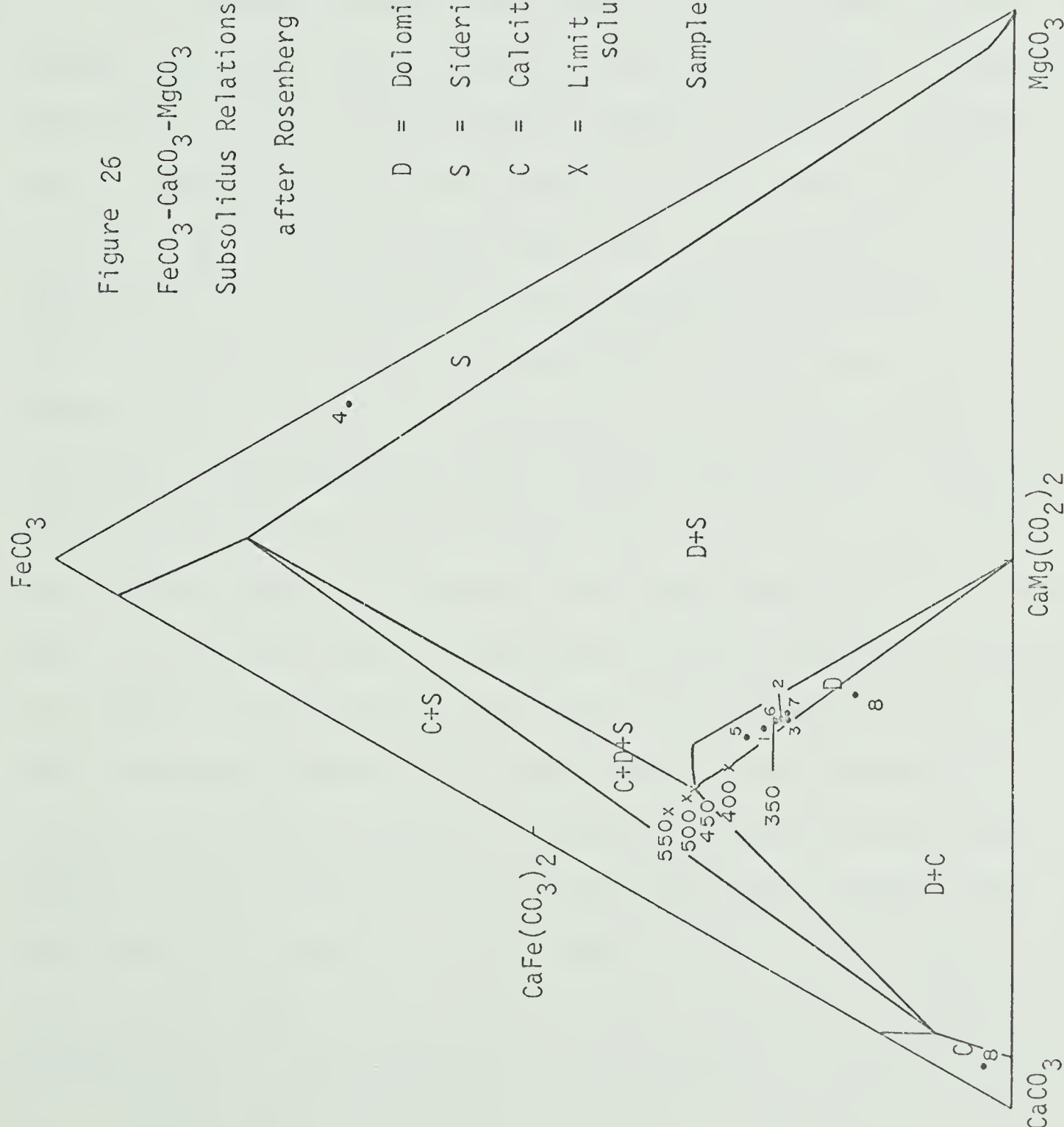


Figure 26

FeCO_3 - CaCO_3 - MgCO_3

Subsolidus Relations at 450°C and 2 Kb

after Rosenberg 1967

D = Dolomite solid solution

S = Siderite solid solution

C = Calcite solid solution

X = Limit of ferroan dolomite solid solution at 450°C etc.

Samples #1-8

CaCO_3 , MgCO_3 , and FeCO_3 , at temperatures ranging from 350°C to 550°C. He found that the system is insensitive to pressure and conducted his experiments between 2-3 Kbars.

The stability field relationships at 450°C are shown in Fig. 26. Stability field shapes are constant across the temperature range, although field sizes vary.

The system includes a three phase field low in Mg CO_3 which includes the phases calcite, siderite, and ferroan dolomite. An ordered solid solution series extends from the $\text{CaMg}(\text{CO}_3)_2$ dolomite end members towards $\text{CaFe}(\text{CO}_3)_2$, the Fe-rich equivalent. This is never attained, as it first reaches the above three-phase field. The maximum Ca and Fe substitution in the dolomite structure is temperature-dependent, and marks the attainment of the three-phase field. The dolomite - ferroan dolomite series lies in a belt containing a constant 50-56% CaCO_3 . This value tends to increase slightly with Fe substitution. The compositions at which the Ca and Fe contents reach a maximum and the three-phase field is reached are marked for the temperatures, 350°, 400°, 500°, 550°C. At 350°C the value is only known in terms of maximum Fe content. It is interesting to note that the amount of Fe solid solution increases with temperature increase, which runs counter to the accepted phyllosilicate trend of Mg enrichment. There are also two disordered solid solution series, a narrow field around calcite, which increases with temperature, and a complete siderite-magnesite solid solution series. Separating the above fields are areas of single carbonate instability. Two-phase areas, calcite-siderite, calcite-dolomite and dolomite-siderite.

Sample #8 presumably falls within the calcite-dolomite field, and Sample #4 the siderite solid solution field. The others all lie in

the dolomite solid solution range. As none of these samples have reached the three-phase field they cannot be considered to be saturated in Fe, and they thus give minimum temperatures only.

The actual Mg/Mg + Fe ratio of the carbonate is closely linked with the coexisting mineralogy and there would appear to be a tendency for ankerite and chlorite to become "saturated" in Mg at Mg/Mg + Fe ratios of 0.5 and 0.38 respectively. Whether the coexisting phyllosilicates impose a constraint on the carbonate Mg/Mg + Fe ratio, or the carbonate ratio constrains that of the silicates remains a problem!

Sample #5, the most Fe-rich sample, gives an ankerite minimum temperature on Figure 26 of $375^{\circ} \pm 25^{\circ}\text{C}$. According to Rosenberg, this carbonate cannot be formed at a lower temperature. Similarly Sample #1 suggests a minimum temperature of $360^{\circ} \pm 25^{\circ}\text{C}$, and the main group of ankerites, by extrapolation of Rosenberg's data, suggest a minimum of $330^{\circ} \pm 25^{\circ}\text{C}$. These values suggest that all the carbonates formed above 325°C , and Sample #5 formed above 375°C .

Winkler (1967, p. 99) states that calcite is the only carbonate phase stable with free quartz in the biotite metamorphic grade. If this is correct then the ankerite and siderite phases must be unstable, or late and retrogressive. There is little evidence to support retrogression, the textural evidence suggests good equilibrium and the late porphyroblasts of chlorite are restricted to biotite-bearing assemblages. They appear to be prograde formed in the biotite-producing reaction.

Chlorite grade carbonate porphyroblasts are poikiloblastic and although re-equilibrated, this textural feature is retained in the biotite grade carbonates, which form "eyes" drawn out by the schistosity and enveloped by biotite and chlorite (Plate IV, #7). This textural

evidence argues against the destruction of chlorite grade carbonate and its regeneration during cooling. Ankerite must have been stable during the biotite grade metamorphism and the remarkable degree of chemical equilibrium suggests only one period of stabilization.

Mg/Mg + Fe Ratio

The octahedral cation plot of the various phyllosilicates (Fig. 16) brings out one of the most important characteristics of the rock mineralogy. The three-phase muscovites, and biotite show some spread in the Mg/Mg + Fe ratio of the phase, whereas chlorite, with the exception of Sample #5 does not. Mg/Mg + Fe plots for the four coexisting ferromagnesian phases (which includes ankerite) illustrate this point and indicate the same tendency in ankerite.

The plot of muscovite Mg/Mg + Fe ratio against ankerite (Fig. 30) suggests an equilibrium linear relationship between the two, with ankerite reaching a saturation point in Mg/Mg + Fe ratio at 0.5, while muscovite continues to increase its ratio. Samples #2, 7, 3 would appear to be "saturated" in Mg. The same result is obtained by plotting biotite Mg/Mg + Fe against ankerite (Fig. 31). As the biotite ratio increases, so does the ankerite ratio until the 0.5 mark, thereafter Sample #7 rises independently in biotite.

The chlorite, ankerite, Mg/Mg + Fe plot (Fig. 27) shows the same relationship, only the chlorite itself appears to cluster at a fixed ratio.

Plots of muscovite Mg/Mg + Fe ratio against chlorite (Fig. 28) and biotite Mg/Mg + Fe ratio against chlorite (Fig. 32) bring out exactly the same relationship.

Two points would appear to be clear, both chlorite and ankerite increase their Mg/Mg + Fe ratios to a fixed maximum. This "saturation" point is at 0.38 and 0.5 Mg/Mg + Fe ratios respectively. Also, there is a definite linear relationship between a phase that "saturates",

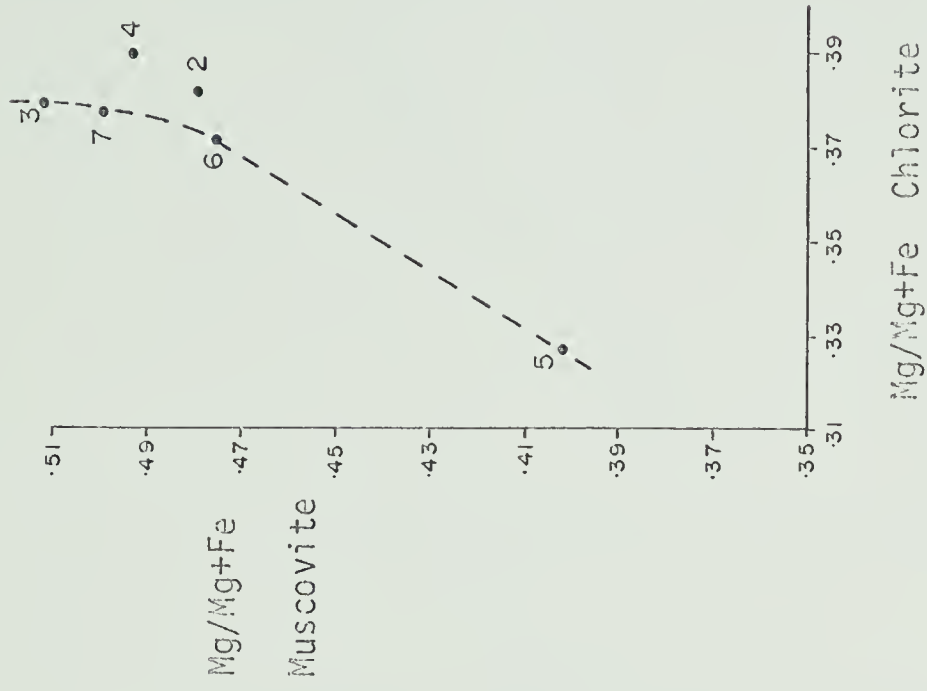


Figure 27

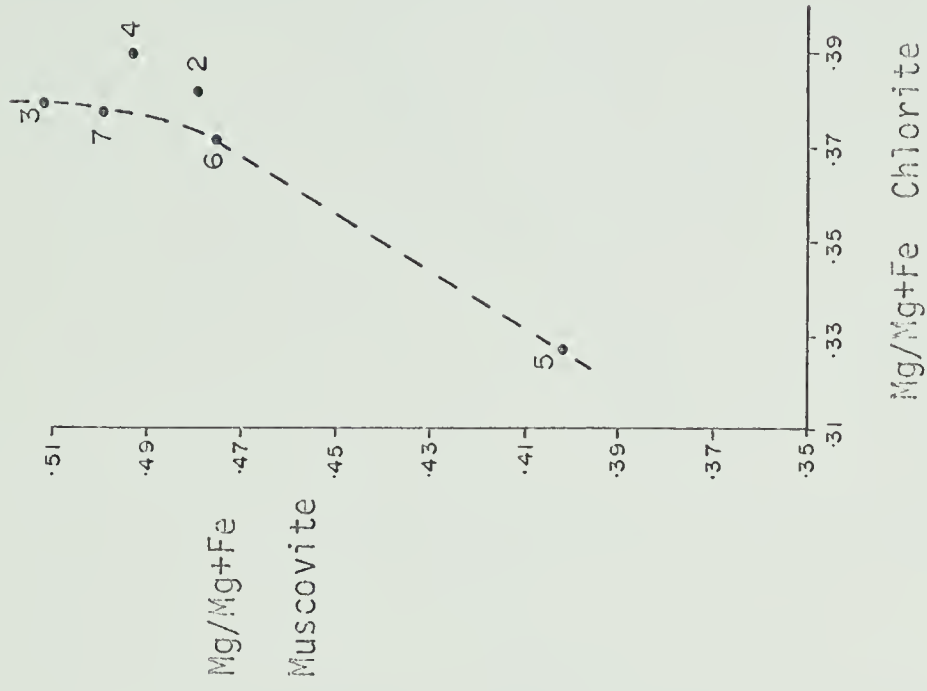


Figure 28

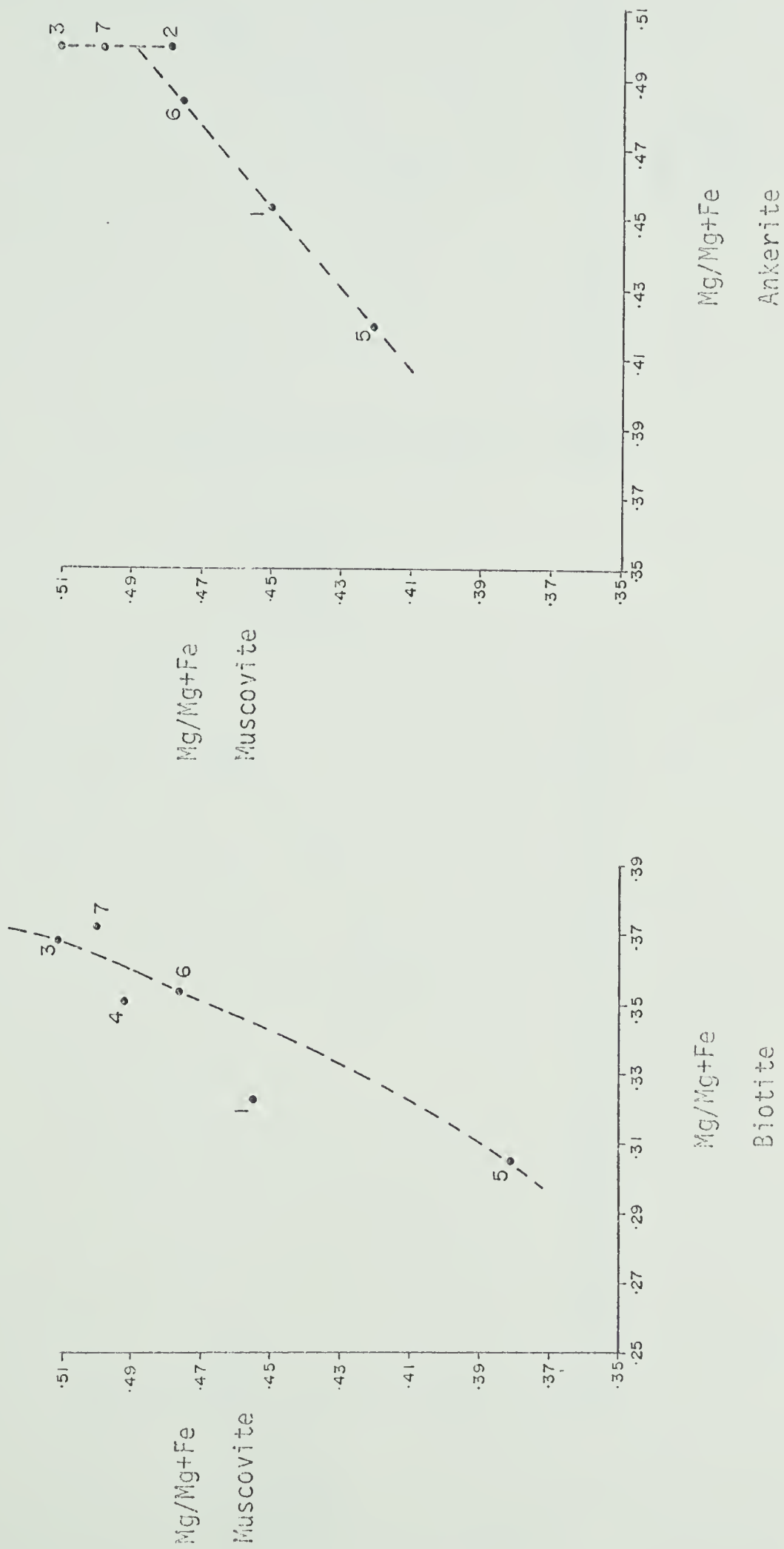


Figure 29

Figure 30

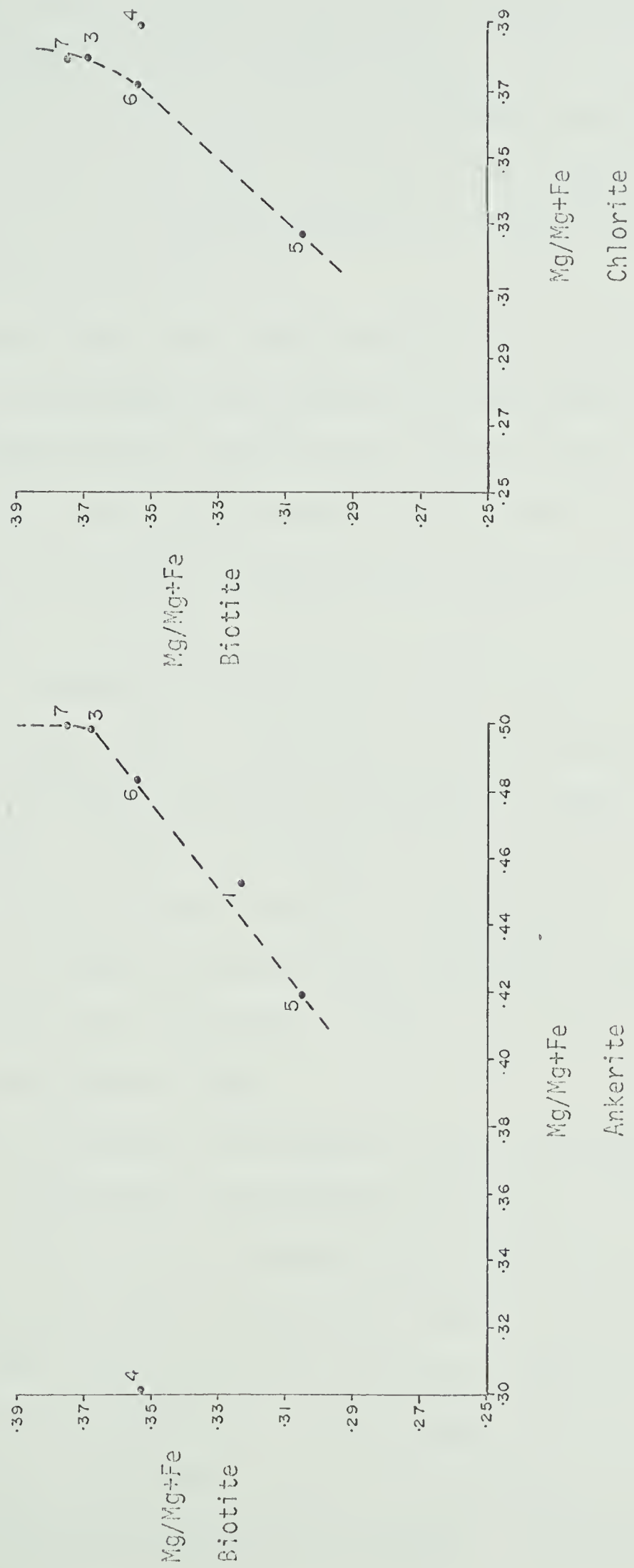


Figure 31

Figure 32

i.e. ankerite and chlorite, and any other phase in terms of their non-"saturated" Mg/Mg + Fe ratios, Samples #5, 6.

The coexisting muscovites, biotites, chlorites and ankerites systematically increase their Mg/Mg + Fe ratios in the sample order, Sample #5, 1, 6, 2, 3, 7, in which Samples #2, 3, 7 reach saturation point in ankerite and chlorite.

The absence of one phase, either biotite or chlorite, appears to alter only one other phase in the system, thus the absence of biotite from Sample #2 leaves chlorite and ankerite "saturated" but reduces the muscovite ratio. Similarly, the absence of chlorite from Sample #1 leaves ankerite and muscovite in equilibrium and reduces the biotite Mg/Mg + Fe ratio.

Normality is measured relative to the set of interrelated Mg/Mg + Fe distribution curves. However, the variations noted above and the effect of the anomalous carbonate in Sample #4 appear to be systematic and real. In the case of Sample #4 the chlorite is too high in its Mg/Mg + Fe ratio and the carbonate is exceedingly low. As noted earlier, however, the total Mg content in the carbonate is slightly high, and this, rather than the Mg/Mg + Fe ratio, may be the controlling factor governing the chlorite ratio.

According to Rosenberg, the stability field of the ankerite increases with Fe substitution and temperature increase. Thus Sample #5, which is high in Fe in all its phases, has a higher minimum temperature of formation than Sample #3 which has a lower Fe content all round. This anomalous state is best explained by allowing a common fluid control and "buffer" the chlorite and carbonate Mg/Mg + Fe ratio.

The carbonate distribution pattern at 50:50 MgCO_3 and FeCO_3 appears to be extremely odd and rather coincidental. Although there is

no known reason why the carbonate should crystallise this $\text{CaFeMg}(\text{CO}_3)_2$ ratio in preference to any other in the series, it would appear to do so. As the carbonate reaches its "ideal" equilibrium ratio it increases the chlorite $\text{Mg}/\text{Mg} + \text{Fe}$ ratio proportionately. Where there is insufficient Mg, it is proportionated between the phases which thus appear undersaturated, e.g. Sample #5.

The $\text{Mg}/\text{Mg} + \text{Fe}$ saturation point may be related to metamorphic grade; however, the apparent grade increase from Sample #5 through to Samples #3, 7 is compositional. The Mg-poor samples (a function of $\text{Mg}/\text{Mg} + \text{Fe}$ and $\text{Al}/\text{Mg} + \text{Fe}$) give a better indication of metamorphic grade because they give a better indication of the minimum temperature of metamorphism. The system is further complicated by Atherton's (1965) observation on the importance of the $\text{Mg}/\text{Mg} + \text{Fe}$ ratio on the stability of a mineral. Thus, the higher the Mg content of the chlorite grade mineralogy, the less likely it will be for it to react. The chlorites from Jasper may be Mg-rich and the temperature of equilibration might well be a lot higher than that suggested by the Fe-rich anomalous minimum in Sample #5.

Albite Occurrence

The anomalously high albite content of the Miette group sediments of Jasper has been attributed to post depositional Na metasomatism of detrital clasts of microcline and plagioclase (Charlesworth et al., 1967). The chemical implications of this period of ionic exchange in the feldspars has been noted elsewhere (see page 137).

Albites with the characteristic "chessboard" pattern, as viewed in thin section under crossed nicols (Plate V, #5) are found part of the coarser sedimentary fraction. Original clastic outlines remain, although mechanical disruption may occur in the Western Zone. The internal structural pattern results from the truncation of the albite lamellae by the [001] cleavage (Charlesworth et al., 1967). Albites of this type are stable throughout the area, although they tend to be lost during the formation of a pronounced recrystallized biotite schist.

Many of the larger chessboard albites contain within them rectangular inclusions of unaltered plagioclase feldspar, with a moderate but variable anorthite content, up to An_{45} . These resemble remnants of plagioclase found by Krupicka (1970, pers. comm.) in Hudsonian microclines. For such remnants to remain after albitization of the clast, they must be compositionally very different from their original host. This was probably microcline, thought by Krupicka to have replaced much of the preHudsonian gneissic plagioclase during a period of K metasomatism associated with the Hudsonian orogeny. The textural relations of these inclusions and their composition argue against exsolution in a perthite. Significantly microlites of white mica are

often associated with albites of this type. Albite formed from microcline has a higher obliquity than its host, thus the lamellae get disrupted and the chessboard pattern results.

Plagioclase laths may also alter to chessboard albite and are converted to the albite composition at very low metamorphic grades. A maximum of 3.0% An is found in the albite produced (Voll in Brown, 1964). The plagioclase twin lamellae may be retained, thus giving deceptive optical An content determinations. In such cases the feldspar tends to be associated with microlites of white mica. Alternatively the plagioclase disrupts completely and becomes cloudy as the structure breaks down into almost submicroscopic crystal domains. According to Voll, who worked on the Dalradian rocks of Scotland, these crystal lattice domains delimited by [010] and [001] cleavages may grow to give the chessboard structure. Voll states that "Carbonate in the rock appears to hasten the domain growth". This point is very interesting as it may tie the occurrence of the chessboard pattern to a high fugacity of carbon dioxide, which is certainly evident in the present study.

Albite X-ray Diffraction Data

A large clast of albite was isolated from a stretched pebble conglomerate belonging to Unit A in the Western Zone.

The sample was analysed using Ni filtered $\text{CuK}\alpha$ radiation, $\lambda = 1.54178 \text{ \AA}$, with slits at 4° . Lithium fluoride was added as an internal standard. A scale factor setting of 8×1.0 and scanning speed of $0.5^\circ 2\theta/\text{minute}$ were used.

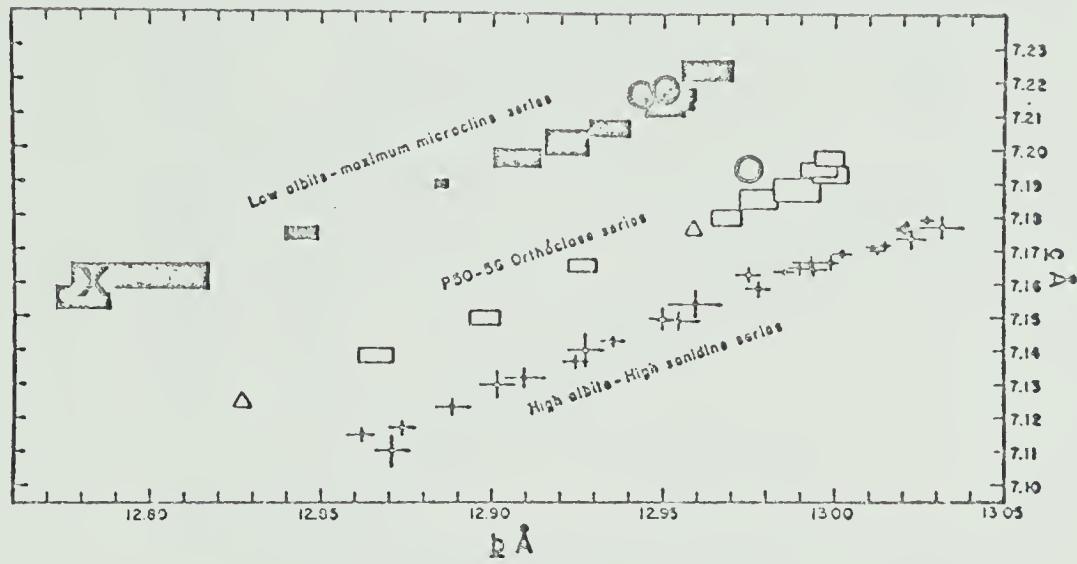
Approximate composition, structural state, and unit cell dimensions were calculated using the formulae of Orville (1967) and these were refined using the "least squares" programme of Evans, Appleman and Handwerker (1963).

The composition of the albite, which lies in the "microcline-low albite" series would appear to approximate to pure albite, with a maximum of 2.0% contamination. Samples analysed on the Electron Microprobe give the following composition; Ab = 98.93, Or = 0.47, An = 0.59, well within the limits determined by X-ray analysis.

The unit cell length 'a' is independent of structural state and is proportional to the composition of the feldspar, whereas unit cell lengths 'b' and 'c' are related to the Al:Si order-disorder state of the lattice structure, and are used to classify the feldspar state. With a decrease in the degree of order 'b' increases, and 'c' decreases in length. Similarly the unit cell α^* and γ^* plot to give a sensitive indicator of structural state (Fig. 33-35).

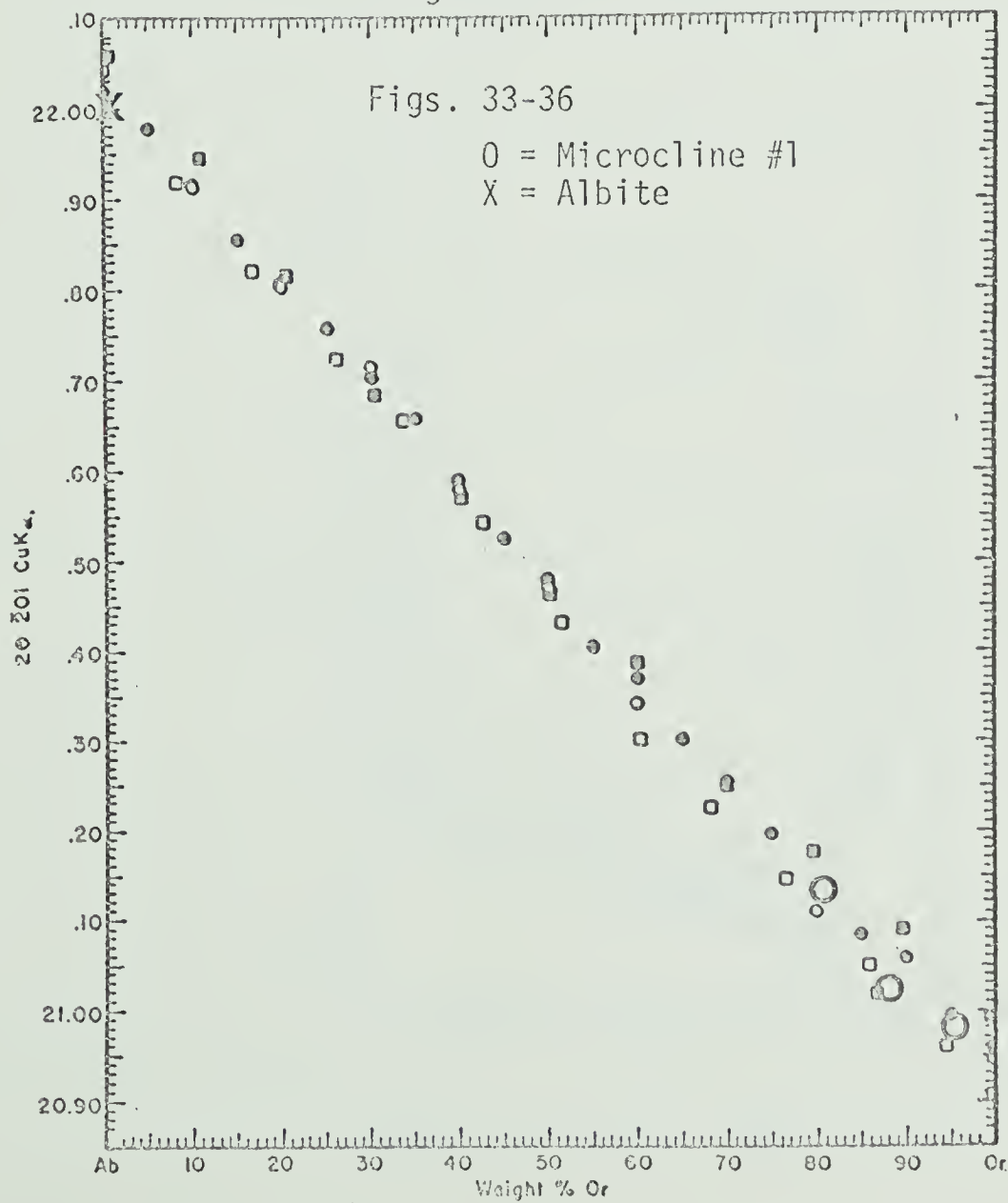
The sample analysed lies close to the "microcline-low albite" series plot of Orville, at the low albite end. The 'c' cell length appears to be slightly longer than is usual, and on a α^* , γ^* plot the sample lies on the projection of the "high albite-low albite" series. The albite is thus anomalously "low". This fact is brought out by the failure of the least squares programme to converge. Only one parameter appears to be out, and this may indicate either an inherited feature, or else a stress effect on the crystal lattice. Possibly the high 'c', a function of good Al:Si order, is inherited from an early microcline phase.

Figure 33



Data from Wright and Stewart, 1968, p. 46

Figure 34



Data from Wright and Stewart, 1968, p. 93

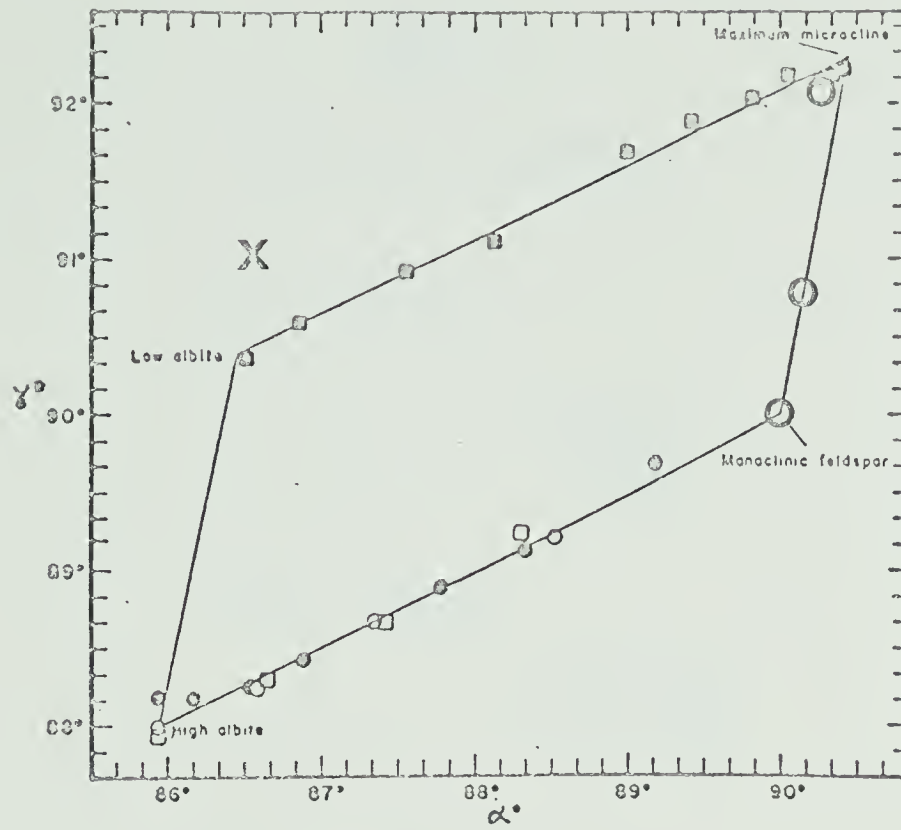


Figure 35

Data from Wright and Stewart, 1968, p. 48

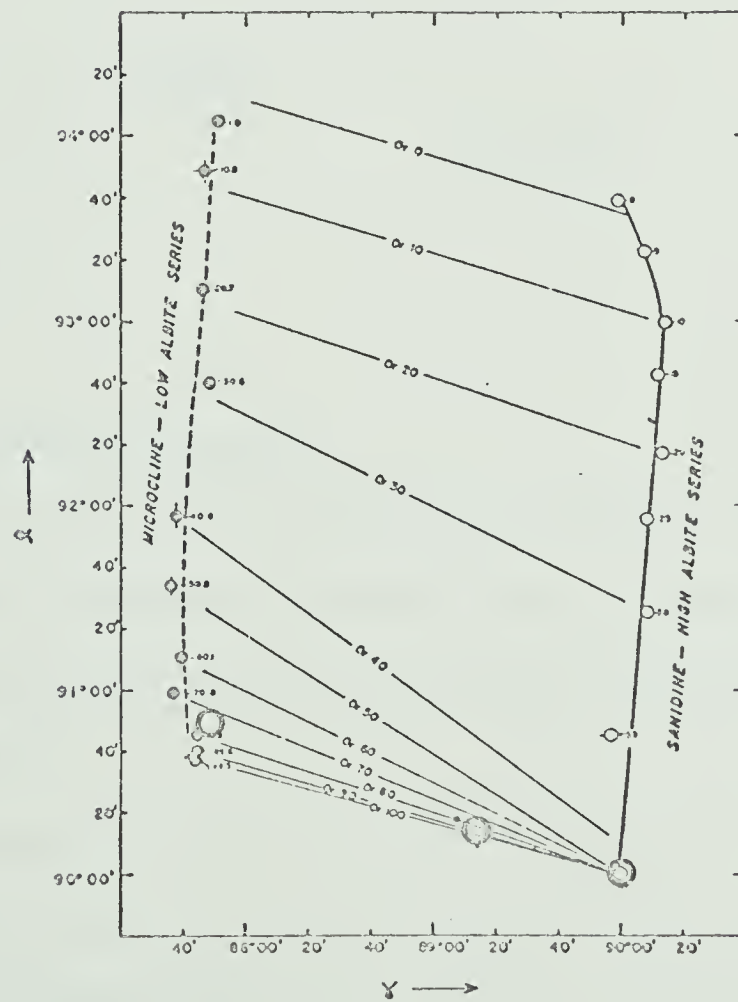


Figure 36

Data from Orville, 1967, p. 78

TABLE 19

Albite Cell Parameters

Cell Dimensions

a	8.13 Å
b	12.78 Å
c	7.16 Å

Normal Lattice

α	94° 20.00'
β	116° 36.00'
γ	87° 10.00'

Reciprocal Lattice

α^*	86° 34.00'
β^*	63° 31.00'
γ^*	91°

Volume

V	663.60 Å
---	----------

Microcline X-ray Diffraction Data

Two large clasts of microcline were isolated from the same hand specimen which produced the albite of the previous section. They were analysed separately, using the same operating conditions as for albite (Fig. 33-36).

The structure of the first microcline (#1) is complex, at least two potash feldspar phases are found with one albite phase. The feldspar is "perthitic" although whether the albite was exsolved or exists in

the form of included fragments is not known.

"Least squares" structural determinations allow different combinations of peaks to "converge" and give a set of cell parameters which may be assigned to maximum microcline, intermediate microcline, and orthoclase, the three structural states. In rocks which have undergone strain these should perhaps be treated with caution; however, the long and complicated history of the microcline might allow the three phases to coexist. The "orthoclase" phase contains approximately 19% albite in solution, judging from its $[\bar{2}01]$ peak position (a function of 'a' cell length). The "maximum microcline" phase contains approximately 12.0% albite, and the intermediate phase 5.0% albite. The cell dimensions in this sample do not comply with the ideal. Both the microcline cell lengths 'b' and 'c' suggest maximum microcline, the cell angles α and γ clearly indicate that one phase is intermediate in structure to between maximum microcline and orthoclase. Possibly one of the two features is "inherited" from the earlier phase. The intermediate microcline is disordered, and the 'b' and 'c' lengths are probably anomalous. The polyphase nature of the feldspar is interesting, in view of the assumed Hudsonian source area, and the possibility of an early period of microclinization (Burwash and Krupicka, 1969). It is, however, impossible to interpret at this stage, in view of the known period of post depositional alkali exchange. These clasts are relicts which survived the albitization process, although their structural state may have been affected.

The second microcline (#2) was also a "perthite" with three distinct potash phases distinguishable on an X-ray diffraction chart. The phases consist of maximum microcline, with 3.0% albite, with a

"normal" structural state lying on the maximum microcline-low albite join, and two intermediate microclines, with 9.0% albite, and 13.0% albite respectively.

Increase in Na is accompanied by a decrease in the 'b' and 'c' cell dimensions. This moves the structure towards the albite disordered state. There is a pronounced shift in the intermediate microclines towards the orthoclase structure, a higher temperature structural state.

Significantly Wright (1967) and Steiger and Hart (1967) find that the maximum microcline structure becomes unstable at $375 \pm 50^\circ\text{C}$ and 460°C respectively. The transition from maximum microcline to orthoclase is usually sharp in a contact metamorphic environment, and intermediate microclines are rarely found as a stable phase. Possibly the maximum microclines presently under study are in the process of conversion to orthoclase.

The cell data given for both albite and microcline probably reflected the genuine order of magnitude of the unit cell parameters. Levels of accuracy are controlled by the original experimental observations and the nature of the "least squares" programme. They are thus hard to estimate without extensive calibration. It is unlikely that the error factor involved is sufficient to alter the arguments presented.

TABLE 20

Microcline #1 Cell Parameters

	Maximum Microcline	Intermediate Microcline	Orthoclase
Lengths			
a	8.567 Å	8.601 Å	8.466 Å
b	12.953 Å	12.947 Å	12.977 Å
c	7.215 Å	7.214 Å	7.206 Å
Volume	718.115 Å	721.732 Å	719.125 Å
α	90°-41.0'	90°-9.00'	90°-00.00'
β	116°-10.0'	116°-2.00'	115°-52.00'
γ	87°-52.0'	89°-16.00'	90°-00.00'
α^*	90°-17.0'	90°-11.00'	90°-00.00'
β^*	63°-51.0'	63°-53.00'	64°-8.00'
γ^*	92°-2.0'	90°-44.00'	90°-00.00'

PHYSICAL AND CHEMICAL CONSIDERATIONS

Physical Conditions

The textural relationships of the coexisting phases and the degree of chemical equilibrium suggest that a high degree of equilibrium was attained throughout the whole system. There is a strong possibility that, within the limitations of the coexisting phases, the physical environment was able to "buffer" the assemblage and influence the phase chemistries of the individual mineral species. The strongest argument for this is the pronounced effect the addition of a carbonate phase makes on the system's Mg/Mg + Fe ratio.

Variables such as temperature, pressure and the fugacities of oxygen, sulphur, and carbon dioxide may influence the system.

Oxides and sulphides both deplete the silicate system in Fe and thus tend to increase the Mg/Mg + Fe of the silicate system. The oxide assemblage itself influences the ratio of $\text{Fe}^{++}/\text{Fe}^{+++}$ in the rock. The addition of an ankeritic carbonate provides a buffer for both Fe and Mg and, as demonstrated, strongly influences the silicate Mg/Mg + Fe ratios.

Fugacity of Oxygen

The oxidation ratio of a rock, as defined by Chinner (1960) is:

$$\frac{\text{Mol } 2\text{Fe}_2\text{O}_3 \times 100}{\text{Mol } 2\text{Fe}_2\text{O}_3 + \text{FeO}}$$

This value is a measure of the degree of oxidation in the rock, and is usually buffered by individual, or pairs of oxide phases. Oxidation ratio values are given in Table 4. Samples #1, 2, 3, 4, 5 have a constant ratio around 34 and are fairly reduced. The mineralogy is buffered by coexisting ilmenite and magnetite. Sample #6 has a low ratio of 14 and contains magnetite alone. Samples #7, 8 are both high, around 54. Sample #7 is buffered by ilmenite alone, and Sample #8 contains an odd haematite-rutile assemblage.

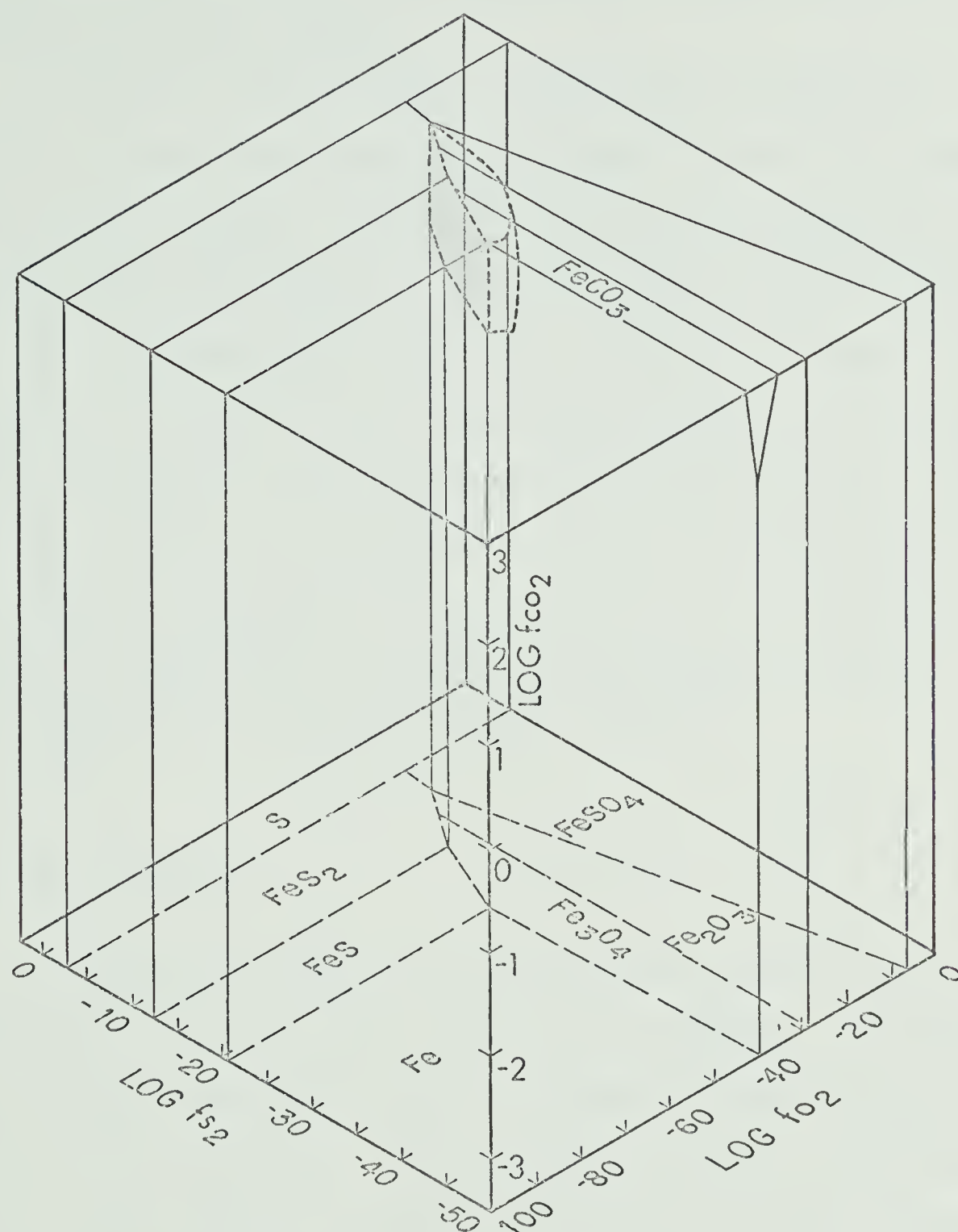
Based on Holland's (1959) fugacity diagram (for the anhydrous state at 600°K or 327°C) (Fig. 22) the magnetite-pyrite assemblage in Sample #6 suggest a minimum fugacity of oxygen of 10^{-35} atmospheres. The fugacity is unlikely to have risen much above 10^{-25} , atmospheres.

The occurrence of graphite in Sample #6 is reflected in the low oxidation state of that sample.

Sulphur Fugacity

Visible sulphides were found in Samples #4, 5, 6, 8. Pyrrhotite associated with magnetite and ilmenite would place a lower limit of 10^{-20} atmospheres sulphur fugacity on the system. The general abundance of pyrite in the Miette group sandstones and shales suggests a slightly higher value; the pyrite-magnetite assemblage in Sample #6 would increase this to 10^{-8} atmospheres of sulphur, and the haematite-pyrite association

Figure 37



After Holland. 1959

Range of S_2 , O_2 and CO_2 fugacities at 600°K as defined by the mixed assemblages

Containing - pyrite, pyrrhotite, siderite (Fe carbonate), haematite, magnetite.

in Sample #8 would increase it still further to a maximum of 10^{-6} atmospheres of sulphur fugacity.

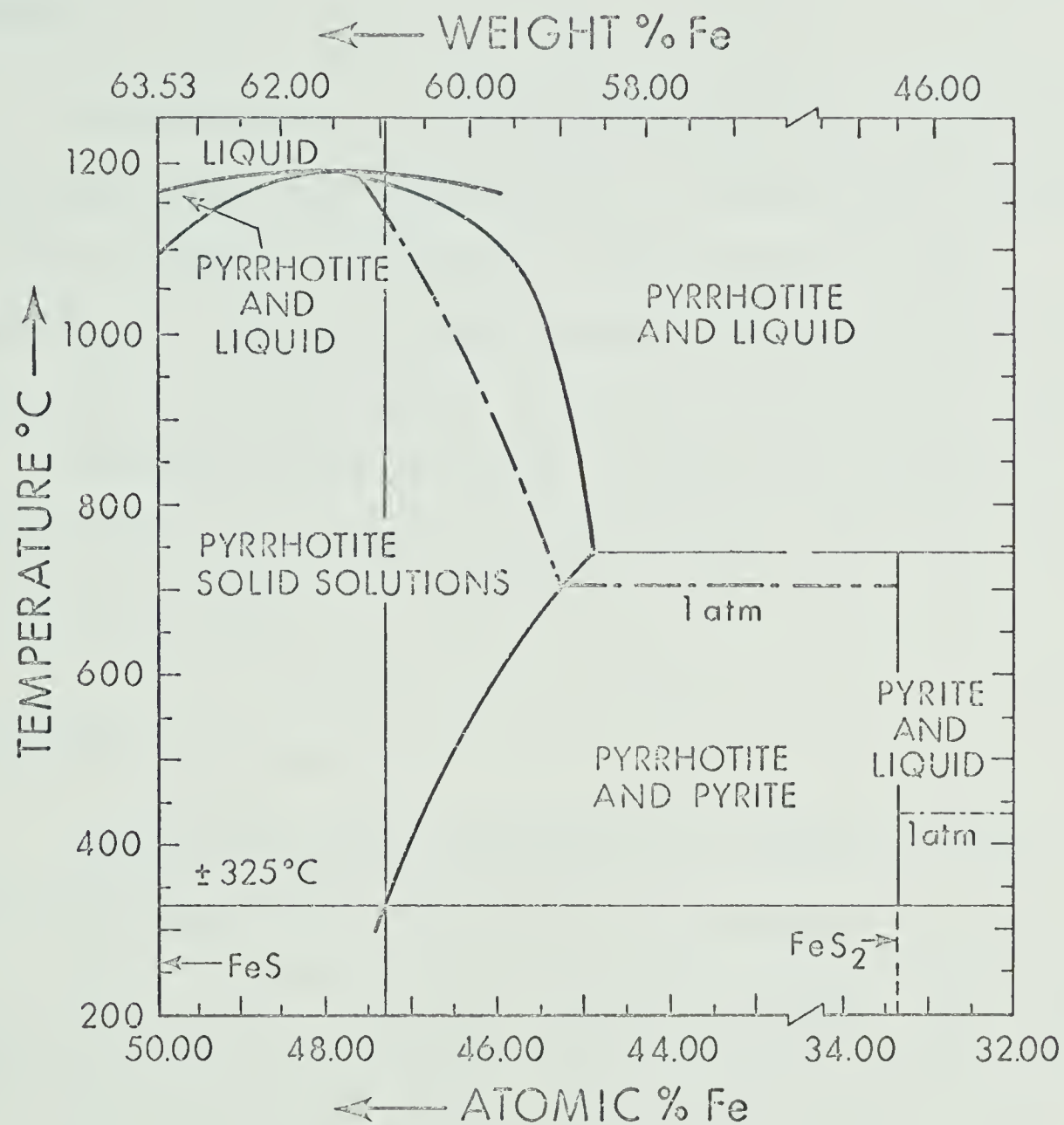
According to Arnold (1962) the composition of pyrrhotite coexisting with pyrite is temperature-dependent, and that the atomic percentage of Fe decreases in pyrrhotite coexisting with pyrite as the temperature rises. Pyrrhotite is non-stoichiometric, and the degree of Fe deficiency is temperature controlled. In the case of Sample #4, where the composition is known, there is no associated pyrite and the value is thus an indication of the minimum temperature of formation. The pyrrhotite in Sample #4 was analysed on the Electron Microprobe and was found to have the composition $\text{FeS}_{1.104}$, equivalent to an atomic Fe percentage of 47.29%. This, on Arnold's geothermometer, gives a minimum temperature of formation of 325°C (Fig. 38).

Carbondioxide Fugacity

The absence of epidote, and the ubiquitous occurrence of a carbonate phase indicates a high carbon dioxide fugacity. The fugacity of CO_2 required to stabilize an Fe-rich carbonate at 600°K (equivalent to 327°C) is 100 atmospheres. The stability of siderite, and presumably ankerite, is much reduced by temperature increase, which may explain Winkler's (1967) statement that calcite is the only stable carbonate in the biotite metamorphic grade. The high fugacity required is probably realistic.

The Upper Miette black shale unit, which overlies the Middle Miette sandstone sequence from which the samples were derived, passes into a calcareous facies west of the Trench. The limestones in this

Figure 38



Arnold, R.G. 1962 Econ. Geol., Vol. 57

Minimum Temperature of Formation of Pyrrhotite
in Sample #4

unit are metamorphosed and deformed and would be a ready source of carbon dioxide.

Pressure

Charlesworth et al. (1967) state that the equivalent Miette group sediments at Jasper were overlain by a minimum of 25,000 feet, or 8 Km of sediment; equivalent to a load pressure of 3 Kbars. Neglecting the effect of tectonic pressures associated with the deformation, the load pressure should approximate to the fluid pressure.

Shearing tends to facilitate reaction and in the Western Structural Zone, where shearing is most evident, biotite formation is locally syntectonic.

Temperature

Minimum temperatures suggested by the carbonates and the pyrrhotite compositions indicate that the temperature of stabilisation was in excess of 325°C definitely, and 375°C probably. The indications given by the muscovite compositions and biotites are that the temperature was in fact much higher than this. However, the addition of the carbonate phase has strongly influenced the muscovite composition and estimates must be treated with caution.

Mineralogical Evolution of Miette Group Sediment

The previous sections have dealt with the chemistry and mineralogy of a few selected specimens. The nature of the biotite grade metamorphosed sediments is, however, the result of a progressive evolution from detrital sediment through diagenesis, chlorite metamorphic grade metamorphism, and into the biotite grade. The route is largely unknown; however, it is very important to the evolution of the rocks and an attempt has been made to reconstruct possible, if not probable, sequence of events. This task is aided by the assumed origin and sedimentary history of the sediments discussed earlier.

A necessary assumption, which appears to be reasonable in view of the present data and the work of Shaw (1956) on meta-pelites, is that there is no ionic migration or metasomatism involved, and the sediments analysed realistically reflect the original sediments. This assumption is also in line with the findings of Allen (1967) on biotite grade Tennessee arkoses.

The rock textures, assumed source area, and bulk chemistry suggest that the original detritus consisted largely of quartz, microcline and plagioclase set in an homogenised clay matrix of illite. Most clay minerals tend to convert to illite in the marine environment and montmorillonite, kaolinite and remnant ferromagnesian minerals will tend to convert to illite after deposition during diagenesis. During this process montmorillonite will accept Mg and K, push Al^{VI} into the tetrahedral sheet, and release Si.

Illite itself, degraded by fluvial action, stabilises its structure by adsorbing K from the marine environment in preference to

Na or Ca. Although this whole process continues with increased depth of burial, the indications are that the clay was essentially illite before its final deposition.

A study by Maxwell and Hower (1967) on the Belt Series' illite in Montana indicates that the illite polymorph changes from 1 Md to 2M, and becomes more micaceous with depth of burial and grade increase, a process complete by the biotite isograd.

Wejner (1966) notes the experimental data of Velde (1964) in which illite, when heated to 300°C, "unmixes" to a "mica"-chlorite-quartz assemblage. This process is sensitive to K availability. The diagenetic-metamorphic boundary is a zone over which illite upgrades to muscovite; this process requires the phyllosilicate K requirement to double. Some of the K is obtained by "albitisation" of clasts of microcline by a process of ionic exchange, in which Na replaces K in the original clast. The rest must come from the illite itself. The formation of chessboard albite is thus likely to be an early event, at the onset of chlorite grade metamorphism (Voll in Brown, 1964). The destruction of illite releases Si, Mg, Fe, Ti, which contributes to the new chlorite grade chlorite phase. The occurrence of ilmenite and magnetite in the Jasper sediments would suggest that some of the Fe went into oxides, accounting for the high Mg content of the chlorite grade chlorite. Textural evidence both at Jasper and Mount Robson supports the idea that a monomineralic clay, illite, splits into two distinct phases.

The detrital feldspars have taken up much of the Na at low metamorphic grades, and although the average Na content of a chlorite grade phengitic muscovite is not known, it is probably slightly low.

According to Ilyama (1964) muscovite is stable in solutions ten times as rich in Na than K, thus albite and muscovite are likely to be formed. Some coarse grits and pebble conglomerates contain both albite and unaltered clasts of detrital microcline. These are unaltered within the biotite metamorphic zone. Presumably the compositions of these rocks plot towards microcline on an A.K.F. diagram, and the clay component was able to upgrade to muscovite without influencing the large resistant clasts of microcline. This illustrates the compositional control of the rock, and argues against large-scale Na metasomatism. The occurrence of chessboard albite and untouched microcline in close proximity reflects the selective nature of the process.

If the chlorite grade muscovite is in fact significantly depleted in Na by this process, then the low concentration of Na in biotite may be a reflection of this Na reduced state.

Biotite Isograd

Mather (1970), working on the Dalradian Rocks of Scotland, suggested that the classical isograd of Tilley (1925), based on the incoming of biotite in vaguely defined "pelitic" rocks, should be redefined relative to a reaction in rocks of greywacke composition. According to Mather, argillaceous sandstones and greywackes, below the classical isograd, mark the first appearance of biotite as a prograde metamorphic mineral. The same phenomenon has been noted elsewhere and Jones and Ghent (1970) record the same feature in rocks belonging to the Horse Thief Creek Formation in the Selkirk Mountains of British Columbia. The strata examined by the above workers are stratigraphically equivalent to the Miette group of the Rocky Mountains and is in accordance with the state of the biotite isograd at Mount Robson.

At Mount Robson argillaceous sandstones stratigraphically and structurally overlie a phyllitic unit (Unit B). These are found to contain biotite whereas the phyllite itself, folded into a series of synclines and anticlines, retains its chlorite grade mineralogy throughout the Rearguard Structural Subzone, and into the more highly deformed Western Structural Zone.

Mather suggests that the critical factor should be the breaking of the chlorite-microcline tie-line on an A.K.F. diagram and the initiation of a biotite-phengite join. The reaction thus defining the biotite isograd would be:

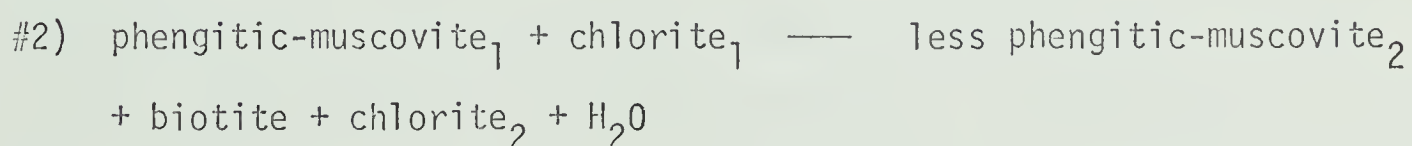
#1) chlorite + microcline + phengitic muscovite ——— biotite +
less phengitic muscovite + quartz + water.

Once this occurs the three-phase field muscovite-biotite-chlorite is

established. According to Mather, once initiated by this reaction, the field increases in size with increase in metamorphic grade. The size increase occurs as the phengitic muscovite apex of the three-phase field migrates towards muscovite. The stable "phengite" thus becomes poorer in celadonite and gradually becomes nearer to the composition of muscovite. The biotite-phengite, and phengite chlorite joins lengthen, and the compositional range compatible with the three-phase mineralogy increases. Increasingly more Al-rich sediments get brought into the expanding field as the metamorphic grade increases, and the celadonite content decreases correspondingly in the muscovite. Pelitic rocks tend to be high in Al and thus rarely mark the onset of biotite formation.

Atherton (1964) notes that Al-rich sediments may not form biotite until the garnet isograd and it is reasonable to assume that Sample #2 has retained its chlorite grade mineralogy because of its high Al/Mg + Fe ratio. The three-phase field has not yet encroached on Sample #2.

In pelitic rocks the formation of biotite is governed by the following equation:



Reaction #1 will commence when the assemblage chlorite + microcline becomes unstable. As mentioned previously, microcline is rare in the Miette group metasediments and this reaction may only apply in a few coarse conglomeratic horizons. Sediments which initially lay in a field to the left of the phengite-biotite join on an A.K.F. diagram, should contain excess microcline and no chlorite. The assemblage phengite-biotite-microcline \pm albite was in fact found in thin section, but no

examples were analysed. It is, however, possible for the whole-rock composition to be within this field, in a sample devoid of microcline! Sample #1, although close to the chlorite-bearing field, belongs to this group as it contains excess albite. The reaction is thus more complicated, as chlorite is unstable and must be completely removed by reaction, once that tie-line biotite-phengite is initiated, regardless of the K-bearing phase.

Added to Mather's reactions there must be a third, between phengitic muscovite and chlorite, producing biotite and a (?) less phengitic muscovite in a microcline free, alkali-rich system. Sample #1, giving a phengitic muscovite and Al/Mg + Fe reduced biotite results from such a reaction. Samples #3, 4, 5, 6, 7 at Mount Robson formed biotite and regenerated a second generation of chlorite. The reaction involved must approximate to reaction #2 of Mather. These sediments are pelitic and lie in the three-phase muscovite-biotite-chlorite field, to the right of the critical biotite-muscovite (phengite) join.

According to Mather, this reaction is initiated after reaction #1 and is progressive and compositionally dependent. The composition of the "phengite" on the muscovite-phengite join is grade-dependent, in line with the suggestions of Lambert and Butler. In Samples #3, 4, 5, 6, 7 the Al/Mg + Fe ratio is clearly fixed, and the sample ratios are not strung out in a line of increasing Al/Mg + Fe ratio, marking the position of the biotite-bearing reaction for each whole-rock analysis. They would seem rather to be continually upgrading their chemistry to the maximum Al/Mg + Fe allowable at any given grade. Thus all six samples represent the maximum grade conditions, and not whole-rock variation.

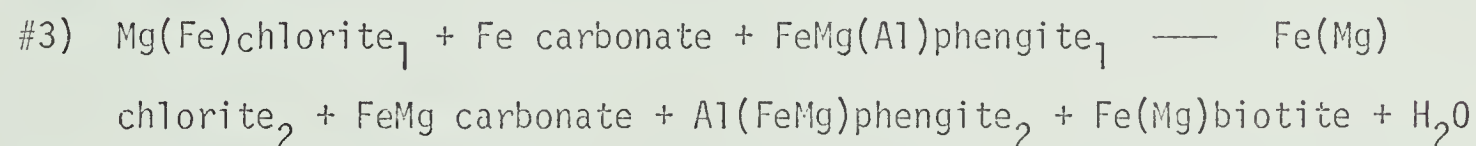
An additional factor in the above is the Mg/Mg + Fe ratio of the

original chlorite grade mineralogy, as chlorites with a high Mg/Mg + Fe content may inhibit the biotite forming reaction until a high metamorphic grade.

The probable chemistry of chlorite grade chlorite as deduced from the sediments at Jasper, has been discussed earlier. There is little to suggest that the chlorite grade chlorite was ever substantially lower in Al/Mg + Fe ratio, although slight deficiencies appear to have been made up to a level presently just below that of Sample #2.

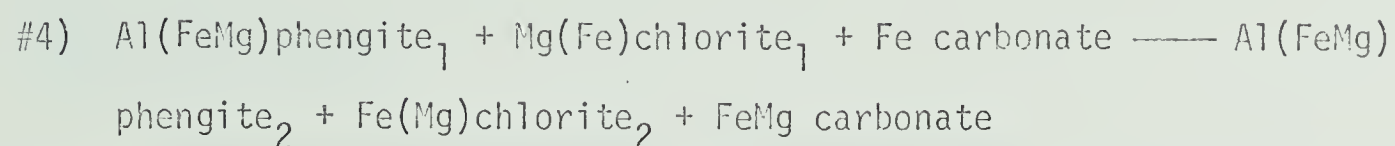
Chinner (1960) discounts the reaction proposed by Ramberg (1952) which calls for a 10% increase in Al_2O_3 in chlorites above the biotite isograd, on the grounds that chlorites above and below contain a relatively constant 20% Al_2O_3 by weight. The biotite grade chlorites at Mount Robson give an average of 21.56% Al_2O_3 and are unlikely to be significantly higher than their chlorite grade counterparts.

The reaction, #2, proposed by Mather would appear to be realistic, however, the addition of a carbonate phase to buffer the Mg/Mg + Fe ratio will affect the reaction. The proposed reaction at Mount Robson is:



Sample #2 retains its chlorite grade Al/Mg + Fe ratio and has not reacted to form biotite; it does, however, have a "normal" Mg/Mg + Fe ratio in terms of the ankerite buffered system and has re-equilibrated its Mg and Fe by partitioning in the muscovite-chlorite-carbonate system.

From this it follows that the carbonate reaction is not dependent on the biotite-producing reaction and it can be represented separately.



Because this buffering reaction is independent of the biotite-producing reaction, it may pre-date, post-date, or occur contemporaneously with the biotite-producing reaction. The 375°C minimum temperature would suggest a prograde reaction. Should it pre-date the biotite-producing reaction, then the resultant drop in Mg/Mg + Fe ratio of the chlorite might trigger the second reaction. The system is complex and worthy of further study.

Age Determinations

Work by Evans, Stauffer, Steiner and Weiner on the Miette group sediments at Jasper not only gives an indication of the age of the detrital material in the sediments and the approximate age of metamorphism, but also contributes to the understanding of the chemical evolution of the sediments.

Steiner (1962) found that there was a linear relationship between the cube of the median diameter of a detrital muscovite and its K^{40}/Ar^{40} age. Thus large crystals show little upgrading during metamorphism and the amount of upgrading increases as the grain size decreases. By extrapolation above and below certain grain sizes the grains should reflect the age of the original detritus on the one hand and the age of metamorphism on the other. In view of the proposed evolution of the sediment from an illitic clay towards muscovite, it is interesting to note that the finer material recrystallising from illite to phengitic-muscovite loses nearly all its radiogenic argon, whereas coarser material, presumably crystallographically nearer to the phengite-muscovite structure, retains its original radiogenic argon into and through the chlorite metamorphic grade.

Weiner suggests that a phyllite consists of three mica components: 1) "new" mica recrystallised parallel to the cleavage, with little or no inherited argon; 2) mechanically orientated cleavage mica which has lost some, and 3) mica still orientated parallel to the bedding plane which has lost somewhat less radiogenic argon. (Weiner, 1966).

Little is known about the chemistry of the chlorite grade muscovite-phengite mica. However, it would be interesting to know if

these stages in structural reorganisation involve chemical reorganisation also.

Weiner also dated two biotite grade samples from the present thesis area near Tête Jaune Cache; the results are shown in Table 21. Sample #661 of Weiner is a phyllite which is apparently devoid of chlorite. It is thus atypical! The chemistry of this sample would place it close to that of Sample #1 which would suggest an early reaction after Mather's reaction #1. The psammitic schist chosen by Weiner is atypical for the same reason - it would appear to represent biotite formation by the early reaction. The biotite age of 93 m.y. is probably realistic; it seems unlikely that it would inherit radiogenic argon from the muscovite and chlorite, although at 105 m.y. the muscovite may be slightly updated. This age then may mark the minimum age of biotite formation by the early reaction.

TABLE 21

Sample	Rock Type	Material	Age by K^{40}/Ar^{40} m.y.
661	Phyllite	Wholerock	69
659	Sandstone	Biotite separate	93
660	Sandstone	Muscovite separate	105

from Weiner 1966, p. 153

REFERENCES

- Aitken, J.D. (1969). Documentation of the subcambrian unconformity, Rocky Mountains Main Ranges, Alberta: Can. Jour. Earth Sci., Vol. 6, pp. 193-200.
- Akehurst, A.J. (1964). The Jasper Formation, Jasper, Alberta: unpublished M.Sc. Thesis, University of Alberta, Edmonton.
- Albee, A.L (1962). Relationships between the mineral association, chemical composition, and physical properties of the chlorite series: Amer. Mineral., Vol. 47, pp. 851-870.
- Allen, G.C. (1967). Chemical variations during prograde metamorphism in the Great Smoky Mountains of North Carolina and Tennessee: Geol. Soc. Amer. Special Paper 115, p. 3 (abst).
- Arnold, R.G. (1962). Equilibrium relations between pyrrhotite and pyrite from 325-743°C: Econ. Geol., Vol. 57, pp. 72-90.
- Atherton, M.P. (1964). The Garnet Isograd in pelitic rocks, and its relation to metamorphic facies: Amer. Mineral., Vol. 49, pp. 1331-1349.
- _____ (1965). The chemical significance of isograds: In Pitcher, W.S. and Flinn, G.W. (eds.) Controls of Metamorphism: Oliver and Boyd.
- _____ (1968). The variation in garnet, biotite and chlorite composition in medium grade pelitic rocks from the Dalradian, Scotland, with particular reference to the zonation of garnet: Contr. Mineral. Petrol., Vol. 18, pp. 347-371.,
- Bally, A.W., Gordy, P.L., and Stewart, G.A. (1966). Structure, seismic data, and orogenic evolution of southern Canadian Rocky Mountains: Bull. Can. Petrol. Geol., Vol. 14, #3, pp. 337-381.
- Bielenstein, H.U. (1964). The Miette Formation, Jasper, Alberta: unpublished M.Sc. Thesis, University of Alberta, Edmonton.
- Brown, A. (1967). McBride map-area (93H), British Columbia: Geol. Surv. Can. Paper 68-1, Part A, pp. 20-21.
- Brown, E.H. (1967). The Greenschist Facies in part of eastern Otago, New Zealand: Contr. Mineral. Petrol., Vol. 14, pp. 259-292.
- Burling, L.D. (1923). Cambro-Ordovician section near Mount Robson: Geol. Soc. Amer. Bull., Vol. 34, pp. 721-748.

- Burwash, R.A. et al. (1964). Precambrian. In Geological History of Western Canada, pp. 14-19: Alcraft Printing Co., Calgary, Alberta.
- Burwash, R.A. and Krupicka, J. (1969). Cratonic reactivation in the Precambrian basement of western Canada. I. Deformation and chemistry: Can. Jour. Earth Sci., Vol. 6, pp. 1381-1395.
- Butler, B.C.M. (1967). Chemical study of minerals from the Moine schists of Ardnamurchan area, Argyllshire, Scotland: Jour. Petrol., Vol. 8, pp. 233-267.
- Campbell, R.B. (1967). McBride map-area, British Columbia: Geol. Surv. Can. Paper 67-1, Part A, pp. 53-55.
- _____ (1968). McBride map-area, British Columbia: Geol. Surv. Can. Paper 68-1, Part A, pp. 14-19
- _____ (1968a). Canoe River, British Columbia: Geol. Surv. Can. Map 15-1967.
- _____ (1970) Structural and metamorphic transitions from infrastructure to superstructure, Cariboo Mountains, British Columbia: Geol. Assoc. Can. Special Paper 6, pp. 67-71.
- _____ and Charlesworth, H.A.K. (1970). Geology of the region between Prince George and Jasper: In Edmonton Geol. Soc. Guidebook 1970, pp. 84-93.
- Charlesworth, H.A.K. et al. (1967). Precambrian geology of the Jasper region, Alberta: Res. Council Alberta, Bull. 23.
- Chayes, F. (1955). Potash feldspar as a by-product of the biotite-chlorite transformation: Jour. Geol., Vol. 63, p. 75.
- Chinner, G.A. (1960). Pelitic gneisses with varying ferrous/ferric ratios from Glen Clova, Angus, Scotland: Jour. Pet., Vol. I, pp. 178-215.
- Coombs, D.S. (1960). Lower grade mineral facies in New Zealand: Rept. 21, Int. Geol. Cong., Pt. XIII, pp. 339-351.
- Deer, W.A., Howie, R.A., and Zussman, J. (1962). Rock Forming Minerals, Vol. 3, Layer silicates: Longmans, London
- Degens, E.T. (1965). Geochemistry of Sediments, A brief survey: Prentice Hall Inc.
- Duncumb, P. and Reed, S.J.B. (1968). The calculation of stopping power and backscatter effects in electron microanalysis. In Quantitative electron probe microanalysis: Nat. Bur. Standards, Special Publ. 298, pp. 133-154.

- Ernst, W.G. (1963). Significance of phengitic micas from low-grade schists: *Amer. Mineral.*, Vol. 48, pp. 1357-1373.
- Evans, C.R. (1961). The Precambrian rocks of the Old Fort Point formation, Jasper, Alberta: unpublished M.Sc. Thesis, University of Alberta, Edmonton.
- _____, Steiner, J., and Weiner, J.L. (1964). Age dating studies on Precambrian rocks at Jasper, Alberta: *Bull. Can. Inst. Min. Met.*, Vol. 57, pp. 33-36.
- Evans, H.T., Jr., Appleman, D.E., and Handwerker, D.S. (1963). The least squares refinement of crystal unit cells with powder diffraction data by an automatic computer indexing method: *Amer. Crystallog. Assoc. Meeting*, Cambridge, Mass., pp. 42-43.
- Fisher, R.A. (1953). Dispersion on a sphere: *Proc. Roy. Soc., Ser. A.*, Vol. 217, pp. 295-305.
- Foster, M.D. (1956). Correlation of dioctahedral potassium micas on the basis of their charge relations. A contribution to geochemistry: *U.S. Geol. Surv. Bull.* 1036-D, p. 57.
- _____. (1962). Interpretation of the composition and classification of the chlorites: *U.S. Geol. Surv., Prof. Paper* 414-A, pp. 1-33.
- Goldsmith, J.R. (1960). Subsolidus relations in the system $\text{CaCO}_3\text{-MgCO}_3\text{-MnCO}_3$: *Jour. Geol.*, Vol. 68, pp. 324-335.
- _____. et al. (1962). Studies in the system $\text{CaCO}_3\text{-MgCO}_3\text{-FeCO}_3$: *Jour. Geol.*, Vol. 70, pp. 659-688.
- Griffiths, R.E. (1962). The geology of the Wynd map-area, Jasper, Alberta: unpublished M.Sc. Thesis, University of Alberta, Edmonton.
- Grim, R.E. (1968). *Clay Mineralogy*: McGraw-Hill Book Company.
- Guidotti, C.V. (1967). On the significance of the variable μS_2 during metamorphism of pelitic schists: *Geol. Soc. Amer. Special Paper* 115, p. 85 (abst).
- _____. (1969). A comment on 'Chemical study of minerals from Moine schists of the Ardnamurchan area, Argyllshire, Scotland' by B.C.M. Butler, and its implications for the phengite problem: *Jour. Petrol.*, Vol. 10, pp. 164-170.
- _____. (1970). The mineralogy and petrology of the transition from the Lower to Upper Sillimanite Zone in the Ognossoc Area, Maine: *Jour. Petrol.*, Vol. 11, pp. 277-336.
- Heinrich, K.F.J. (1967). The absorption correction model for microprobe analysis: *Trans. 2nd Nat. Conf. Electron Microprobe Analysis*, Boston, Paper 7, 2 p.

- Mountjoy, E.W. and Aitken, J.D. (1963). Early Cambrian and Late Precambrian paleocurrents, Banff and Jasper National Parks: Bull. Can. Petrol. Geol., Vol. 11, pp. 161-168
- Muecke, G.K. (1964). Fracture Analysis in the Canadian Rocky Mountains: Unpublished M.Sc. Thesis, University of Alberta, Edmonton.
- Orville, P.M. (1967). Unit-cell parameters of the microcline-low albite, and the Sanadine high albite solid solution series: Amer. Mineral., Vol. 52, pp. 55-85.
- Price, R.A. and Mountjoy, E. (1970). Geologic structure of the Canadian Rocky Mountains between Bow and Athabasca Rivers - a progress report: Geol. Assoc. Can., Special Paper 6, pp. 7-25.
- Ramberg, H. (1952). The Origin of Metamorphic and Metasomatic Rocks: Chicago University Press.
- Reed, S.J.B. (1965). Characteristic fluorescence corrections in electron-probe microanalysis: British Jour. Appl. Phys., Vol. 16, pp. 913-926.
- Remington, D.B. (1960). Precambrian rocks of the Whistlers Mountain Trail map area, Jasper, Alberta: unpublished M.Sc. Thesis, University of Alberta, Edmonton.
- Rosenberg, P.E. (1967). Subsolidus relations in the system CaCO_3 - MgCO_3 - FeCO_3 between 350°C and 550°C: Amer. Mineral., Vol. 52, pp. 787-796.
- Shaw, D.M. (1956). Geochemistry of pelitic rocks. Part III. Major elements and general geochemistry: Bull. Geol. Soc. Amer., Vol. 67, pp. 919-934.
- Shirozu, H. (1958). X-ray powder patterns and cell dimensions of some chlorites in Japan, with a note on their interference colours: Min. Jour., Vol. 2, #4, pp. 209-233.
- Smith, D.G.W. (1963). Pyrometamorphism of phyllites by a dolerite plug: unpublished Ph.D. Thesis, Cambridge University.
- _____ and Tomlinson, M.C. (1970). An A.P.L. language computer program for use in electron microprobe analysis: Computer Contrib. 45, University of Kansas. Amer. Assoc. Petrol. Geol., pp. 1-28,
- Snelling, N.J. (1957). Notes on the petrology and mineralogy of the Barrovian Metamorphic Zones: Geol. Mag., Vol. 94, pp. 297-304.
- Sorenson, M.K. (1955). Some observations on the geology of the Rocky Mountain Trench between latitudes 53° and 53° 30': Alberta Soc. Petrol. Geol., 5th Ann. Field Conf. Guidebook (Jasper National Park), pp. 53-67.

- Stauffer, M.R. (1961). The geology of the Ski-lodge Road map area, Jasper, Alberta: unpublished M.Sc. Thesis, University of Alberta, Edmonton.
- Steiger, R.H. and Hart, S.R. (1967). The microcline-orthoclase transition within a contact aureole: *Amer. Mineral.*, Vol. 52, pp. 87-115.
- Steiner, J. (1962). Lower Miette Rocks at Jasper, Alberta: unpublished M.Sc. Thesis, University of Alberta, Edmonton.
- Sweatman, T.R. and Long, J.V.P. (1969). Quantitative electron-probe microanalysis of rock forming minerals: *Jour. Petrol.*, Vol. 10, Pt. 2, pp. 332-379.
- Tilley, C.E. (1925). A preliminary survey of metamorphic zones in the southern Highlands of Scotland: *Quart. Jour. Geol. Soc. Lond.*, Vol. 81, pp. 100-112.
- Towe, K.M. (1962). Clay mineral diagenesis as a possible source of silica cement in sedimentary rocks: *Jour. Sed. Pet.*, Vol. 32, pp. 26-28.
- Velde, B. (1964). Low grade metamorphism of micas in pelitic rocks: *Ann. Rept. Director, Geophys. Lab. Carnegie Inst., Washington D.C.* (1963), pp. 137-147.
- _____ (1965). Phengite micas: synthesis, stability and natural occurrence: *Amer. Jour. Sci.*, Vol. 263, pp. 886-913.
- _____ (1967). Si^{+4} content of natural phengites: *Cont. Mineral. Petrol.*, Vol. 14, pp. 250-258.
- Voll, G., *in* Brown, W.L. (1964). Crystallographic aspects of feldspars in metamorphism. *In* *Controls of Metamorphism*: Oliver and Boyd Limited.
- Walcott, C.D. (1913). Cambrian formations of the Robson Peak district, British Columbia and Alberta, Canada: *Smithsonian Misc. Coll.*, Vol. 57, pp. 328-343.
- Weaver, C.E. (1958). The effects and geological significance of potassium "fixation" by expandable clay minerals derived from muscovite, biotite, chlorite, and volcanic material: *Amer. Mineral.*, Vol. 43, pp. 839-861.
- Weiner, J.L. (1966). The Old Fort Point Formation, Jasper, Alberta: unpublished Ph.D. Thesis, University of Alberta, Edmonton.
- Wenk, E. (1970). Distribution of Al between coexisting micas in metamorphic rocks from the central Alps: *Contr. Mineral. Petrol.*, Vol. 26, pp. 50-61.

- Winkler, H.G.F. (1967). Petrogenesis of metamorphic rocks: Springer Verlag.
- Wright, T.L. (1967). The microcline-orthoclase transformation in the contact aureole of the Eldora Stock, Colorado: Amer. Mineral., Vol. 52, pp. 117-136.
- _____ and Stewart, D.B. (1968). X-ray and optical study of alkali feldspar. I. Determination of composition and structural state from refined unit cell parameters and 2V: Amer. Mineral., Vol. 53, pp. 38-104.
- Yoder, H.S. and Eugster, H.P. (1955). Synthetic and natural muscovites: Geochim. Cosmochim. Acta, Vol. 8, p. 225.
- Young, F.G. (1968). McBride area, British Columbia; Lower Cambrian stratigraphic studies: Geol. Surv. Can., Paper 68-1, Part A, pp. 21-23.

APPENDIX A

MAPSMap 1

Regional Geological Map
Mount Robson, Jasper and Cariboo Mountains

Map 2 (three parts) 1:12,500

Geological Map of the Fraser River Valley between Tête Jaune
Cache and the Robson River
(Mount Robson Map Area)

Part 1. Western Zone*, and western part of the Central Zone*
Part 2. Eastern part of the Central Zone*
Part 3. Eastern Zone*

* Zones as defined in the text

Map 3 1:25,000

Geological Map of the above area, omitting outcrop data

Map 4 1:25,000

Topographic Map of the above area illustrating structural
domains and sample location points of analysed specimens.

Legend Maps #2 and #3

Map #1

Middle Cambrian (Chancellor Group)

limestone, shale, siltstone



Lower Cambrian (Gog Group)

sandstone, quartzite



Precambrian Miette Group

Unit F (mainly argillaceous)

Unit E (mainly arenaceous)

Unit D (mainly argillaceous)

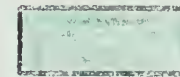
Unit C (mainly arenaceous)

Unit B (mainly argillaceous)

Unit A (mainly arenaceous)



Precambrian, undifferentiated gneiss

Map SymbolsGeological Boundary
Formation, Member
Known

Assumed



Bedding

Inclined
Overturned

Vertical



Fault

Assumed



Thrust-Fault

Assumed



Anticline

Defined



Syncline

Defined



Overturned Anticline

Defined



APPENDIX B

ANALYTICAL METHODS

Electron Microprobe

The mineral phases which constitute samples #1-8 were analysed individually by means of a three channel A.R.L. "EMX" Electron Microprobe with light element facilities. The standards of the Electron Microprobe Laboratory of the Department of Geology, University of Alberta, were used and are listed with the operational conditions Table . The elements used for each standard on each sample are also given.

Muscovite, biotite, chlorite and carbonate were completely analysed for their major constituents, and their coexisting oxide, sulphide and feldspar phases were analysed in a reconnaissance manner.

Data from the Electron Microprobe was corrected for the effects of atomic number (see Duncumb and Read, 1968), mass absorption (see Heinrich, 1966), and fluorescence (see Reed, 1965). Corrections were made utilising the A.P.L. language programme "Probedata" written by Smith and Tomlinson (1970).

Standards were kept moving during analysis in order to average out inhomogeneities in the sample. The mica phases were analysed by a series of "spot counts", and the carbonate which became damaged under the beam were also kept moving during analysis.

Standard backgrounds and then peaks were first taken as a series of 5 x 50 second counts. The sample peaks were then measured as 5 x 20 second "spot counts" on 5 or more mineral grains. The mica was not

noticeably damaged by this count rate. Calcite in Sample #8 tended to burn, although this effect was less evident in ankerite.

Standard peaks were remeasured after the samples (5 x 50 second counts) in order to detect any long term shift in the count rate. Standard backgrounds were then retaken in the same manner. Unless interference from neighbouring peaks prevented it, backgrounds above and below the element peak were taken. Sample backgrounds were measured in the same way, and both standard and sample values were averaged out and converted to a 100 second count rate for comparison.

The samples were mounted as blocks and were viewed by reflected light. The clean cut crystal outlines observed in thin section, and the characteristic form of the micas aided in identifying mica species. One diagnostic element was also run in each set of three in order to differentiate, on a basis of count rate, between one mica and another. The lack of observed contamination in thin section, and the constancy of count rates throughout a grain or group of grains would indicate near equilibrium conditions.

Efforts were made to keep conditions uniform throughout and avoid undue bias; however, certain effects cannot be avoided. These are thought to be insignificant in the present study. Such effects as errors inherent in standard analyses, carbon coating variations, polishing defects in flakey samples, deviations from a perfectly horizontal sample surface with a consequent change in "take off" angle, these and others must contribute to minor errors. These errors are kept to a minimum, and are hard to evaluate (see Sweatman and Long, 1969).

Mica corrections are usually slight. Muscovite Sample #3 gives representation values of maximum deviation from unity. Fluorescence

values range from 0.9954 (Fe) to 1.0118 (Ba). Absorption values from 0.8653 (Al) to 1.0345 (Ca) and atomic number corrections from 0.9724 (Ba) to 1.025 (Ca). Most values for all three fall close to unity.

Biotite and chlorite values are similar, and are generally good. Fluorescence corrections are small.

Ba, Sr, and Mn atomic number corrections are slightly high and P has a high absorption correction.

In all cases where Si, Al, Fe, Mg, K, constitute an important constituent in a mineral the confidence limit, in terms of 99.0% confidence level is between 0.5-2.0%. The analysis of 5 grains is usually sufficient to give enough counts for a realistic estimate; however, the confidence level drops to around 8.0% when dealing with trace amounts of elements and low concentrations. The analyses are thought to be good.

The water contents shown in tables of mineral chemical analyses are not measured but are calculated relative to the coexisting cation content of the mineral.

TABLE B1

Microprobe Analytical Standards

	Biotite EP/S ₁₂₋₂	Muscovite EP/S ₁₂₋₃	Muscovite EP/S ₅₋₂	Fluorapatite EP/S ₃₋₈
SiO ₂	38.62	44.70	47.31	0.34
TiO ₂	2.29	0.87	0.15	-
Al ₂ O ₃	10.72	31.50	32.42	0.06
Fe ₂ O ₃	1.80	4.50	0.65	0.06
FeO	16.51	1.08	2.12	-
MnO	0.95	0.03	0.05	0.01
MgO	14.01	0.99	1.67	0.01
CaO	0.02	0.02	0.19	54.02
Na ₂ O	0.69	0.67	0.75	0.23
K ₂ O	9.20	10.45	10.11	0.01
P ₂ O ₅	-	0.04	-	40.88
H ₂ O ⁺	2.66	4.40	4.46	-
Rb ₂ O	0.03	-	0.06	-
Ba	0.10	0.29	0.22	-
Sr	-	-	0.02	0.06
Cl	-	-	-	0.41
S	-	-	-	0.15
F	3.30	-	-	3.53

EP/S₃₋₄ = 46.54% Fe (marcasite)
53.46% S

EP/S₃₋₁₂ = 60.32% Mg (magnesium oxide)
39.68% O

EP/S₉₋₄ = 100.00% Mn (manganese metal)

Biotite and Chlorite Standards

EP/S ₁₂₋₂	Si, Ti, Al, Mg, K, Na
EP/S ₅₋₂	Ba, Sr
EP/S ₃₋₈	Ca, P, Cl, F
EP/S ₃₋₄	Fe
EP/S ₉₋₄	Mn

Muscovite Standards

EP/S ₁₂₋₂	Ti, Mg, Al
EP/S ₁₂₋₃	Si, K, Na
EP/S ₅₋₂	Ba, Sr
EP/S ₃₋₈	Ca, F
EP/S ₃₋₄	Fe

Carbonate Standards

EP/S ₃₋₈	Ca
EP/S ₃₋₄	Fe
EP/S ₉₋₄	Mn
EP/S ₅₋₂	Sr
EP/S ₃₋₁₂	Mg

Operating Conditions

"Take off" angle	=	52.5 degrees
Operating voltage	=	15 KV
Beam Current	=	0.1 mA \pm 0.01 mA
Threshold voltage	=	1.0 V
Window	=	7.0 V

APPENDIX C

COMPUTER PROGRAMMES

The following APL programmes were used in the assessment of structural data. Reference to each has been made in the text.

```

VFOLD[[]]V
V A FOLD B;E;G;L;K;H;J;I;F;P;R;C
[1] J←((I←+/C[1;]*2)×H←+/C[2;]*2)-(G←+/C[1;]×(C←A DCOS P)[2;])*2
[2] E←((G×L←+/C[2;]*C[3;])-H×K←+/C[1;]*C[3;])÷J
[3] P←I×R+(1+(E*2)+(F←((G×K)-L×I)÷J)*2)*0.5
[4] 'STN ' ;A[4]; ' WITH ' ;H; ' RDINGS'
[5] 'TRHD AND PLUN OF FLD-AK: ' ;1 RHD RA×((P×R) TRHD P),(-1)OR; ' DEG'
V

VLINE[[]]V
V B LINE C;D;E;K;LS;HS;GS;X;Y;Z;XY;KK
[1] D←DCOS B
[2] E←DCOS C
[3] K←(((D←(D[2;]*E[3;])-E[2;]*D[3;])*2)+((Y←(E[1;]*D[3;])
-P[1;]*E[3;])*2)+(X←(D[1;]*E[2;])-D[2;]*E[1;])*2)*0.5
[4] LS←A÷K
[5] HS←Z÷K
[6] GS←X÷K
[7] 'TREND OF LINEAR STRUCTURE: ' ;1 RHD XY+360×0>XY←((( -3)O-LS÷LS)
×RA)×180×HS<0; ' DEGREES'
[8] 'PLUNGE OF LINEAR STRUCTURE: ' ;1 RHD KK-2×KK×0>KK←((-1)OGS)
×RA; ' DEGREES'
[9] 'OUTCROP NUMBER: ' ;A
V

VMEASURE[[]]V
V MEASURE B;H;Y;D;H
[1] 'NO. OF SURFACES: ' ;H÷(pB)÷2
[2] C←DCOS B
[3] D←(+/C)÷R←(+/(+/C)*2)*0.5
[4] 'DIP-DIRECTION OF MEAN SURFACE: ' ;1 RHD Y+360×0>Y←((( -3)O-D[2]÷
D[1])×RA)+180×D[1]>0; ' DEGREES'
[5] 'DIP OF MEAN SURFACE: ' ;1 RHD((-2)OD[3])×RA; ' DEGREES'
[6] 'ESTIMATED PRECISION PARAMETER (H-1/H-R): ' ;1 RHD(H-1)÷H-R
V

```


APPENDIX D

Sample #1

Quartz, Muscovite, Albite, Biotite, Ankerite, Schist

Recrystallised quartz and mica forms a matrix around slightly larger grains of quartz and feldspar. Muscovite (40%) laths 0.5-1.0 mm long are intermeshed to give a poorly orientated mica base with grains of quartz (40%) 0.5-3.0 mm long and feldspar (5%) 0.5-2.0 mm long.

The feldspar is albite which contains microlites of white mica, and is either structureless or exhibits polysynthetic twinning. The larger quartz grains show signs of strain but are otherwise unaltered. Some foliation is found in the matrix, and this is again reflected in the later biotite (10%) flakes. Biotite is found as small (0.5-1.0 mm) flakes with a uniform distribution within the matrix.

Lenses of fine-grained quartz are found in the matrix; these commonly contain carbonate granules which appear to be replacing the quartz. This ankerite (5%) is interstitial and develops into porphyroblasts and grain clusters 2.0 mm long.

Sample #2

Quartz, Albite, Muscovite, Chlorite, Ankerite, Schist

Muscovite (15%) laths, 0.5-2.5 mm long and chlorite (5%) 0.5-1.0 mm give a pronounced foliation to an otherwise quartzose metasediment. Mica is sparsely developed except in partings of originally argillaceous material. The coarser crystalline laths of muscovite and chlorite are

interwoven and appear to envelope original, now recrystallised, grains of quartz (65%) averaging 4.0 mm in length and feldspar (10%) of similar size. Albite clasts exhibit either chessboard twinning or else normal polysynthetic twinning. They contain small stubby micro-lites of white mica, and are embayed by crystals of quartz.

Individual clasts of quartzite may be outlined by grain size and purity. The bulk of the rock comprises a mosaic of poorly sutured quartz crystals 0.5-1.0 mm long, derived from the original sediment.

Ankerite (5%) which is found within the quartz mosaic replaces the quartz and develops into porphyroblasts of carbonate up to 3.0 mm long orientated parallel to the mica foliation.

Tourmaline, zircon, apatite and iron oxide are found as accessory constituents.

Sample #3

Muscovite, Quartz, Ankerite, Biotite, Albite, Chlorite, Schist

A network of irregularly orientated and intricately interwoven (0.5-1.0 mm) laths of muscovite (50%) enclose grains of recrystallised quartz (20%) and embayed crystals of albite (5%), both averaging 1.0 mm in length. Within the mica network are distinct 'eyes' of quartz and ankerite (10%) in which the carbonate replaces and envelopes quartz to become a poikiloblastic porphyroblast up to 3.0 mm long. Associated with the carbonate porphyroblasts are feathery chlorite (5%) porphyroblasts of 1.5 mm length, which are clearly imprinted on the above network at a later date.

Biotite (10%) porphyroblasts, which are smaller (0.5-1.0 mm), were also generated at a later date and have no apparent orientation.

The ankerite, biotite, chlorite, assemblage is best developed in layers of suitable composition.

The feldspar, albite, displays polysynthetic twinning or else is structureless.

Sample #4

Quartz, Muscovite, Siderite, Biotite, Chlorite, Schist

The rock matrix consists of a fine (0.5 mm) regular mixture of muscovite (45%) and quartz (40%). Both are clearly crystalline and intermeshed to give a poorly defined foliation to the rock. Coarser grains of quartz (up to 1.0 mm) are few. Very large and irregular porphyroblasts of biotite (5%) and chlorite (5%), averaging 1.0 mm in length, have been superimposed on the muscovite-quartz matrix. These irregular laths are commonly found in association with the carbonate siderite (5%). Within the matrix assemblage are found 'eyes' of quartz and carbonate. The carbonate sizes range from 1.5-3.0 mm and they tend to be poikiloblastic, enclosing small (0.5 mm) grains of quartz. They are found lying in a quartz halo, rarely adjoining muscovite although they commonly adjoin either chlorite or biotite.

Sample #5

Quartz, Muscovite, Ankerite, Albite, Chlorite, Biotite, Schist

Quartz (45%) and muscovite (25%) form a 0.5 mm groundmass mosaic. The quartz is recrystallised and distributed with albite (10%) throughout a sparse network of muscovite. The muscovite laths average 0.5 mm in length and the network shows only a slight sign of preferred

orientation. Similarly 0.5-1.0 mm biotite (5%) laths are randomly distributed throughout the rock. Ragged porphyroblasts of chlorite (5%) 1.0-1.5 mm long occur sporadically and are imprinted on top of the muscovite-quartz groundmass. The chlorite laths are orientated and define the same preferred orientation detected in the groundmass.

Albite grains are full of white mica microlites and are either structureless or else exhibit polysynthetic twinning.

Ankerite (10%) porphyroblasts ranging from 0.5-2.0 mm are found throughout replacing quartz in the groundmass and engulfing quartz crystals. The carbonate has no obvious orientation and appears to develop into granular clusters and larger porphyroblasts.

Sample #6

Quartz, Albite, Muscovite, Ankerite, Biotite, Chlorite, Schist

A mosaic of quartz (70%) consisting of ellipsoidal fragments of recrystallised quartzite up to 5.0 mm long and poorly sutured quartz grains 0.25 mm long are elongated parallel to a mica defined foliation. Muscovite (15%) laths (0.25-1.0 mm) are orientated to define this foliation. Muscovite is poorly developed and is found to wrap around original clasts of quartz, and more particularly feldspar grains up to 1.0 mm long. Albite (5%) embayed by quartz and found full of white mica microlites, may exhibit chessboard twinning, polysynthetic twinning, or none at all.

Thin poorly crystalline laths of biotite (0.5-1.0 mm long) and chlorite (total 5%), up to 2.5 mm long, are also found to parallel the muscovite foliation.

Ankerite (5%) replaces the finer quartz mosaic and forms

1.0-1.5 mm poikiloblastic porphyroblasts parallel to the foliation.

Tourmaline, zircon, apatite and iron oxide are found within the rock.

Sample #7

Muscovite, Quartz, Biotite, Chlorite, Ankerite, Schist

0.5-2.0 mm crystalline and intermatted laths of muscovite (40%) and clearly developed biotite (15%) porphyroblasts (0.5-2.5 mm) define a pronounced mica foliation in the sample. Quartz (20%) grains (0.5 mm long) are found throughout the matted mica, and occur also within lenses of quartz and ankerite (15%). The original quartz lenses have been impregnated by the carbonate which replaces the quartz along grain boundaries and develops into porphyroblasts of up to 5.0 mm, enclosing quartz remnants.

Feathery, matted porphyroblasts of chlorite (10%), up to 3.0 mm long, are imprinted on the mica foliation and are subparallel to it. Chlorite is best developed with biotite in proximity to the ankerite and is often associated with granules of iron oxide.

Sample #8

Calcite, Ankerite, Muscovite, Quartz

Coarsely crystalline carbonate (25%) enclosing detrital grains of quartz (25%) is interlayered and interlensed with a strongly foliated muscovite (50%) quartz assemblage. The carbonate, (averaging 2.5 mm in length, is itself elongated parallel to this foliation and it displays deformation and lamella twinning. Interlayered with the carbonate, the

muscovite occurs as interleaved laths, 0.5-3.0 mm long, cleanly crystalline and well developed.. The quartz grains (0.25-0.5 mm long) appear to be intermixed with both muscovite and carbonate, and are streaked out into lenses parallel to the foliation.

Apatite, iron oxide, tourmaline and chloritoid are found as accessories.

PLATE I

Figure

1) Swiftwater Subdivision

Unit C sandstones with a shallow undulatory dip to the southwest; northeast of Morey Station. Taken from Highway 16 southwest of Swift-current Creek.

2) Emperor Subdivision

Shallow to flat lying Unit C sandstones overlies the recessive core of the Robson Ranch anticline (Unit B). Taken from above locality.

3) Swiftwater Subdivision

Western part of the Swiftwater subdivision illustrating the wide glacial valley of the Fraser River, and the scarcity of outcrop, which is restricted to the two incised railway lines. Taken from above locality.

4) Rearguard Falls

Below Rearguard Station the Fraser River has broken through the crest of a major anticlinal structure and exposes a mixed interbedded sequence of Unit C sandstones, which weather out in accordance with their argillite content. The exposed limb has a shallow dip to the southwest.

5) West-Central Shear Zone

A minor fold associated with the above shear zone, the northeasterly limb is drawn out into the plane of the schistosity (S_2), and the south-westerly limbs become compressed and bulbous. Above the new road bridge at Tête Jaune Cache.

6) Unit F

Finely bedded sequence of shales and siltstones, thicker siltstone layers disrupted by joints which are now filled with calcite. Joints orientated perpendicular to the bedding die out in the more incompetent shale interbeds. Highway 16. Eastern Zone.

7) Unit B

Glaciated surface exposing colour banded Unit B phyllite in the core of a major anticline. Shear folding with shear movement "slicing" the original foliation. S_2 schistosity associated with F_1 folds plunging to the WNW. Rearguard subdivision below Highway 16.

8) Western Zone

Massive arenaceous beds with flaggy phyllitic interbeds, typical outcrop pattern in the Western Zone. Upper railway track, at the southwestern limit of Miette outcrop.

PLATE I

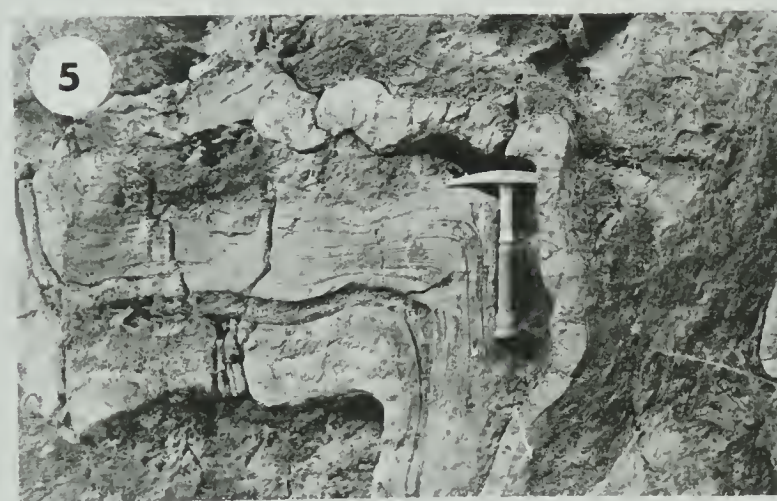


PLATE II

Figure

1) Outcrop

Smooth weathering of a typical Unit C argillaceous sandstone sequence near Rearguard Station on the lower track. Softer horizons are etched out at the expense of the more massive sandstones.

2) Outcrop

Active weathering of a graded sequence of Unit C sandstones. The schistosity is refracted within a sediment bed. The schistosity shallows towards the top of a thick horizon (hammer located right centre). Rearguard subdivision.

3) Sedimentary Structures

Coarse sediment in the form of a flame has disrupted the underlying lower Unit C argillaceous sandstone. The sediment weathers smooth, and cubes of pyrite weather to give a rusty stain on outcrop surfaces. Close to Rearguard Station, on the lower track.

4) Sedimentary Structures

A laminated, finely bedded interbed sequence between uniform argillaceous sandstone and a coarser more feldspathic sequence is disrupted and replaced by the coarser sediment. Unit C. Near Rearguard Station.

5) Quartzo-feldspathic Pebble Conglomerate

Ellipsoidal lenses of quartz, and slightly boudinaged clasts of feldspar form part of a stretched and sheared out pebble conglomerate which is part of Unit A in the Western Zone.

6) Sedimentary Structures

A series of small scours disrupt the top of a thin argillaceous graded sequence above a thick sandstone bed. The scours are filled by coarse sediment which marks the base of a typical graded bed. Highway 16. Rearguard subdivision.

7) Stretched Conglomerate

Elongated pods of quartz, and slightly boudinaged feldspars are orientated parallel to the F_1 fold axis. The pods are ellipsoidal and appear to be kinked by the later F_2 compression event. Unit A downstream from the Tête Jaune bridge in the Western Zone.

8) Stretched Conglomerate

S_2 schistosity face showing a feldspathic sandstone interbed separating two thick pebble conglomerate horizons. Exposure above the bridge at Tête Jaune Cache, Highway 16, in the Western Zone.

PLATE II

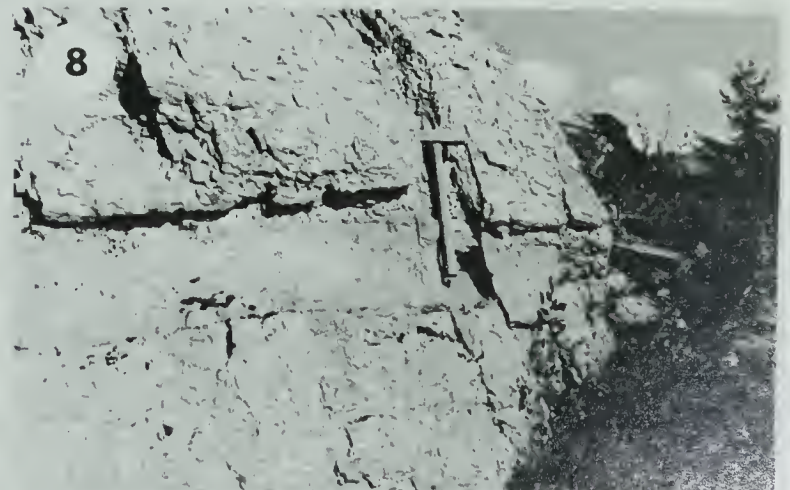
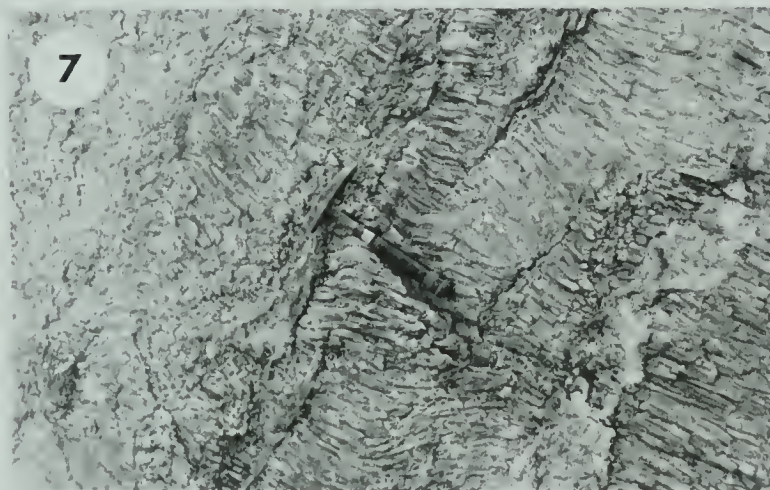


PLATE III

Figure

1) Fold (F_1)

Argillaceous sandstones at the base of Unit D folded into an anticlinal structure with an (S_2) axial plane schistosity, $117^\circ-84^\circ\text{SW}$, with a bedding pitch of 11° , indicating an axial (F_1) plunge to the WNW. Lower track between Tête Jaune Cache and Rearguard. Rearguard Subdivision.

2) Fold (F_1)

Asymmetrically folded sandstone Unit from base of Unit C, with a poorly defined (S_2) axial plane schistosity $121^\circ-90^\circ$, and a steep northeasterly limb. Rearguard Subdivision, Upper track.

3) Schistosity (S_2)

Highly schistose Unit C sandstones near the core of a major anticlinal structure in the Western Zone. Crops out along the oil pipeline. Schistosity (S_2) orientated $115^\circ-71^\circ\text{SW}$.

4) Schistosity (S_2)

Colour banded interbedded shales and siltstones belonging to Unit B, on the limb of a major anticlinal structure in the Rearguard subdivision. Pronounced axial plane schistosity (S_2) $115^\circ-83^\circ\text{SW}$, with a bedding pitch of 11° , indicated a fold axis (F_1) plunge to the WNW lower track east of Rearguard Station.

5) Kinks

Irregular, poorly orientated kink bands restricted to arenaceous and argillaceous sediment interfaces. The kinks, displayed in the Fraser River below Rearguard Station, are a rudimentary form of crenulation which dies out to the northeast.

6) Crenulation

S_2 schistosity plane with a pronounced bedding plane intercept indicative of an (F_1) axial plunge to the WNW. Pebbles and micas are elongated and orientated parallel to this intercept. The less competent phyllite horizon is crenulated, and has a characteristic 70°SE pitch on the S_2 face. Western Zone.

7) Fold (S_2)

Minor fold with an axial orientation parallel to the above crenulations. $165^\circ\text{--}54^\circ\text{SE}$. The S_2 foliation is folded, and an incipient S_3 schistosity is formed. Western Zone, downstream from the Tête Jaune bridge.

8) Schistosity (S_3)

Crenulation cleavage orientated $160^\circ\text{--}53^\circ\text{NE}$. Axial plane schistosity to the above fold, and crenulations formed by the transportation of mica into the S_3 plane. Western Zone, downstream from the Tête Jaune bridge.

PLATE III



PLATE IV

Photomicrographs

Figure

1) Quartz Clast

Detrital, slightly corroded, quartz clast from an argillaceous sandstone in Unit C at Morey Station in the Swiftwater subdivision. Chlorite grade mineralogy, with large chessboard albites (top left corner)

[Sample #E7(7)1 - (99)] x 25

2) Metasandstone

Argillaceous sandstone from the chlorite grade of metamorphism with a poorly defined phengite-chlorite foliation. Mixed quartz, feldspar and carbonate. Base of Unit C, Swiftwater subdivision

[Sample #C₅(4)1 - (83)] x 25

3) Metasiltstone

Poikiloblastic carbonate 'eye' enveloped by a poorly defined muscovite-quartz assemblage. Chlorite porphyroblasts post-date muscovite and cluster about the carbonate. Biotite porphyroblasts are smaller and subparallel to the foliation. Western Zone.

4) Metasiltstone

As above Crossed Nicols

[Sample #F₄(21)1(34)] = [Sample #3 (this study)] x 25

5) Carbonate "Augen"

Lenses or "augen" of carbonate and quartz enveloped by chlorite and biotite porphyroblasts, and set in a phyllitic biotite schist. Muscovite and biotite define the S_2 schistosity. Chlorite is partially superimposed. Plane light, biotite dark, chlorite light. Western Zone.

[Sample #F₄(54)1(46)] \equiv Sample #7 (this study) x 25

6) Carbonate "Augen"

Same feature as above, but a different example

[Sample #F₄(54)1(46)] \equiv Sample #7 (this study) x 25

7) Poikiloblastic Carbonate

Ellipsoidal "augen" of carbonate, as above, with poikiloblastic texture. The carbonate encloses particles of quartz, and is set in an lens of quartz. Muscovite envelopes the whole lens, but is usually insulated from the carbonate by chlorite or biotite porphyroblasts. Plane light. Biotites dark, chlorite light. Western Zone.

[Sample #F₄(51)2B(135)] x 25

8) Poikiloblastic Carbonate

As above, carbonate with a poikiloblastic core elongated parallel to the S_2 schistosity. Porphyroblast of chlorite in juxtaposition to the carbonate.

[Sample #F₄(51)2B(135) x 25

PLATE IV

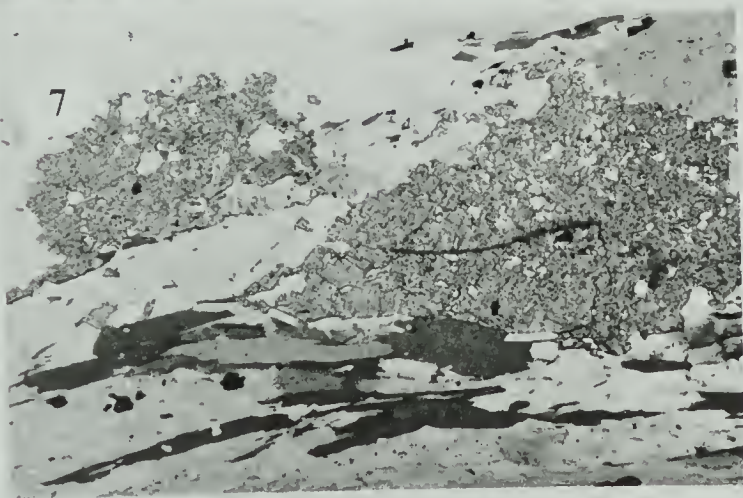
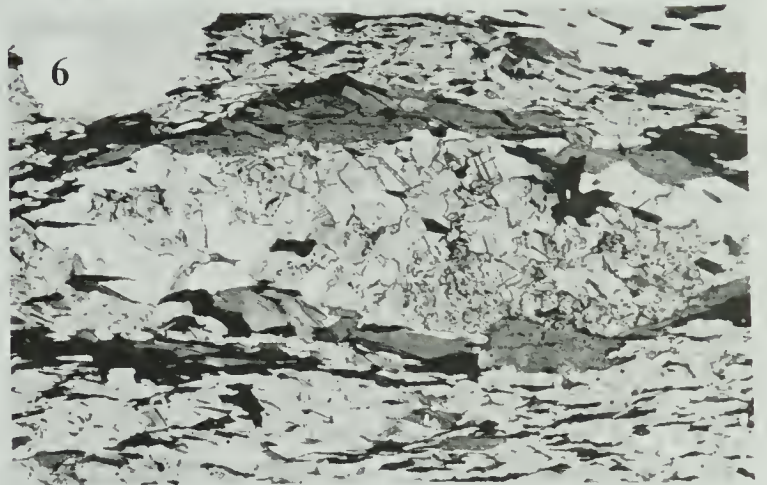
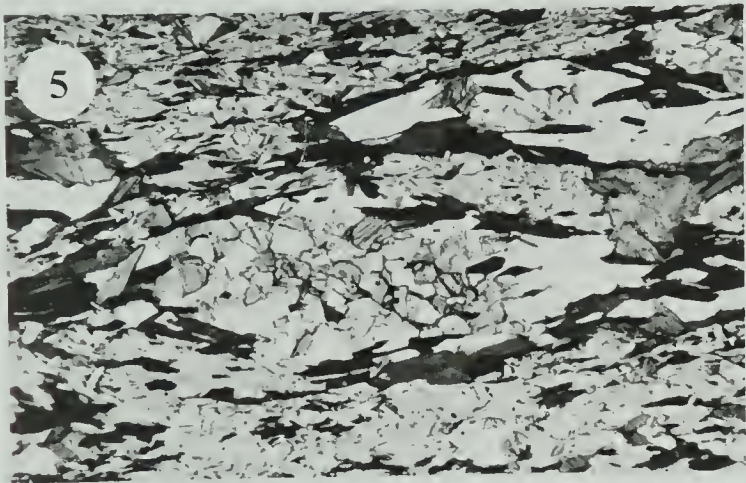
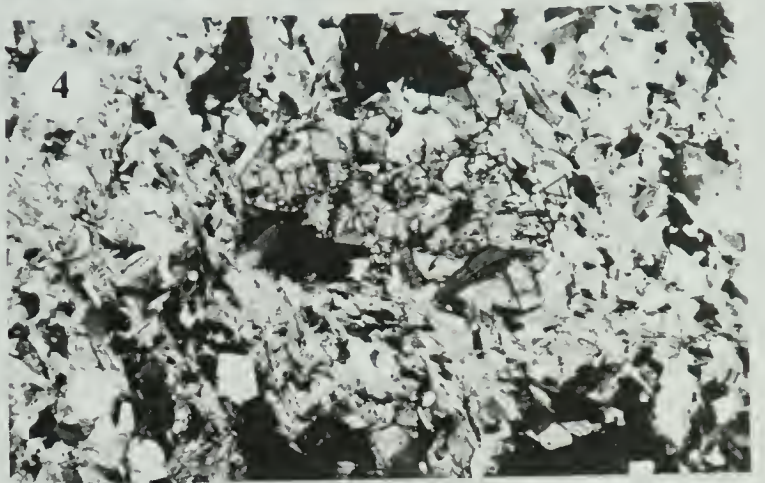
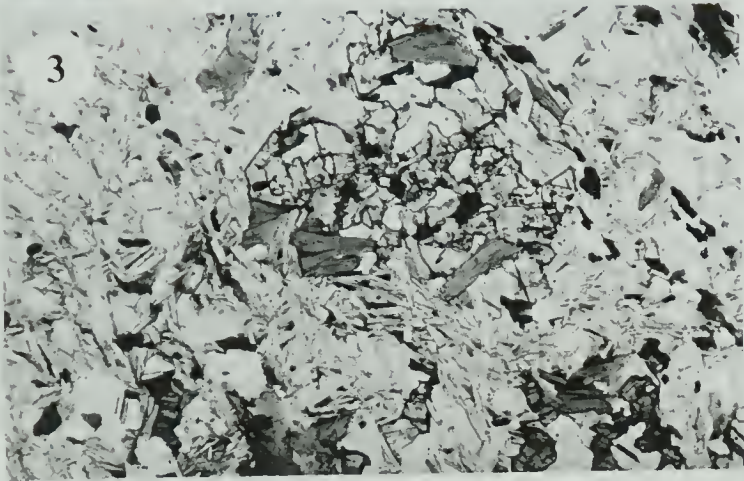
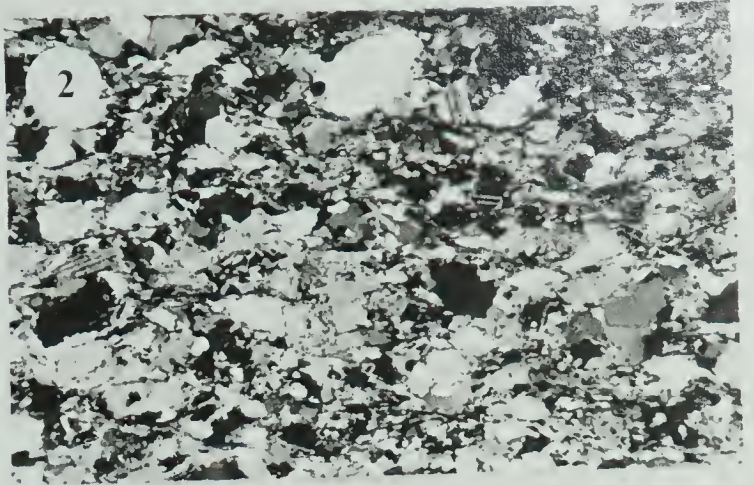
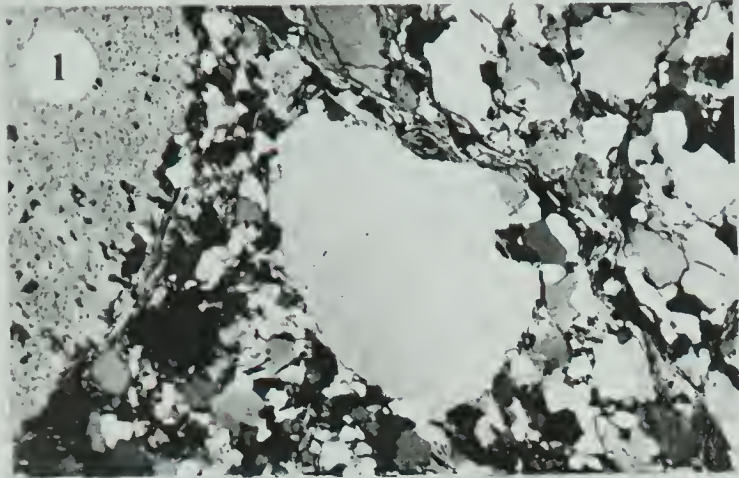


PLATE V

Photomicrographs

Figure

1) Chloritoid

Porphyroblast aligned with the chlorite-phengite defined S_1 schistosity. Unit C phyllitic schist, Swiftwater subdivision.

[Sample #E₄(2)2B(88)] x 25

2) Crenulation

Crenulation of S_2 surface to produce an incipient S_3 foliation. Phengite-chlorite assemblage defines S_2 and is rotated into S_3 , and overprinted with carbonate. Unit B. Rearguard subdivision.

[Sample #F₅(22)1(112)] x 25

3) Microcline

Detrital clast of Hudsonian microcline set in a matrix of quartz and phengite. An unaltered relict, found in a coarse feldspathic sandstone in Unit C, in the Swiftwater subdivision.

[Sample #E₈(11)13(103)] x 25

4) Microcline

Rock fragment containing quartz, microcline (dark), and albite (light). The relict microcline contains fragments of an earlier calcic plagioclase, now albite. Quartzo-feldspathic schistose pebble conglomerate sample, from the Western Zone.

[Sample #F₄(51)2B(134)] x 25

5) Chessboard Albite

Shattered detrital feldspar clast, set in a quartz, phengite matrix. Contains orientated inclusions of plagioclase feldspar with polysynthetic twins perpendicular to the chessboard long axis.

Western Zone.

[Sample #G₆(3)1(129)] x 25

6) Chessboard Albite

Detrital feldspar clast enveloped by a phengite quartz matrix. Chequered, chessboard albite with relict inclusions of an early, Carlsbad twinned plagioclase. Western Zone.

[Sample #G₆(3)1(129)] x 25

7) Chessboard Albite

Detrital clast of feldspar set in a matrix of quartz and phengite. (No chlorite, although chlorite grade) Chessboard pattern to albite which contains rounded inclusions and a corroded edge, consisting of relict plagioclase. Unit C. Swiftwater subdivision.

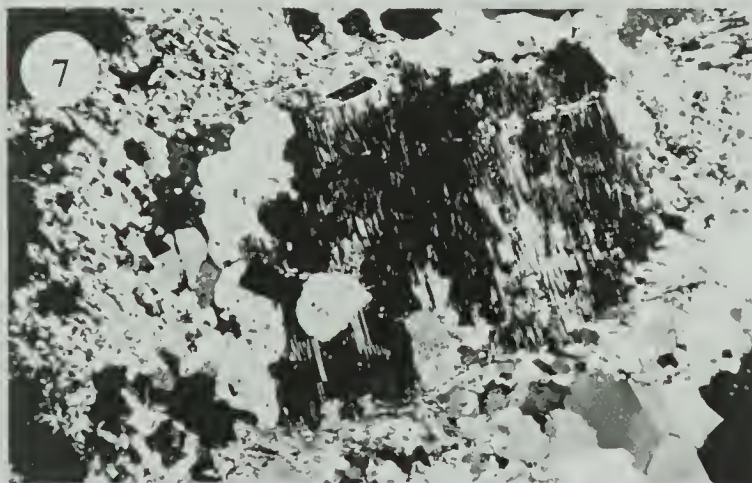
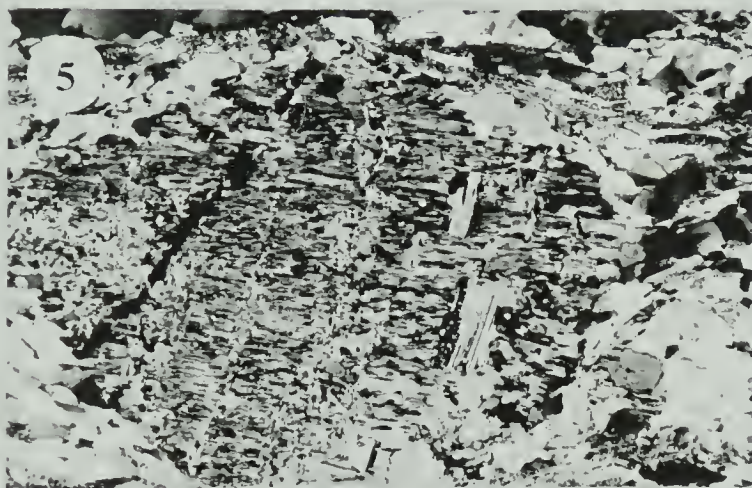
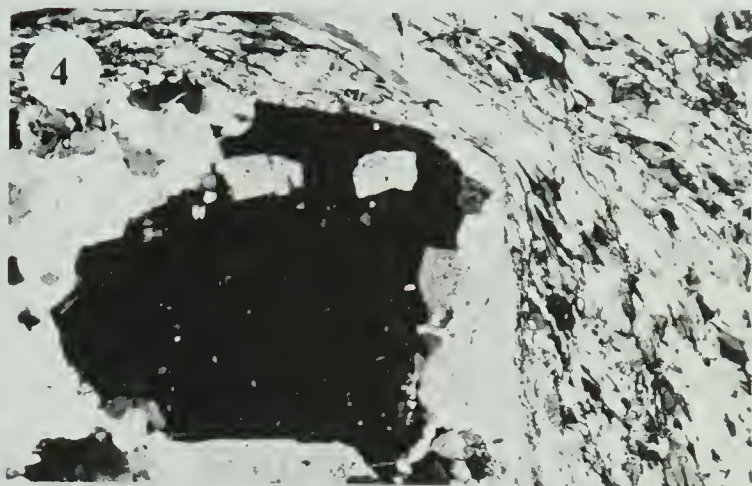
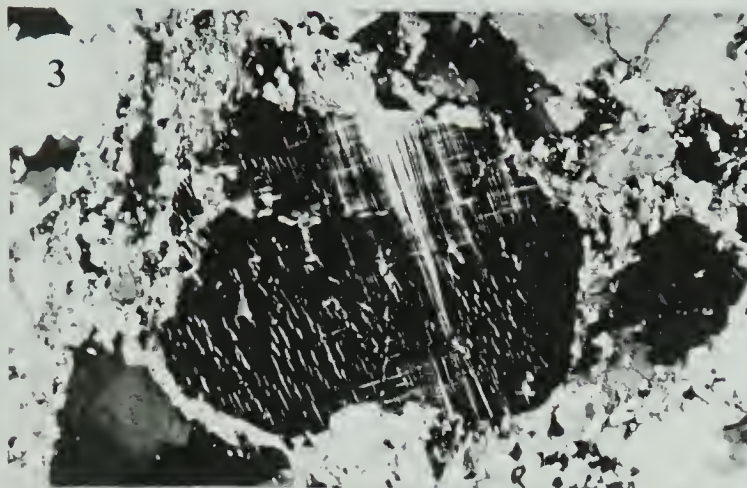
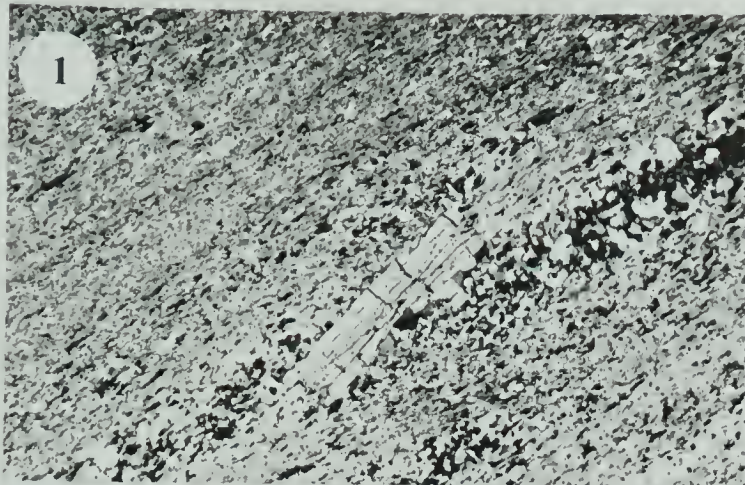
[Sample #E₈(11)13(103)] x 25

8) Microclinised Plagioclase

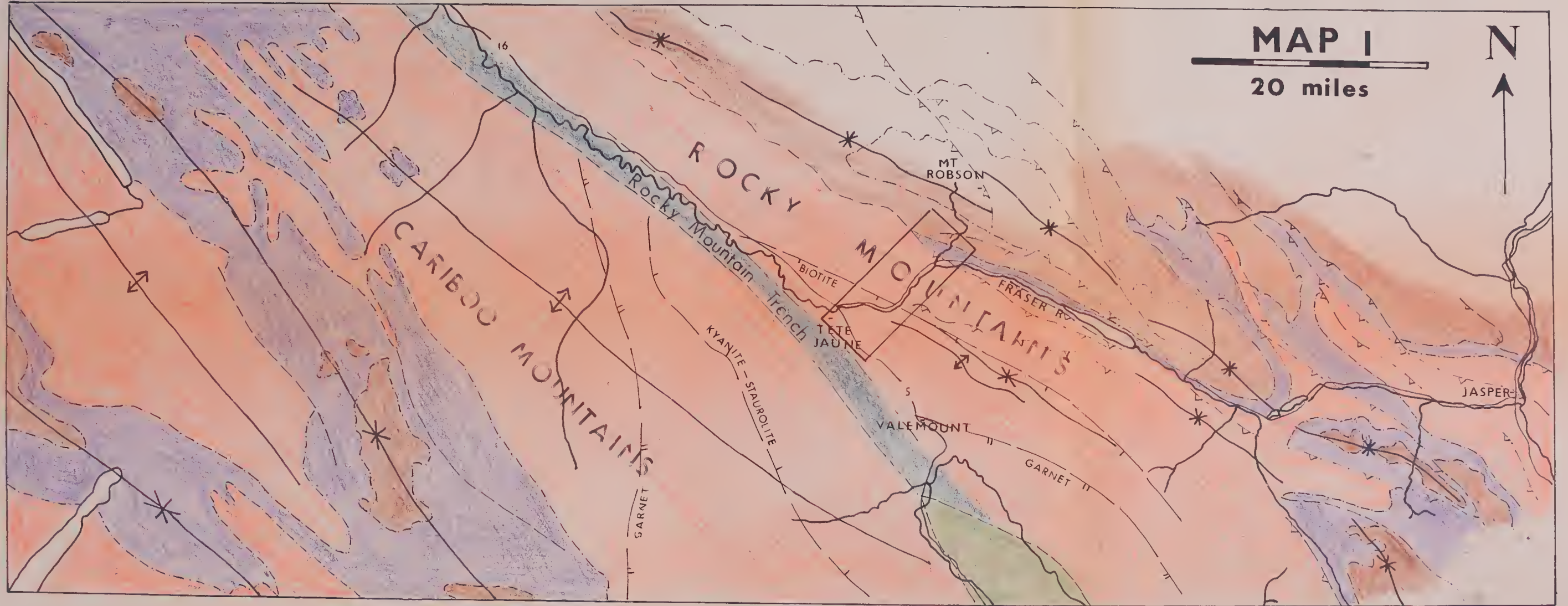
Rounded clast of feldspar set in a matrix of quartz and phengite. Clast enveloped by mica. Plagioclase lamella twins are disrupted by pervasive conversion to microcline (black). Pre-depositional microclinisation of the plagioclase. Western Zone.

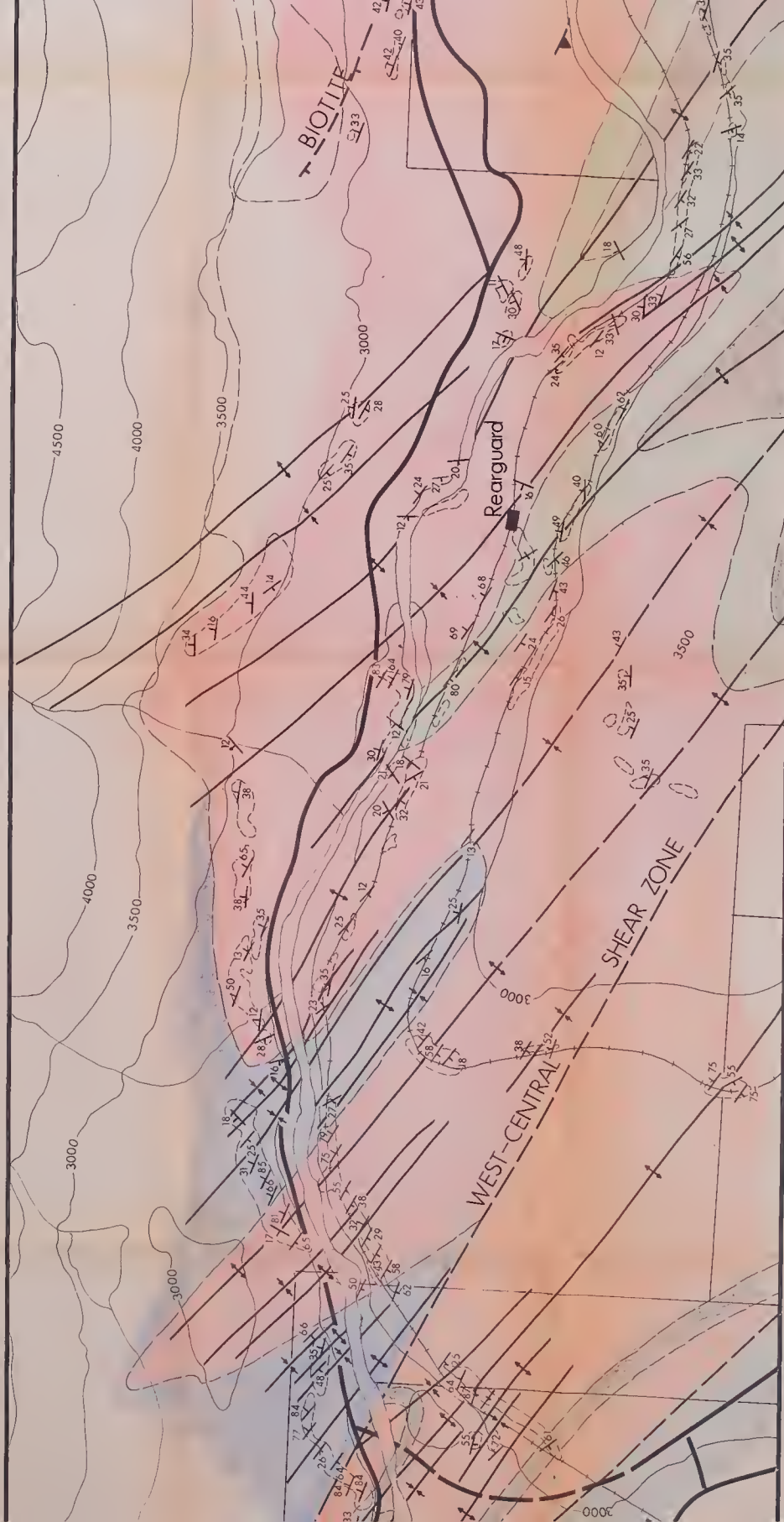
[Sample #F₄(51)2B(134)] x 25

PLATE V

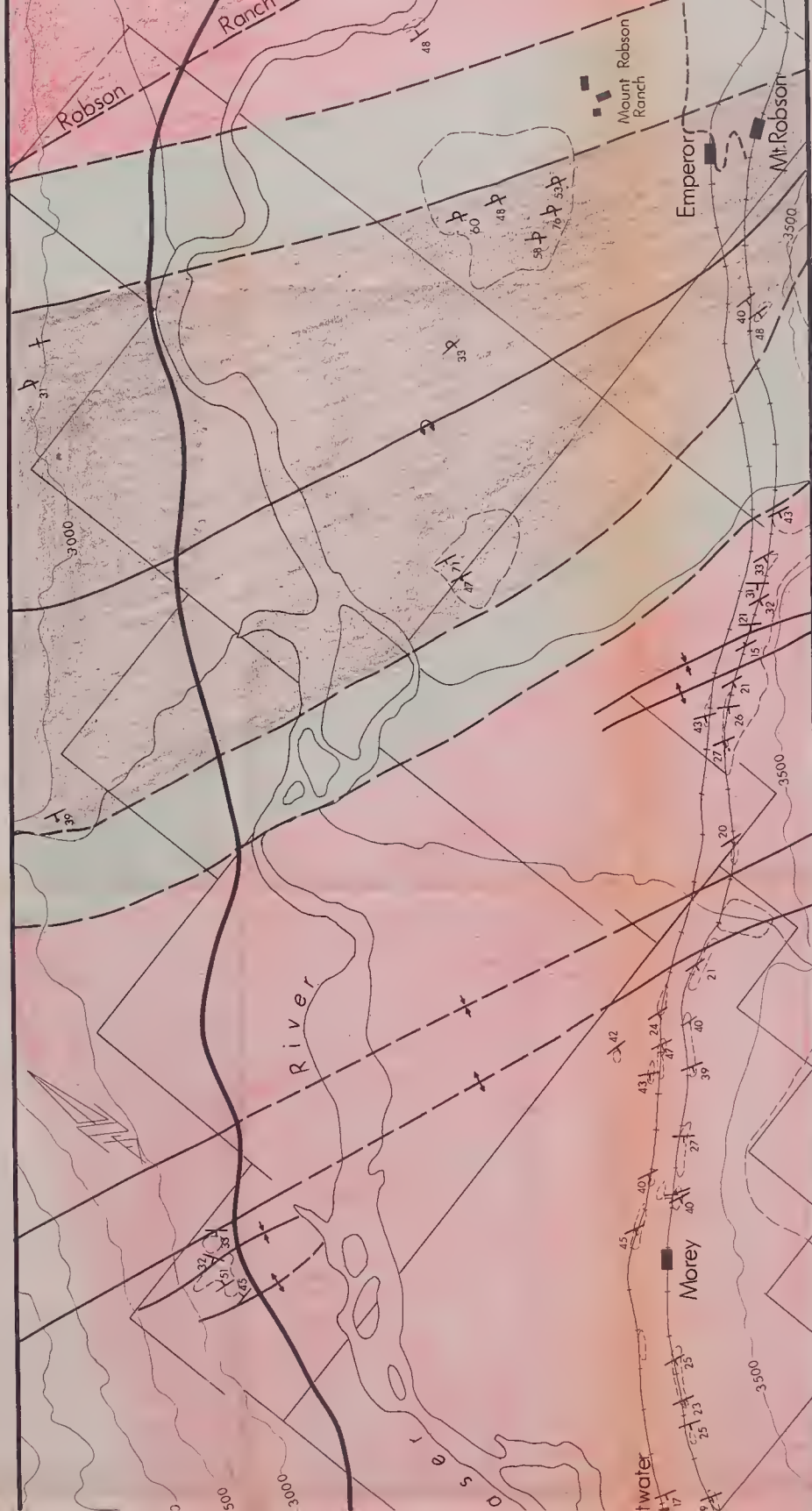






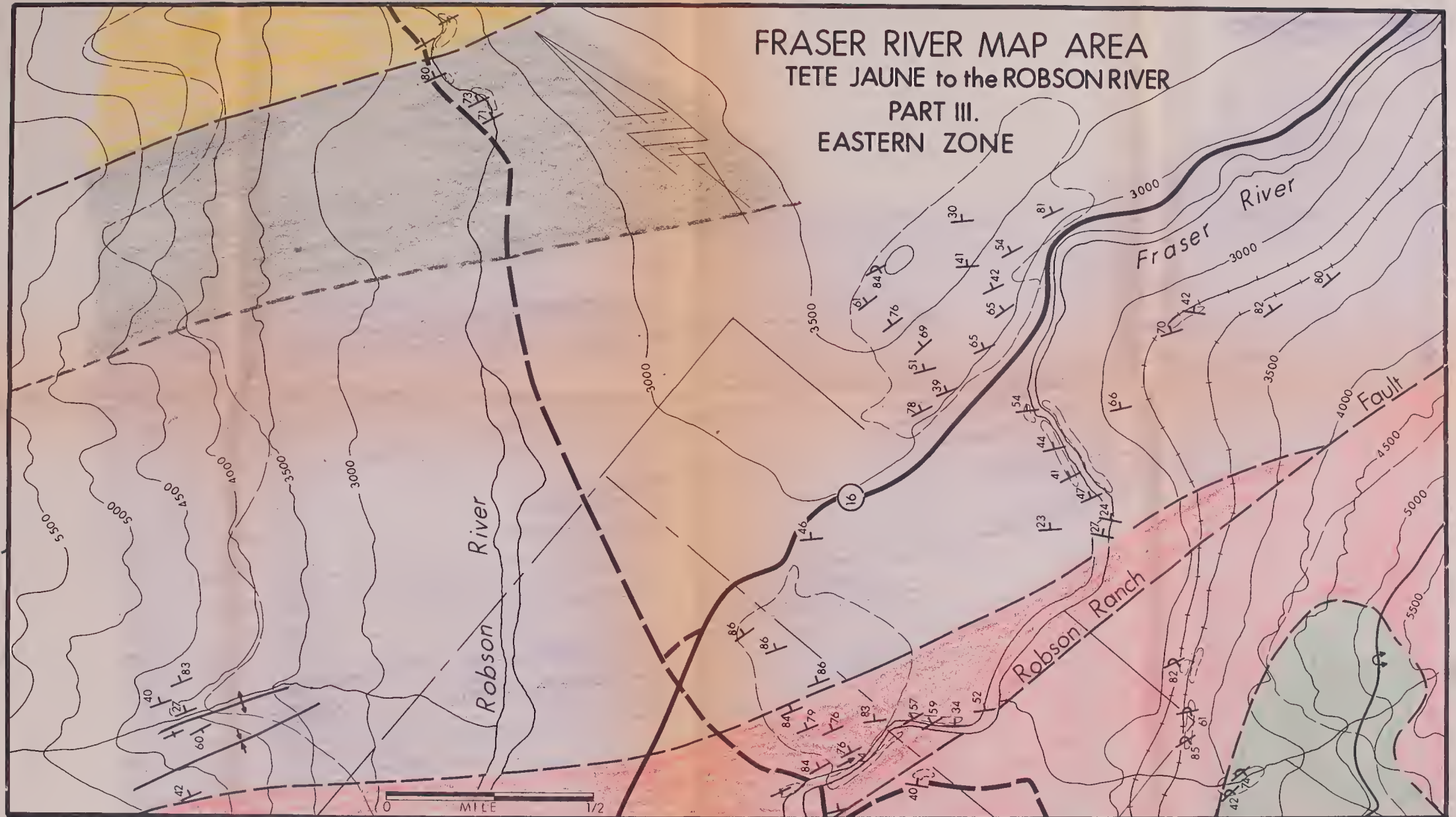


R RIVER MAP AREA TÊTE JAUNE to the ROBSON RIVER PART I. WESTERN & WEST CENTRAL ZONES

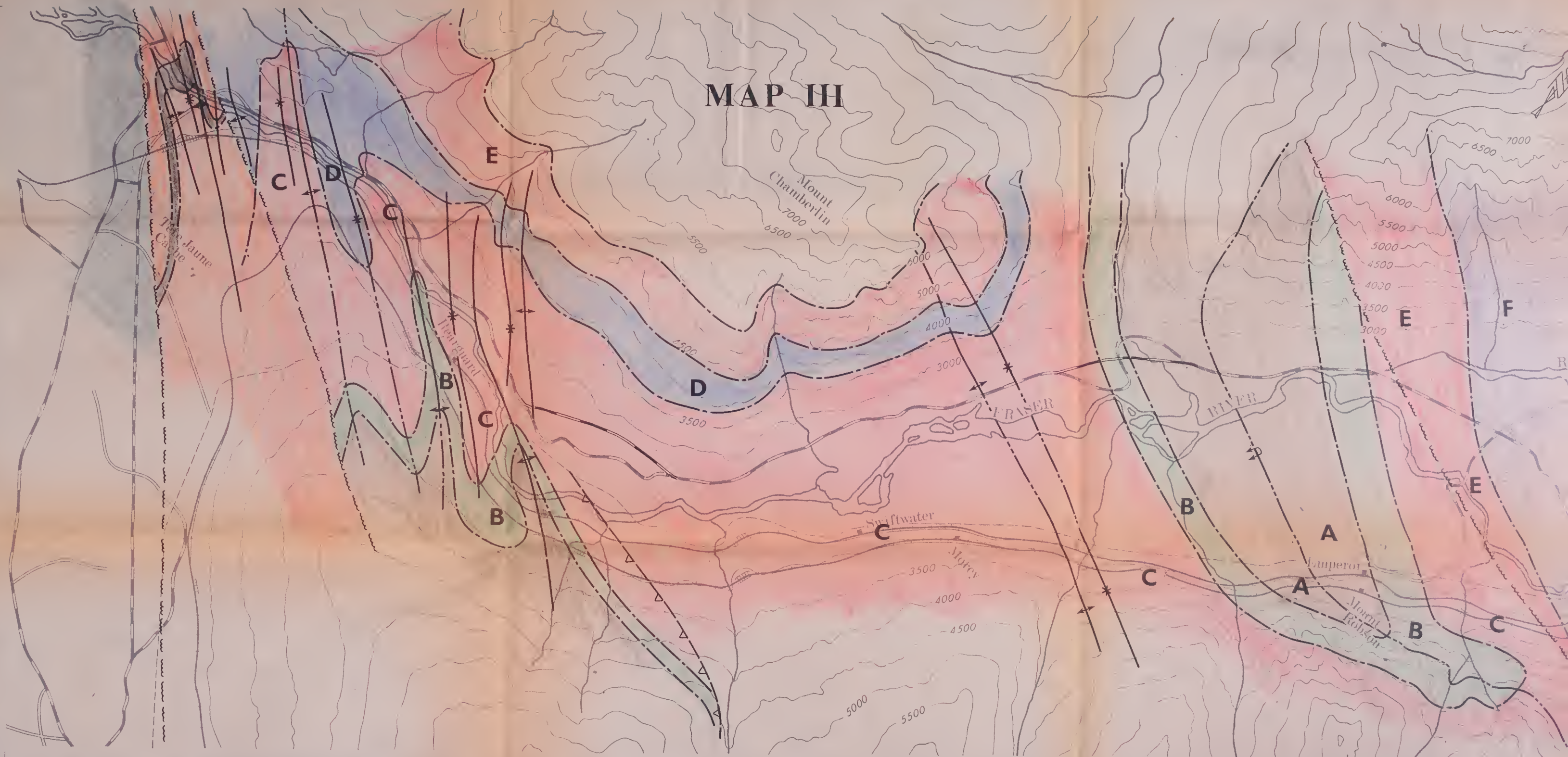


EA TÊTE JAUNE to the ROBSON RIVER PART II. EAST CENTRAL ZONE

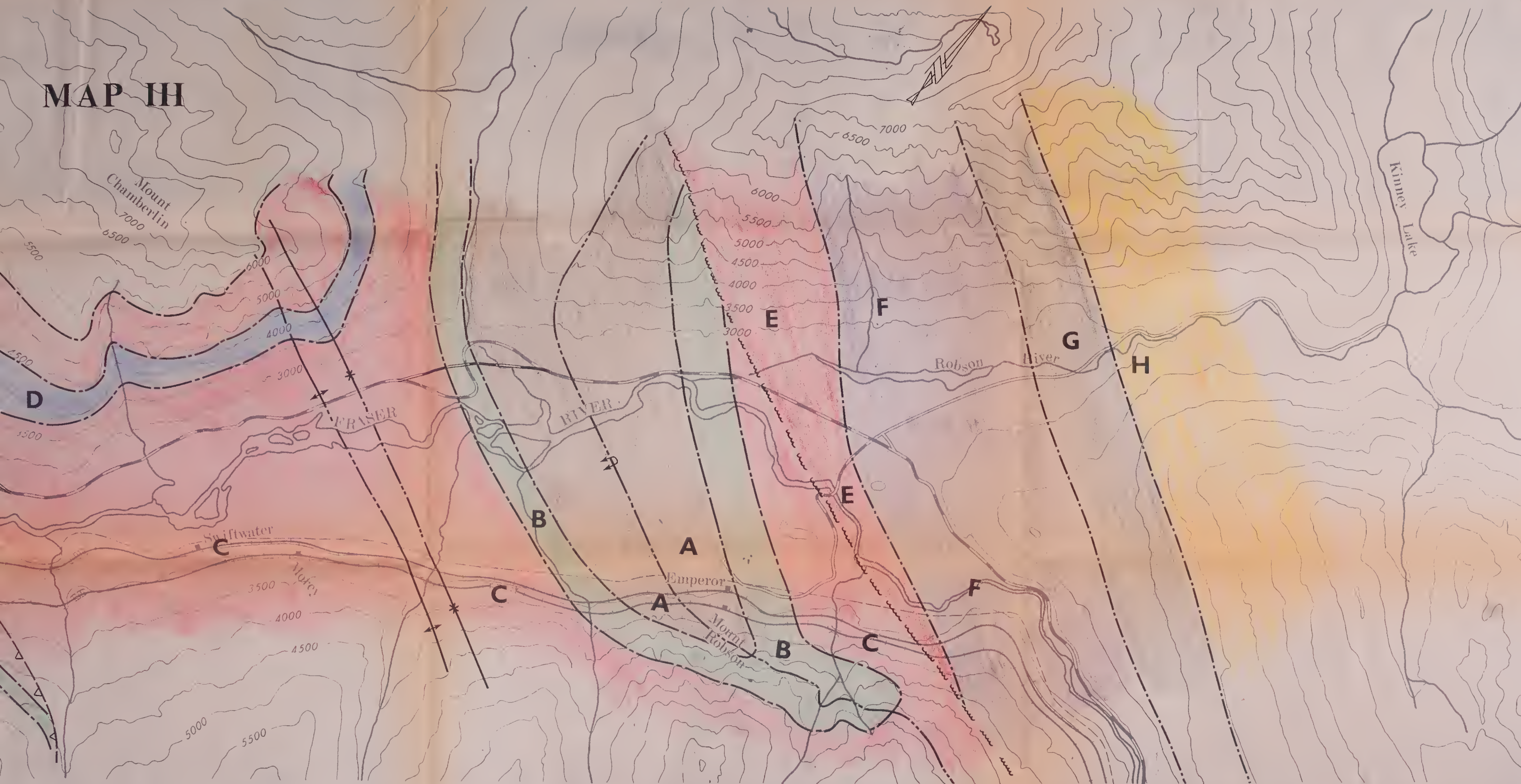
FRASER RIVER MAP AREA
TETE JAUNE to the ROBSON RIVER
PART III.
EASTERN ZONE



MAP III



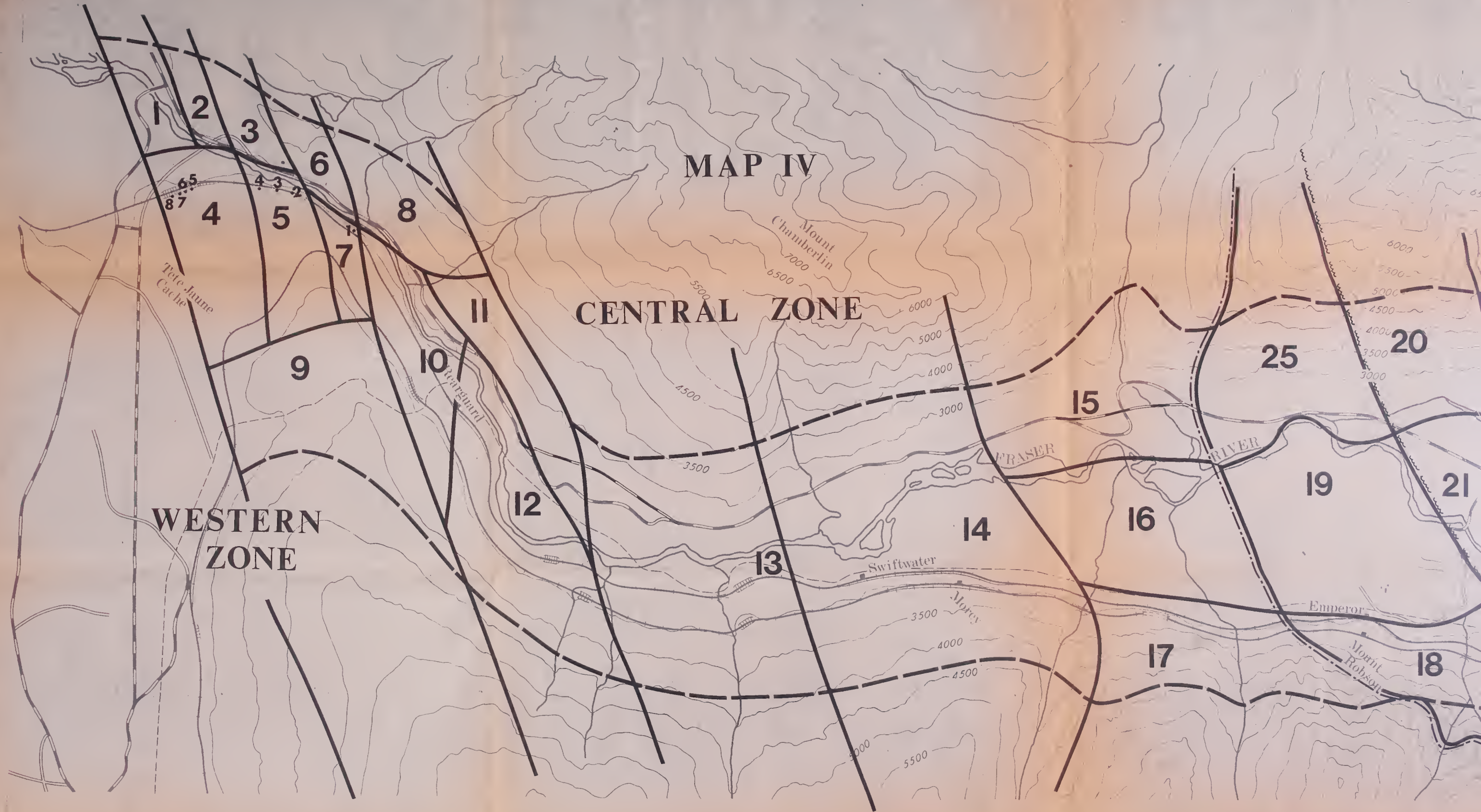
MAP III



MAP IV

CENTRAL ZONE

WESTERN ZONE



MAP IV

CENTRAL ZONE

EASTERN ZONE



B29998